Addendum to the 1998-1999 Hydrodynamic Modeling Report

Massachusetts Water Resources Authority

Environmental Quality Department
ENQUAD Report 2002-17

HydroQual. 2002. **Addendum to the 1998-1999 hydrodynamic modeling report**. Boston: Massachusetts Water Resources Authority. Report ENQUAD 2002-17. 82 p.

TABLE OF CONTENTS

LIST OF FIGURES

LIST OF FIGURES (Cont.)

LIST OF FIGURES (Cont.)

SECTION 1

INTRODUCTION

This addendum was prepared in response to comments made by the Model Evaluation Group (MEG) on the hydrodynamic model calibration documented in the report "Calibration of the Massachusetts and Cape Cod Bays Hydrodynamic Model: 1998-1999" (HydroQual, 2001). Specifically, the MEG requested additional information on the model's estimation of vertical mixing, the heat flux model, and the assigned boundary condition relaxation times. Information was also requested regarding the Gulf of Maine Model, which was not used during the model calibration, but had been used in a previous modeling analysis. This addendum provides additional documentation on these topics.

SECTION 2

VERTICAL MIXING

2.1   INTRODUCTION

The MEG expressed some concern as to whether or not the hydrodynamic model computed enough vertical mixing to reproduce the physical processes occurring within Massachusetts Bay. The evidence cited for the under prediction of the vertical mixing, was the use of a model coefficient allowing all of the shortwave solar radiation to penetrate through the water column in order to reproduce the temperature profile in the water column. The idea being that more shortwave radiation should be absorbed in the surface layer where a model that is mixing properly would distribute the energy appropriately to reproduce the temperature profile. In order to investigate this issue, the vertical diffusivity was examined at two locations, the outfall site (depth = 30.5 m) and the middle of Stellwagen Basin (depth = 89.9 m) during three periods of time. These three periods were the same three periods examined in the calibration report, a wind driven mixing event (May 1998), a cooling event (June-July 1999), and a destratification event (October 1999).

2.2   OUTFALL SITE

Figure 2-1 was originally presented in the calibration report, and shows the observed and computed wind, temperature and salinity during May 1-20, 1998 at the Boston Buoy. (Note the time scale begins at day 0.) The wind begins blowing in a constant direction with a velocity greater than 10 m/s on May 9, 1998. Figures 2-2 and 2-3 present the vertical diffusivity between the top eleven layers in the model at the outfall site for the May 1-20 period. The bottom layer was omitted to save space and did not contribute any additional information to the analysis. (Recall that the top three layers represent 1%, 3%, and 6% of the depth respectively and that each subsequent layer contributes another 10% of the total depth.) The mixing between layers 1 and 2 remains moderately high through the 20-day period, with values, in most cases, between $1x10^{-4}$ and $2x10^{-3}$ m^2/s. Deeper in the water column, periods of high mixing occur less often, but many times with a greater magnitude than between layer 1 and 2. The magnitude of mixing in the deepest layers is often at the model specified minimum mixing of $5x10^{-6}$ m^2/s.

The effect of the prolonged high winds on the mixing is clearly evident throughout the water column during the May 9 to May 14 period. High mixing is observed all the way to the bottom layer of the hydrodynamic model, although there is a time lag with depth, and the duration of high mixing is shorter closer to the bottom of the water column. The effect of the higher mixing can be observed

Figure 2-1. Observed and modeled salinity and temperature as well as the wind forcing on May 1-20, 1998 at the Boston Buoy.
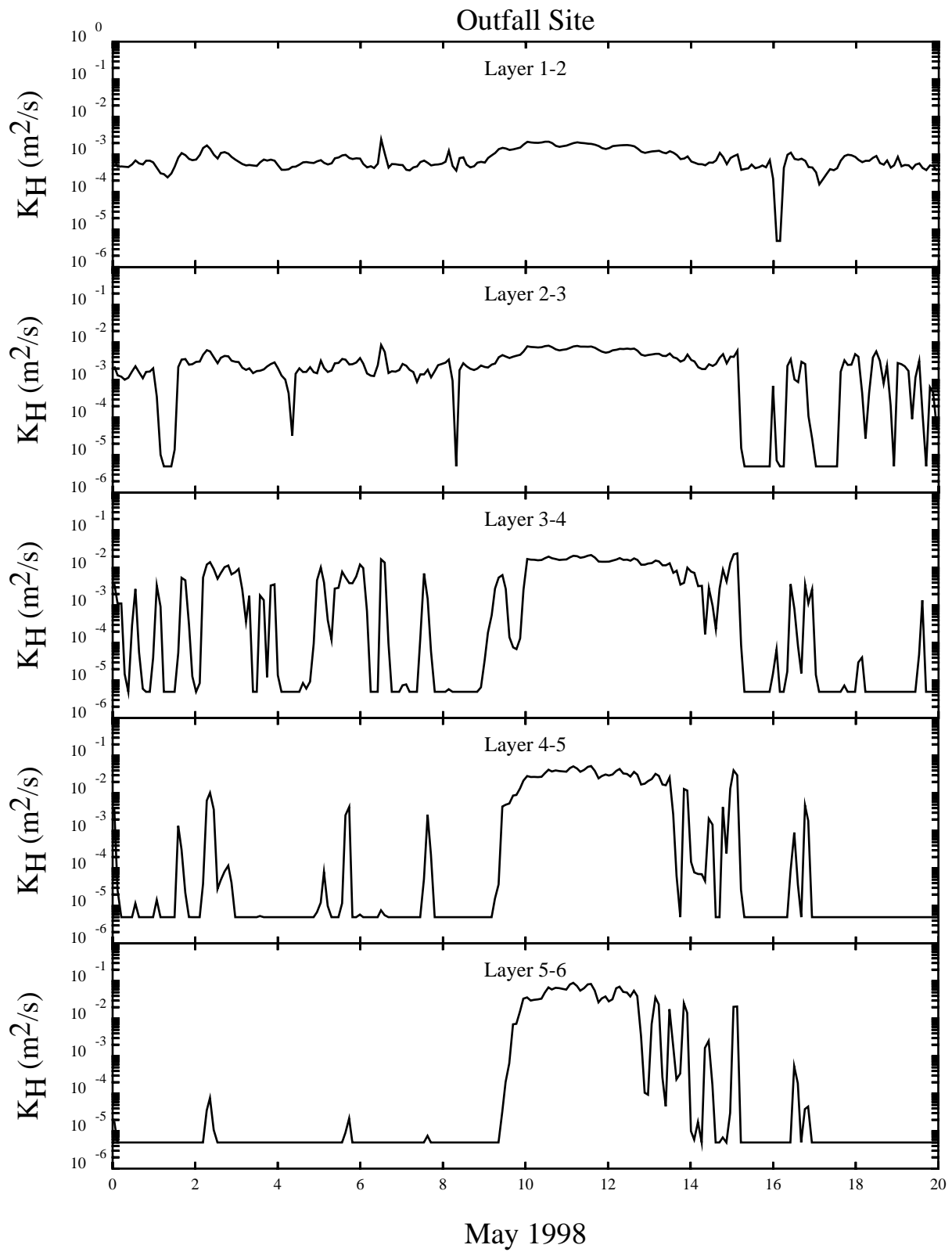
Figure 2-2. Model computed vertical diffusivity at the top five model layer interfaces during May 1998 at the outfall site.

Figure 2-3. Model computed vertical diffusivity at the interfaces of model layers 6-11 during May 1998 at the outfall site.

in the density computed by the model. Figures 2-4 and 2-5 show the time variable change in sigma-t with depth during this period. In general, the model computes an increase in the density in the top five layers and a decrease in density in layers 6 – 10 during the high wind period. The water column becomes completely mixed, at the outfall site, from May 11 to May 13.

Vertical profiles of the vertical diffusivity for one tidal cycle on May 10, 1988 are shown in Figure 2-6. The model output is displayed at 2.07 hr averaged intervals. Day 202.04 occurs near high tide. By May 10, higher mixing is beginning to penetrate down through the water column. A combination of wind and tidal effects increase the vertical mixing. The increased vertical mixing has its effect on density as shown in Figure 2-7. After a period of 12.42 hours the water column is much more well mixed.

Figure 2-8 presents the salinity, temperature, and wind model to data comparison for the period of June 15 to July 15, 1999 as shown in the calibration report. This period included a surface cooling event , which occurred between June 26 and July 3, during a portion of the year that the water column is very stratified. The effect of the cooling event on vertical mixing is less pronounced than the wind mixing event. Below the layer 5-6 interface (9.1 m), the mixing remains at or near the minimum assigned model values as shown in Figures 2-9 and 2-10. Similarly, the larger changes in sigma-t that occur during this time are calculated in the top four layers (Figures 2-11 and 2-12). Figures 2-13 and 2-14 show the vertical diffusivity and the associated density during the initial portion (June 28) of the cooling event. The mixing is restricted to the upper six meters of the water column and the density of the upper six meters changes with the higher mixing. As the cooling event progresses, (July 2) the vertical diffusivity increases further down the water column (Figure 2-15), and the upper nine meters becomes well-mixed as indicated by the density (Figure 2-16).

The last period to be examined, October 1-15, 1999, is presented in Figure 2-17. During this portion of the year, the surface well-mixed layer is approximately 9 to 12 meters deep, and the onset of the fall overturn is beginning. Figures 2-18 and 2-19 show that beginning on or around October 4 there is increased mixing down to the layer 7-8 interface (18.3 m). Sigma-t, presented in Figures 2-20 and 2-21, has an upward trend in the first five days of October in the upper layers, and there is evidence of a decline in the density on October 5th in the lower layers of the water column. The vertical profile of vertical diffusivity on October 5th is presented in Figure 2-22 and shows mixing down to 15 meters. During this particular tidal cycle, the well mixed layer increases from 15 meters to 18 meters, and there is a small decrease in the bottom layer sigma-t as shown in Figure 2-23.

A more complete writeup of these events can be found in HydroQual (2001).
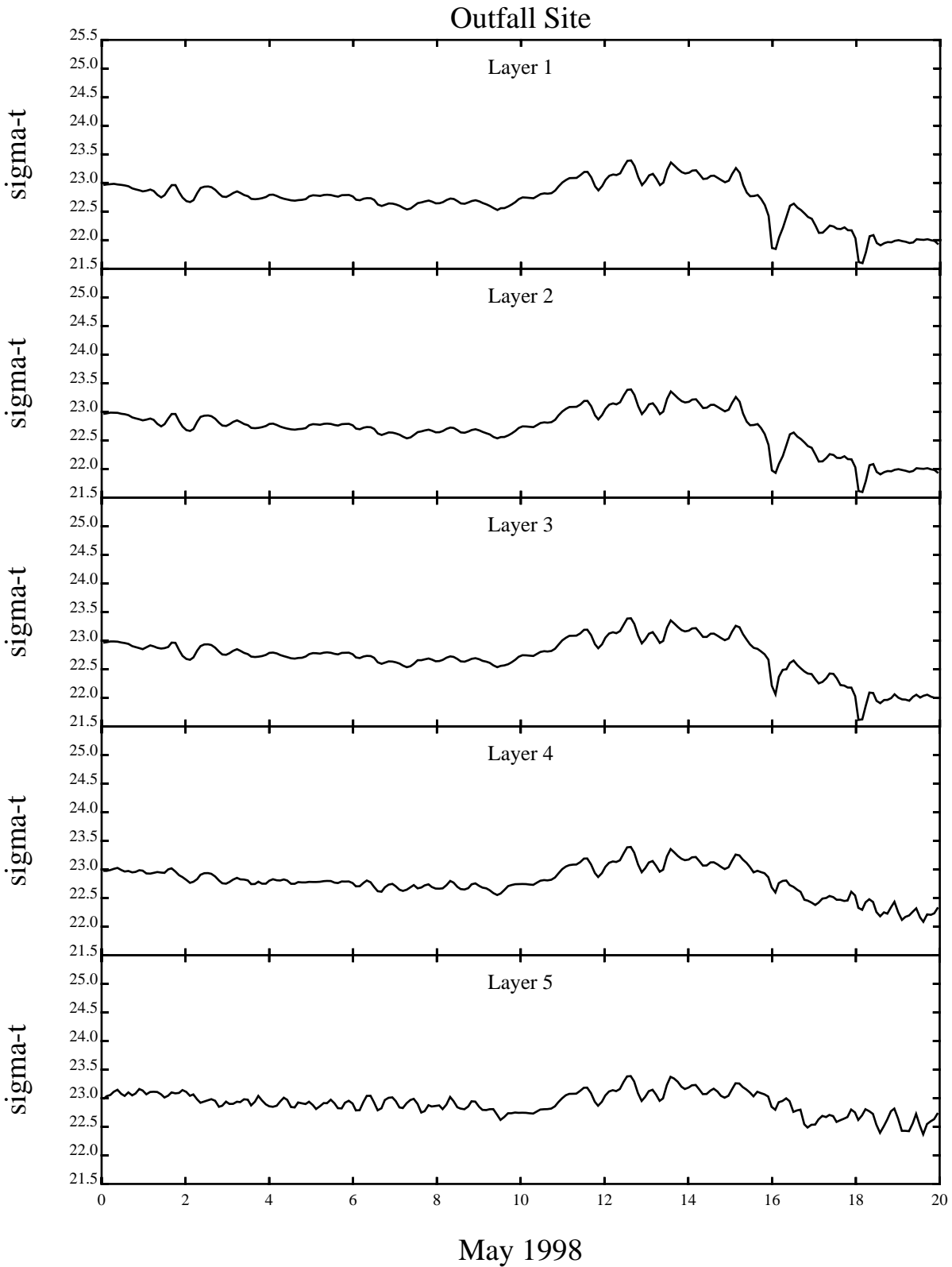
Figure 2-4. Model computed sigma-t in the top five model layers at the outfall site during May 1998.

Figure 2-5. Model computed sigma-t in model layers 6-10 at the outfall
site during May 1998.
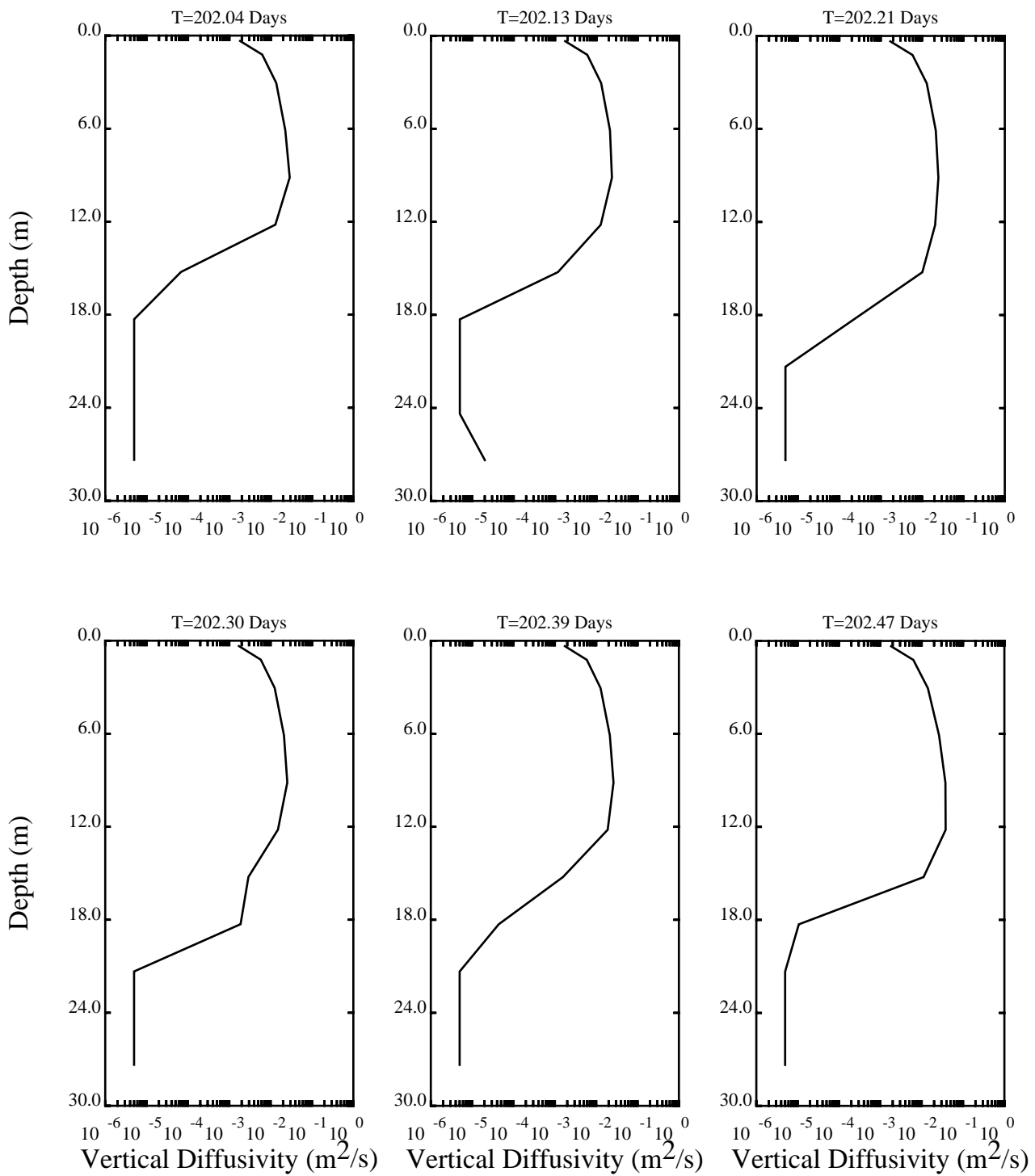
Outfall Site - May 10, 1998

Figure 2-6. Vertical distribution of vertical diffusivity during a tidal cycle on May 10, 1998 at the outfall site.

Outfall Site - May 10, 1998

Figure 2-7. Vertical distribution of sigma-t during a tidal cycle on May 10, 1998 at the outfall site.
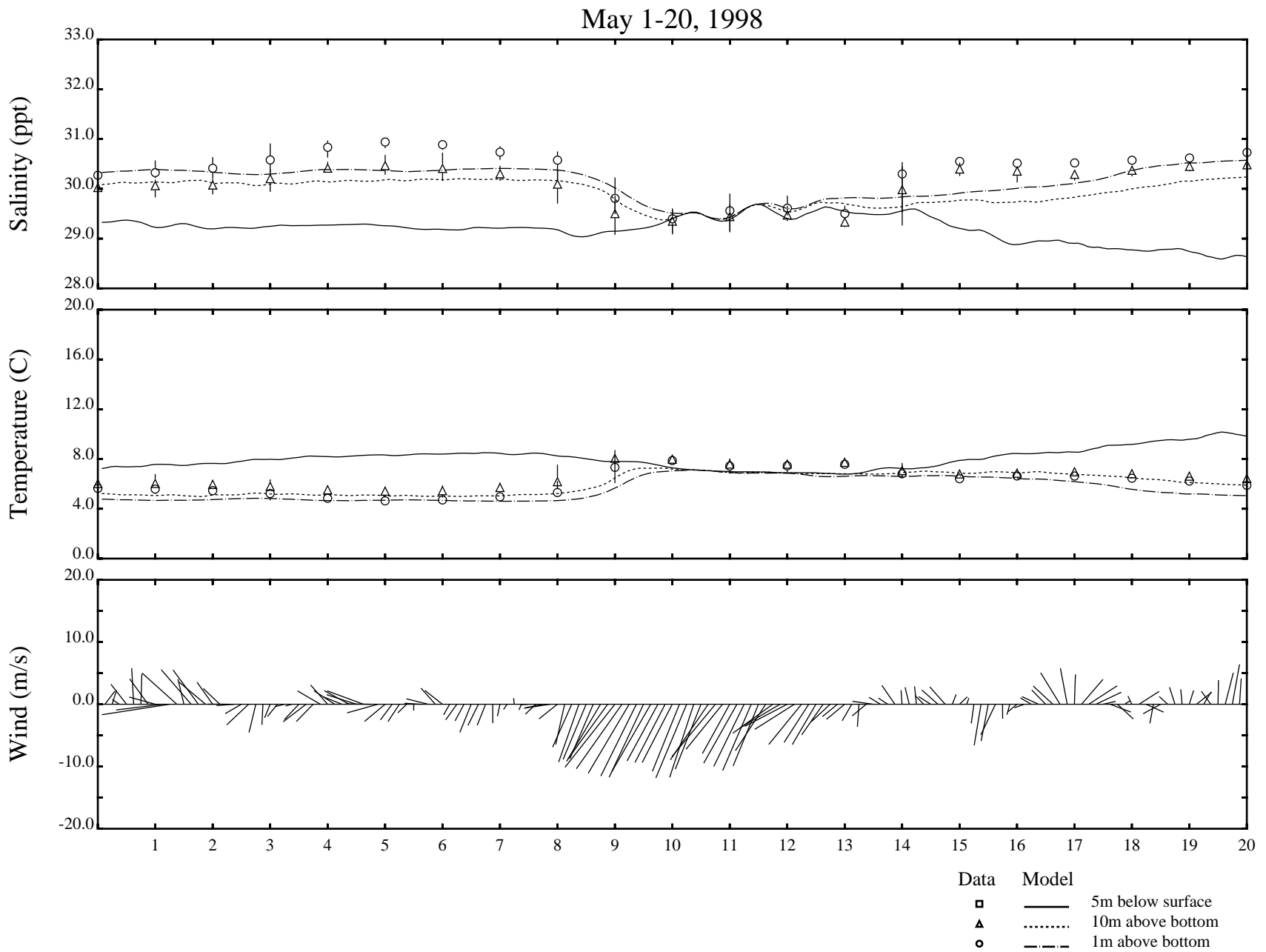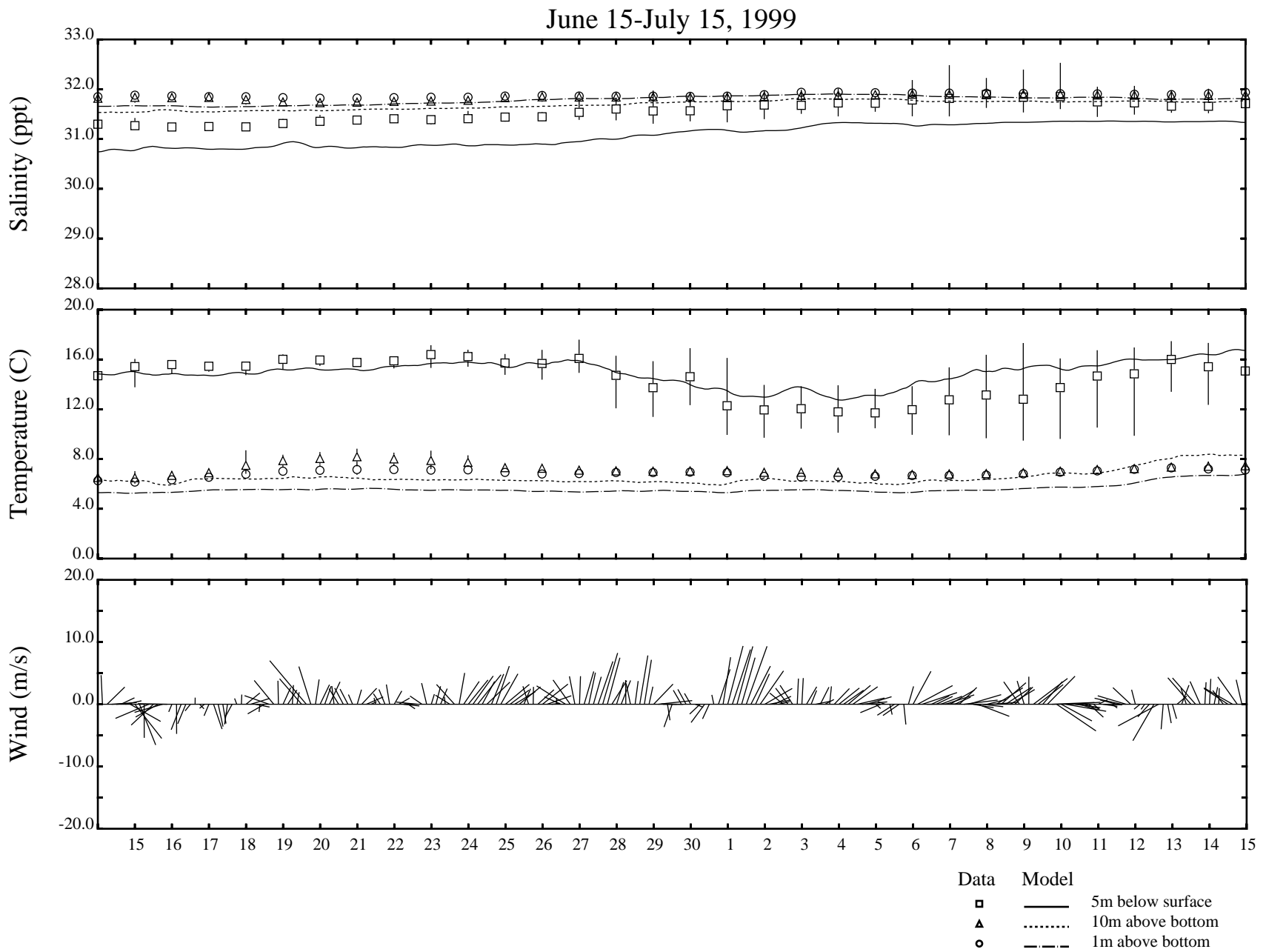
Figure 2-8. Observed and modeled salinity and temperature as well as the wind forcing on June 15-July 15, 1999 at the Boston Buoy.
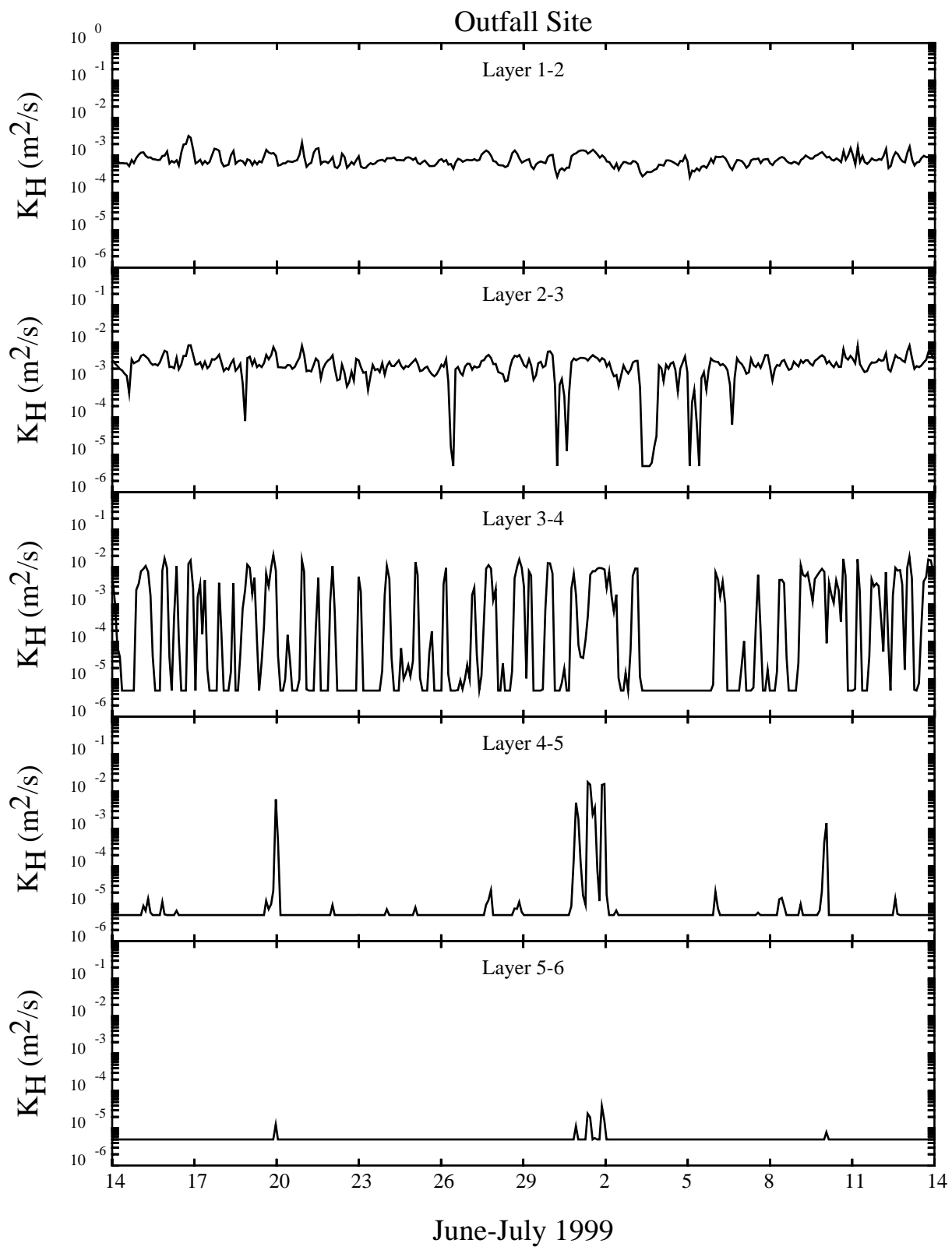
Figure 2-9. Model computed vertical diffusivity at the top five model layer interfaces during June-July 1999 at the outfall site.
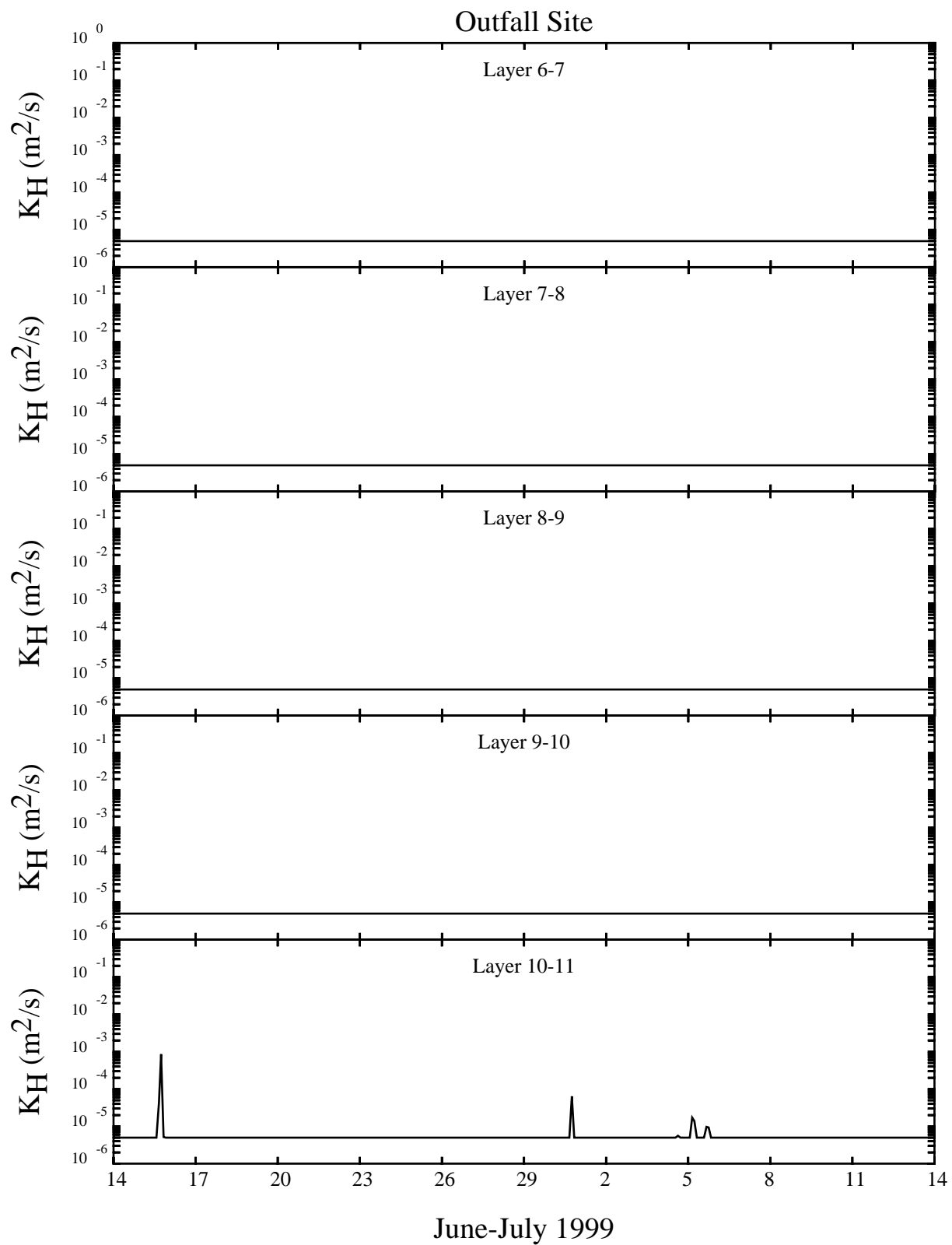
Figure 2-10. Model computed vertical diffusivity at the interfaces of model layers 6-11 during June-July 1999 at the outfall site.
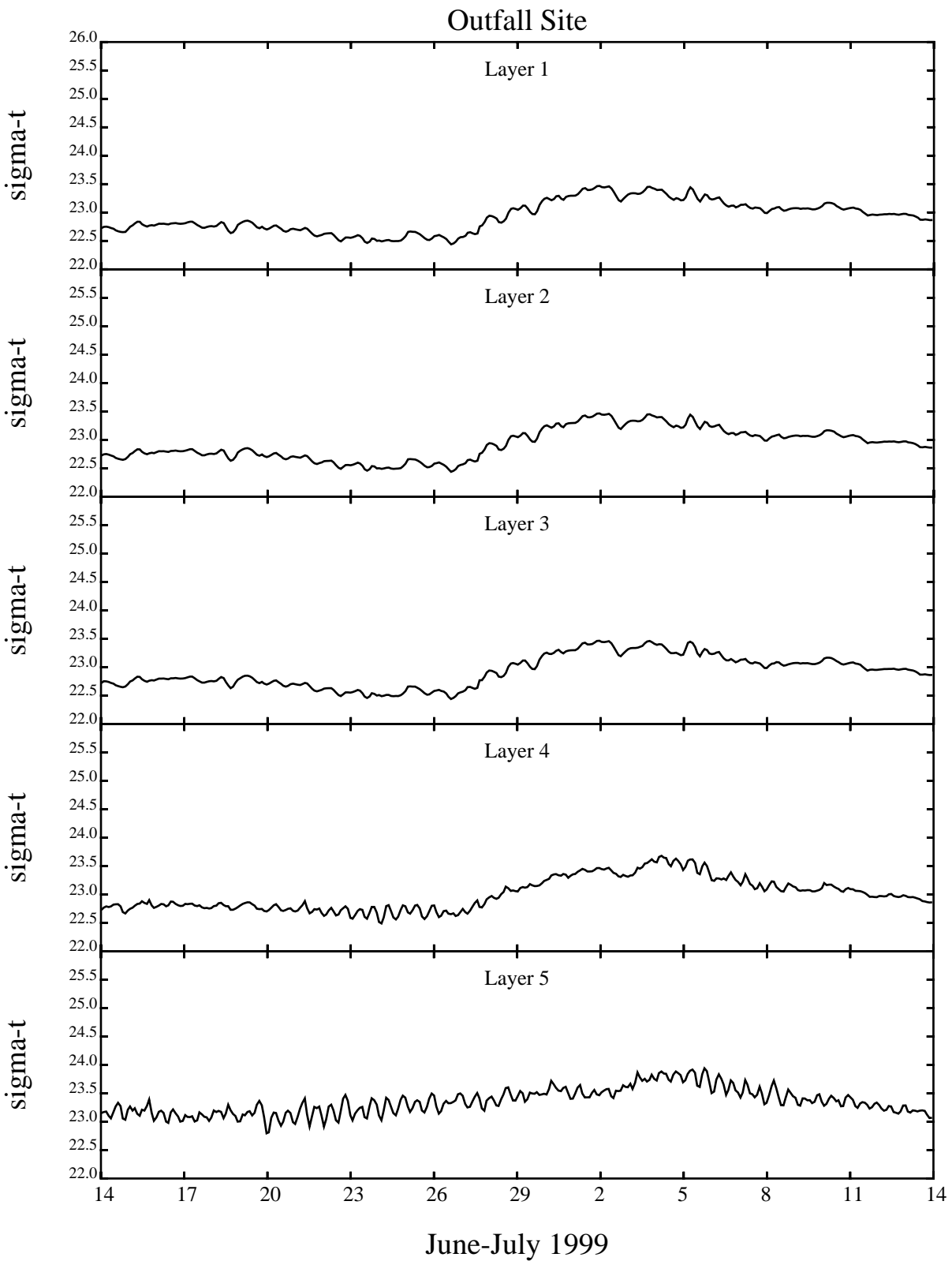
Figure 2-11. Model computed sigma-t in the top five model layers at the outfall site during June-July 1999.

Figure 2-12. Model computed sigma-t in model layers 6-10 at the outfall site during June-July 1999.

Figure 2-13. Vertical distribution of vertical diffusivity during a tidal cycle on June 28, 1999 at the outfall site.
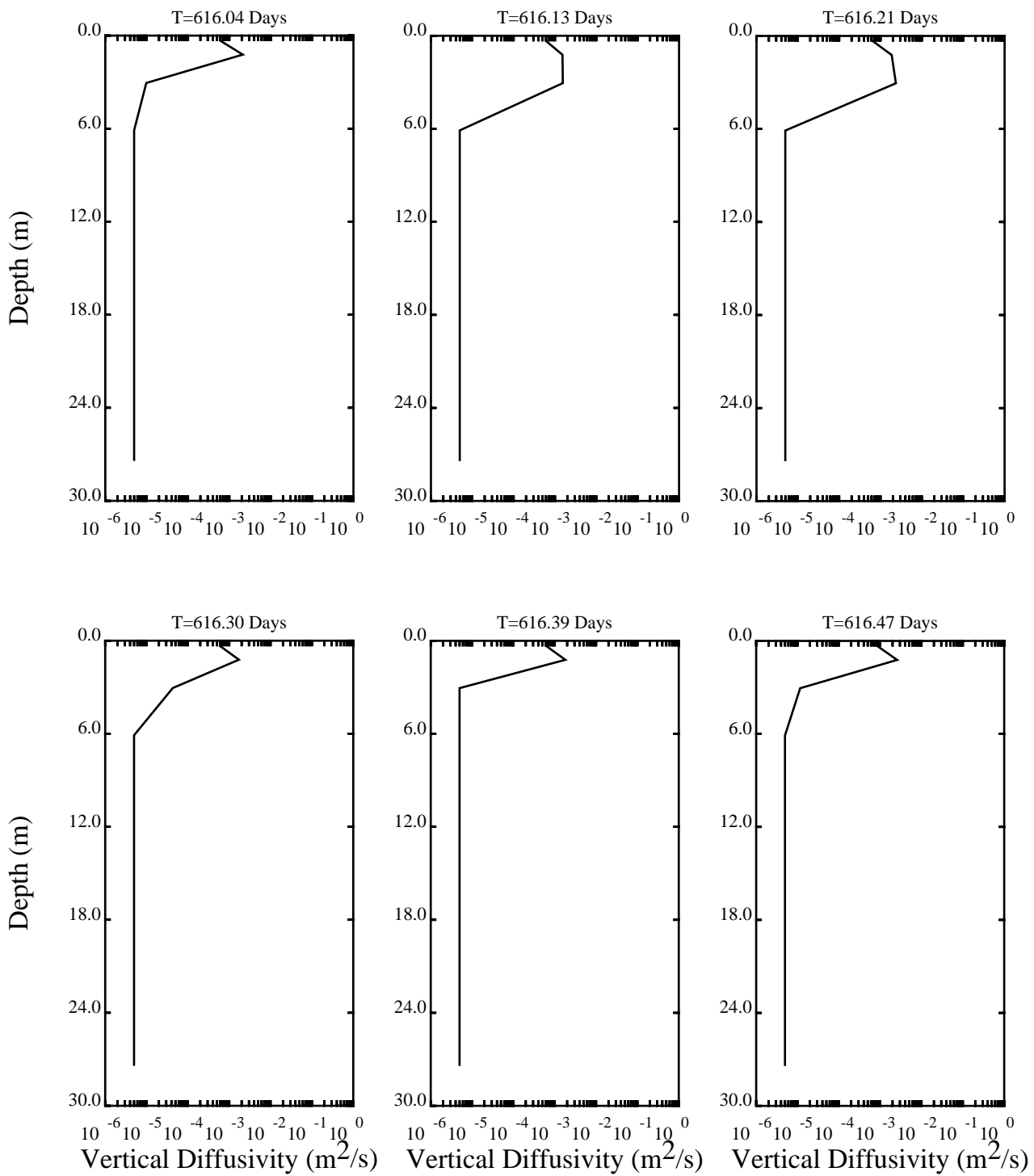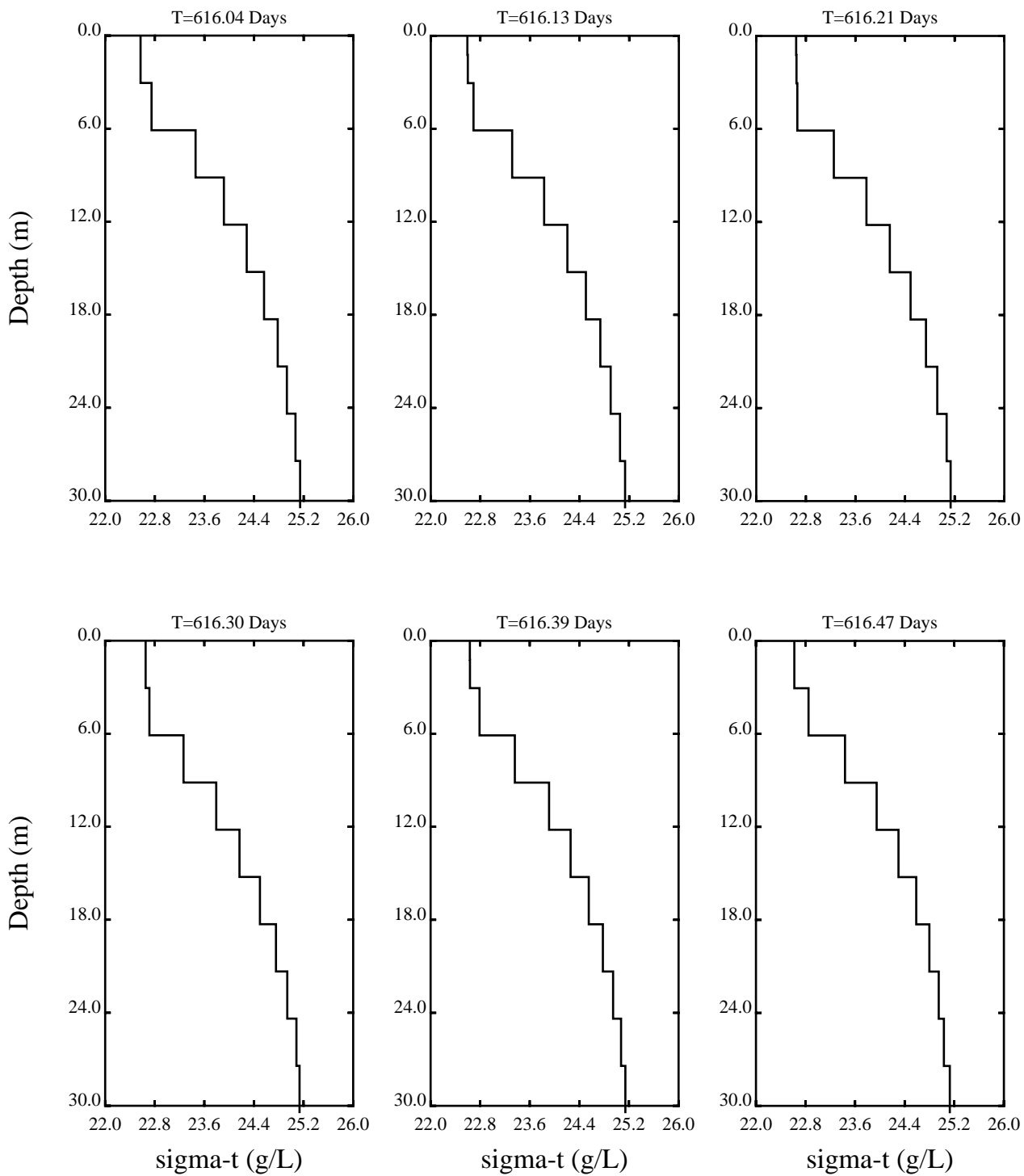
Outfall Site - June 28, 1999

Figure 2-14. Vertical distribution of sigma-t during a tidal cycle on June 28, 1999 at the outfall site.
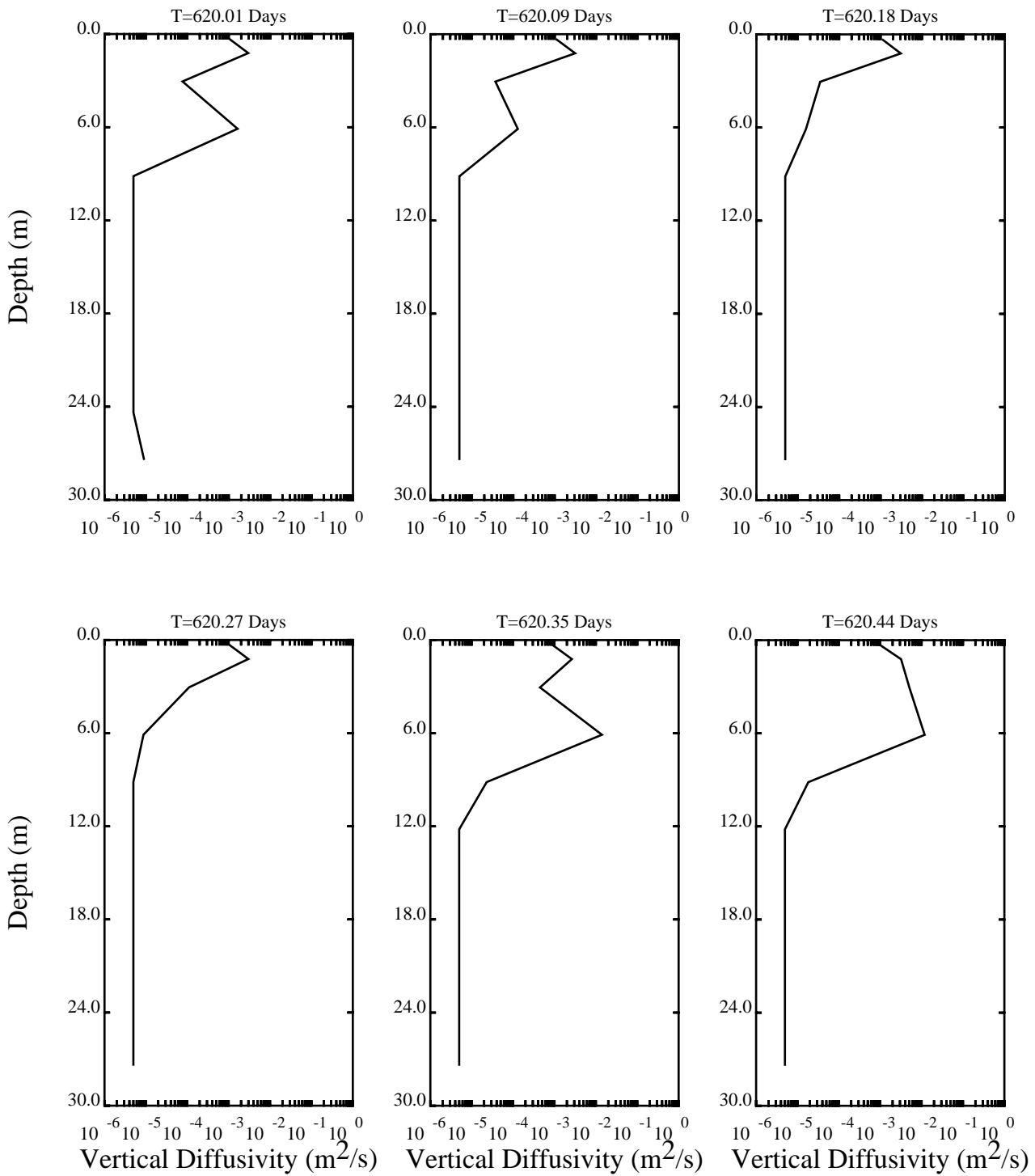
Figure 2-15. Vertical distribution of vertical diffusivity during a tidal cycle on July 2, 1999 at the outfall site.
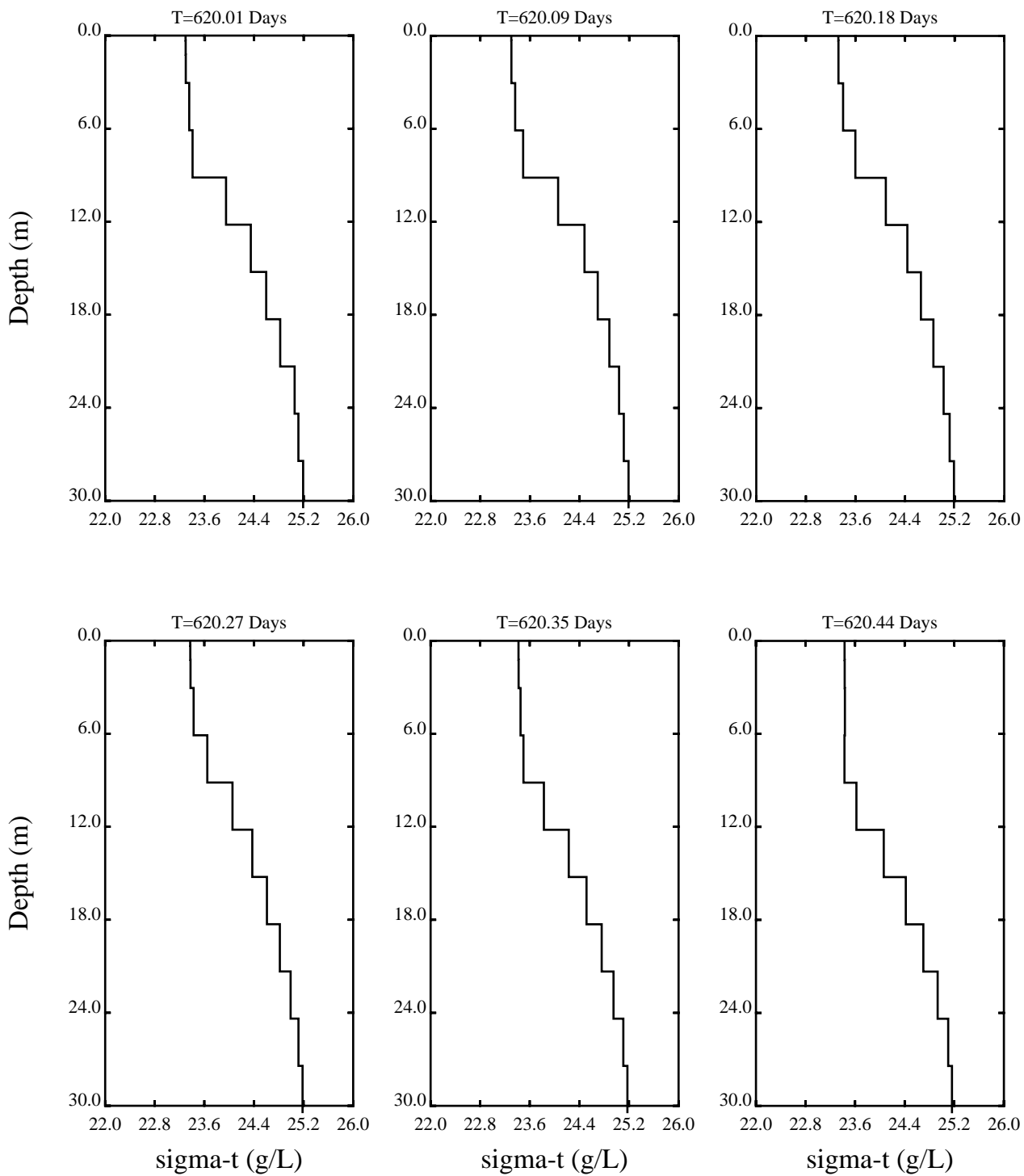
Figure 2-16. Vertical distribution of sigma-t during a tidal cycle on July 2, 1999
at the outfall site.
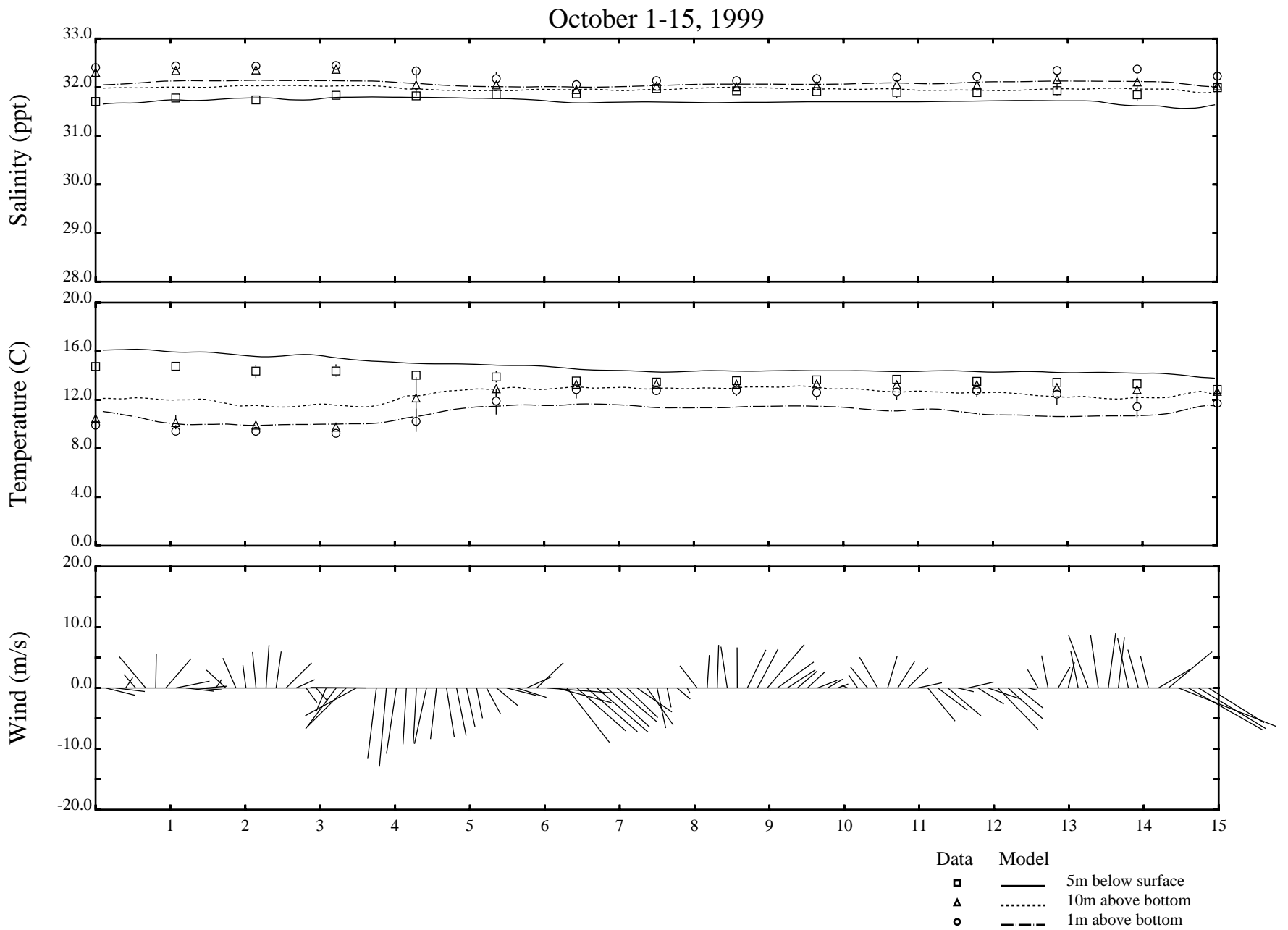
Figure 2-17. Observed and modeled salinity and temperature as well as the wind forcing on October 1-15, 1999 at the Boston Buoy.

Figure 2-18. Model computed vertical diffusivity at the top five model layer interfaces during October 1999 at the outfall site.
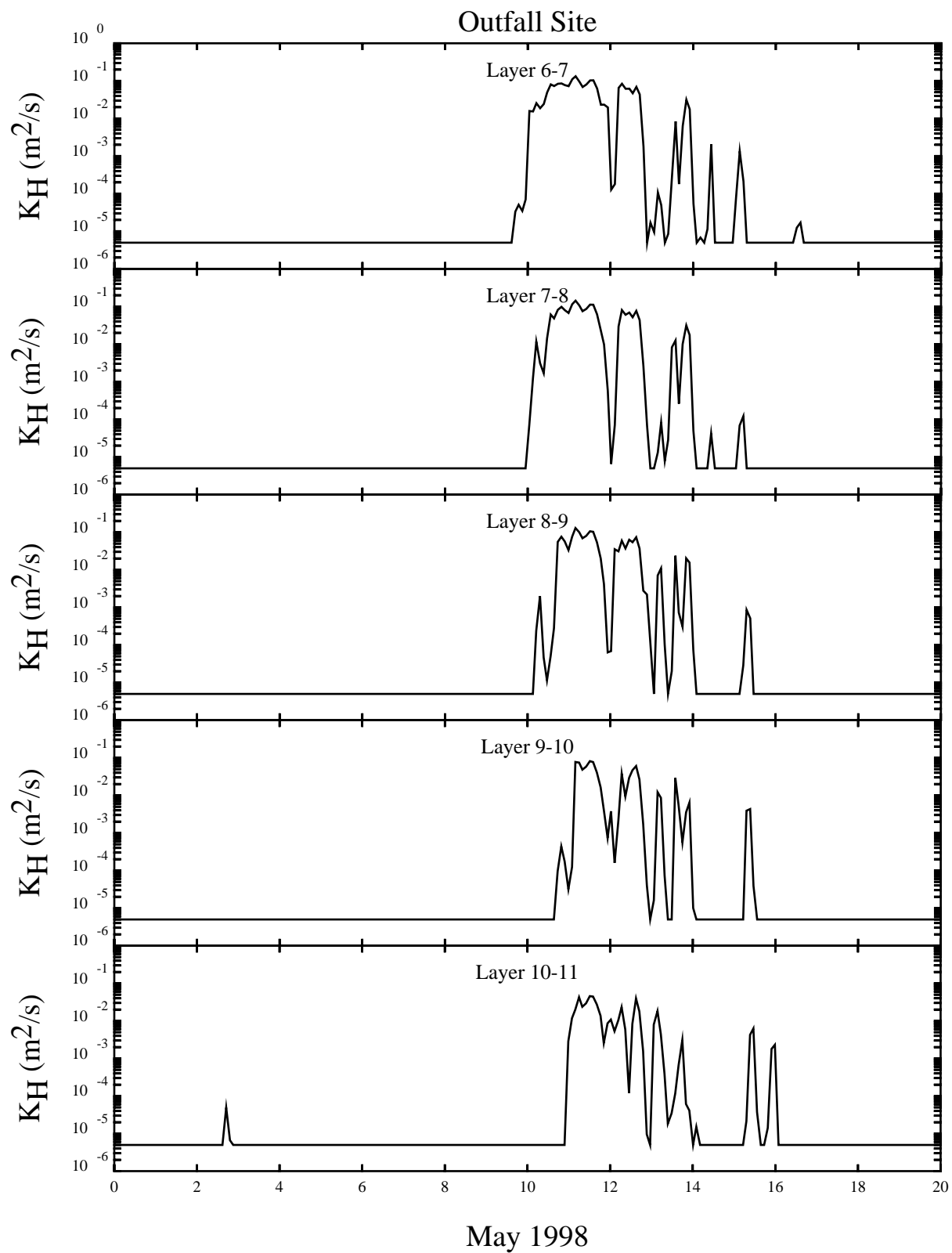
Figure 2-19. Model computed vertical diffusivity at the interfaces of model layers 6-11 during October 1999 at the outfall site.

Figure 2-20. Model computed sigma-t in the top five model layers at the outfall site during October 1999.
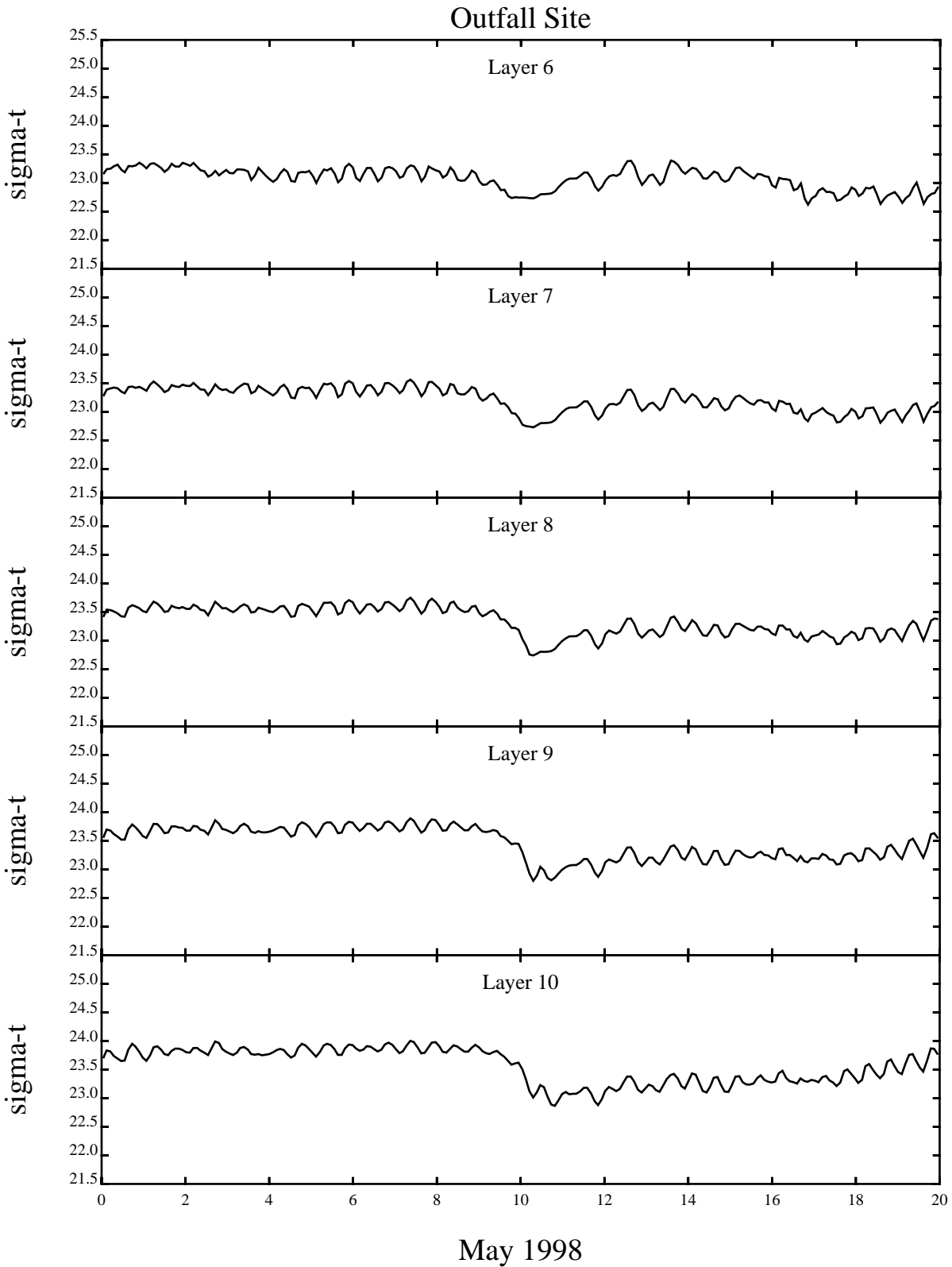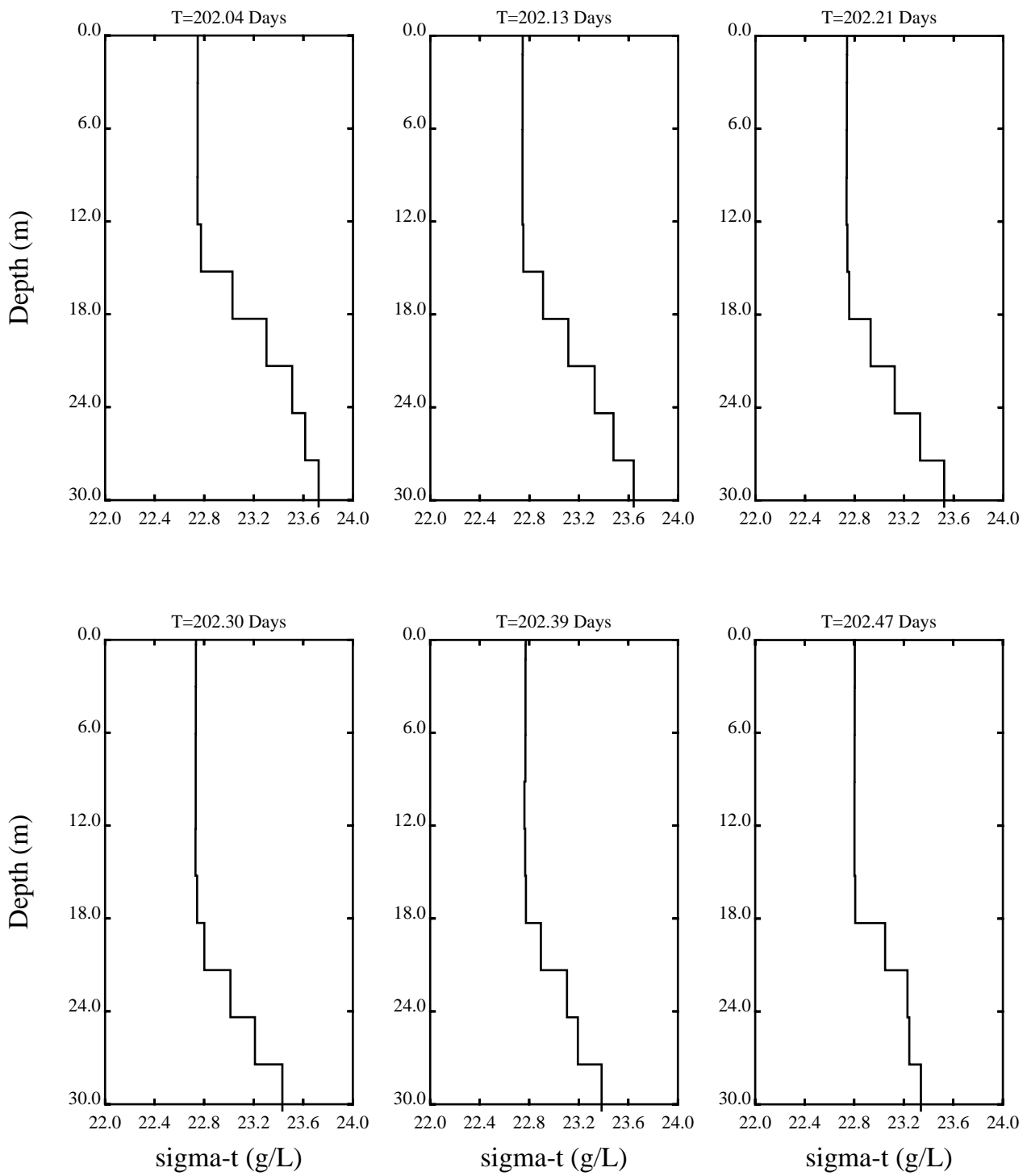
Figure 2-21. Model computed sigma-t in model layers 6-10 at the outfall
site during October 1999.
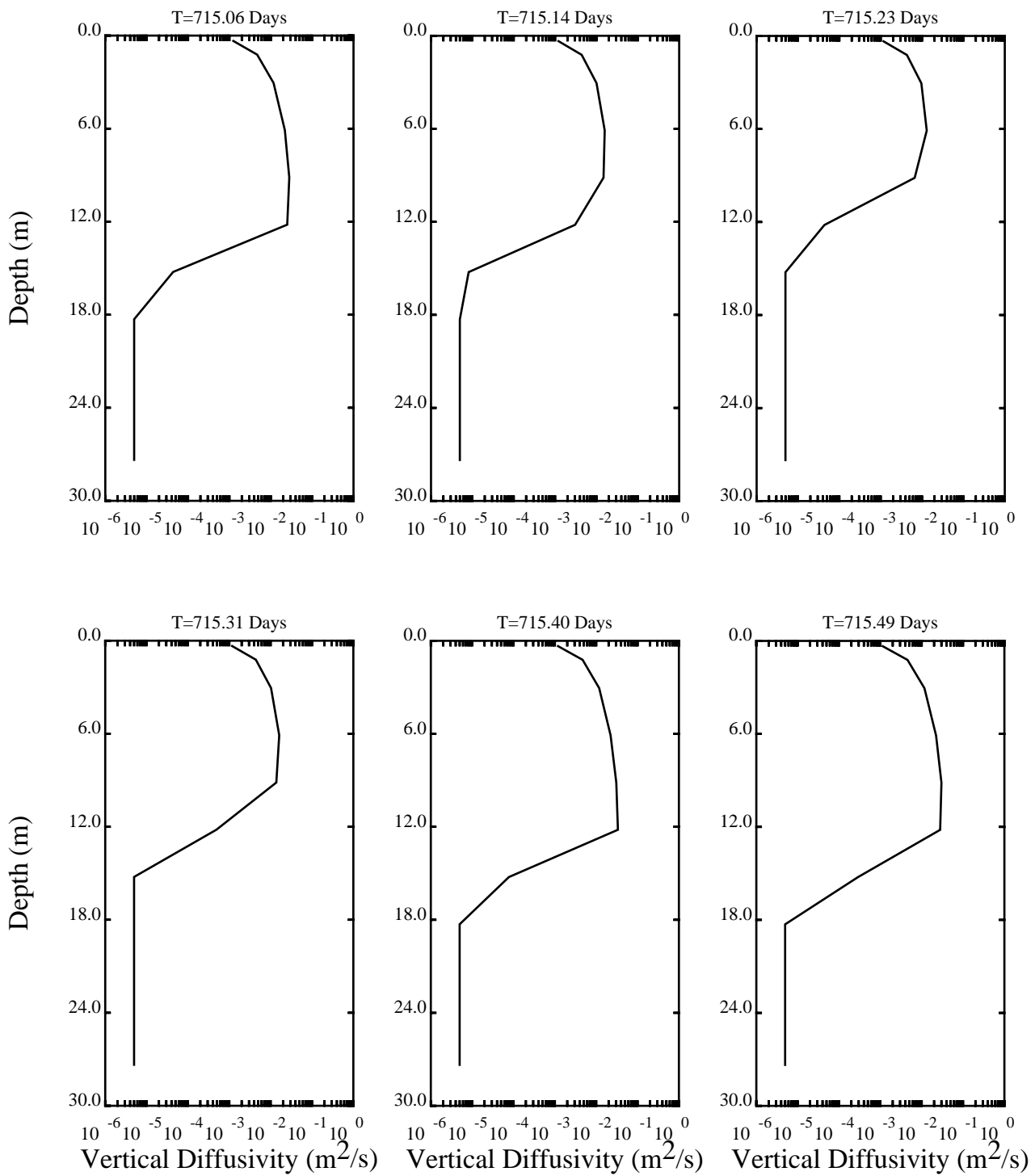
Outfall Site - October 5, 1999

Figure 2-22. Vertical distribution of vertical diffusivity during a tidal cycle on
October 5, 1999 at the outfall site.
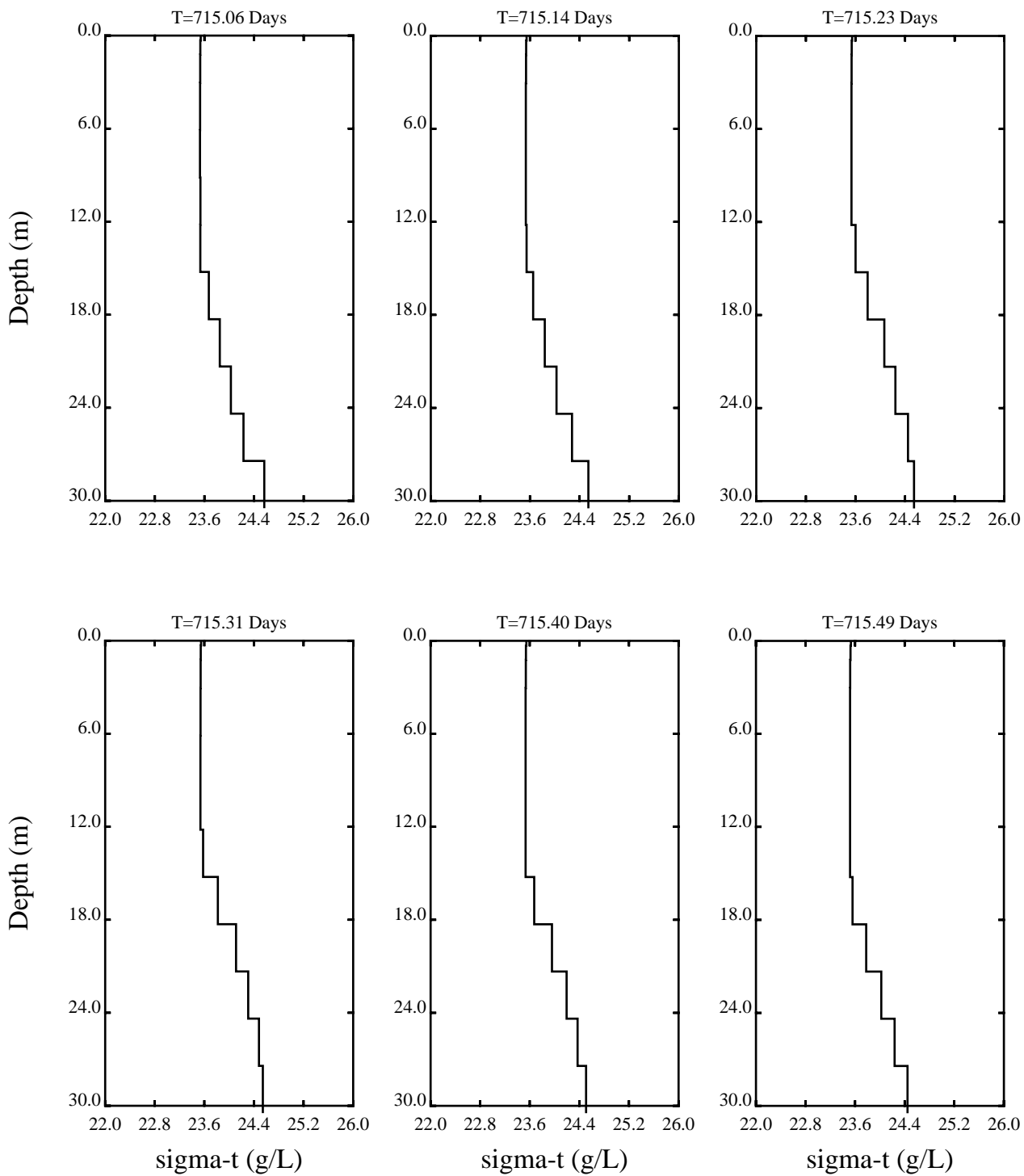
Outfall Site - October 5, 1999

Figure 2-23. Vertical distribution of sigma-t during a tidal cycle on October 5, 1999 at the outfall site.

2.3   STELLWAGEN BASIN

Stellwagen Basin is significantly deeper than the outfall site. Consequently, the surface mixing processes such as wind and cooling do not affect as great a percentage of the water column depth in Stellwagen Basin as compared to the outfall site. Also, the density stratification tends to be greater from surface to bottom in Stellwagen Basin. Figures 2-24 and 2-25 present the vertical diffusivity during the first 20 days of May 1998. The mixing due to wind reaches down to the layer 4-5 interface (18.0 m). This is somewhat shallower than was observed at the outfall site. It is possible that the thickness of the model layers are a partial barrier to the vertical mixing. Below this depth the model computations approach the minimum assigned mixing. Changes in the density during May 10-11 appear to be associated with the wind mixing event (Figures 2-26 and 2-27). However, changes in the density that are computed on May 1-2 and 19-20 must be associated with other phenomenon. The vertical profiles of vertical diffusivity and sigma-t presented in Figures 2-28 and 2-29 also show mixing down to 18 m.

During the more stratified period of June and July 1999, higher vertical diffusivities are confined to the top two layer interfaces as shown in Figures 2-30 and 2-31. In Figures 2-32 and 2-33, there are only small temporal changes in sigma-t observed in the surface layers. The decline in sigma-t followed by an increase is of smaller magnitude than was observed at the outfall site and somewhat lagged in time. Middle layer sigma-t varies with tidal fluctuation. The vertical profiles of vertical diffusivity and sigma-t, Figures 2-34 and 2-35 respectively, show higher mixing occurring in only the top several meters of the water column.

Finally, in October 1999, higher vertical diffusivities are computed to a depth of approximately 18 meters, as shown in Figures 2-36 and 2-37. The fall turnover occurs somewhat later in Stellwagen Basin than at the outfall site. During this period, there is a gradual increase in sigma-t in the top four layers (Figures 2-38 and 2-39). In the remaining layers, the model computes relatively constant sigma-t values. Figures 2-40 and 2-41 present the vertical profiles of vertical diffusivity and sigma-t, respectively, for October 5, 1999. Both figures show mixing down to 18 meters with small variations during the tidal cycle.

2.4   VERTICAL MIXING CONCLUSIONS

The model seems to respond in a reasonable manner to the physical forcings to which it is exposed, although the response varies over the model domain. That is, the model computes more vertical mixing with greater physical forcings. Aside from the model's reproduction of the temperature and salinity data and the Scituate Buoy and Boston Buoy current meter data, to which the model compares favorably, there are no data available that can be used to determine how well the model computes vertical diffusivity. The model computes vertical diffusivity values that are well within generally accepted ranges.
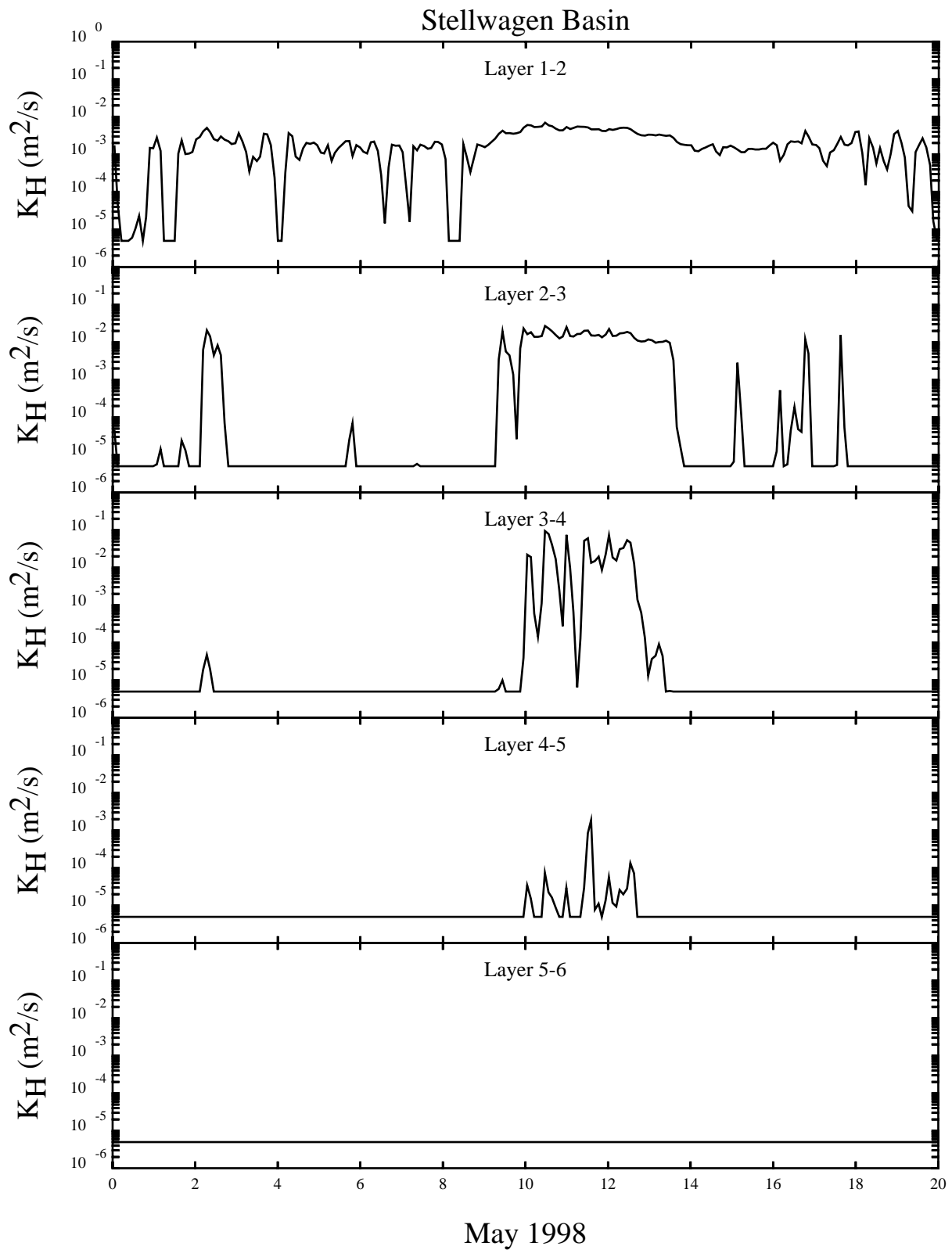
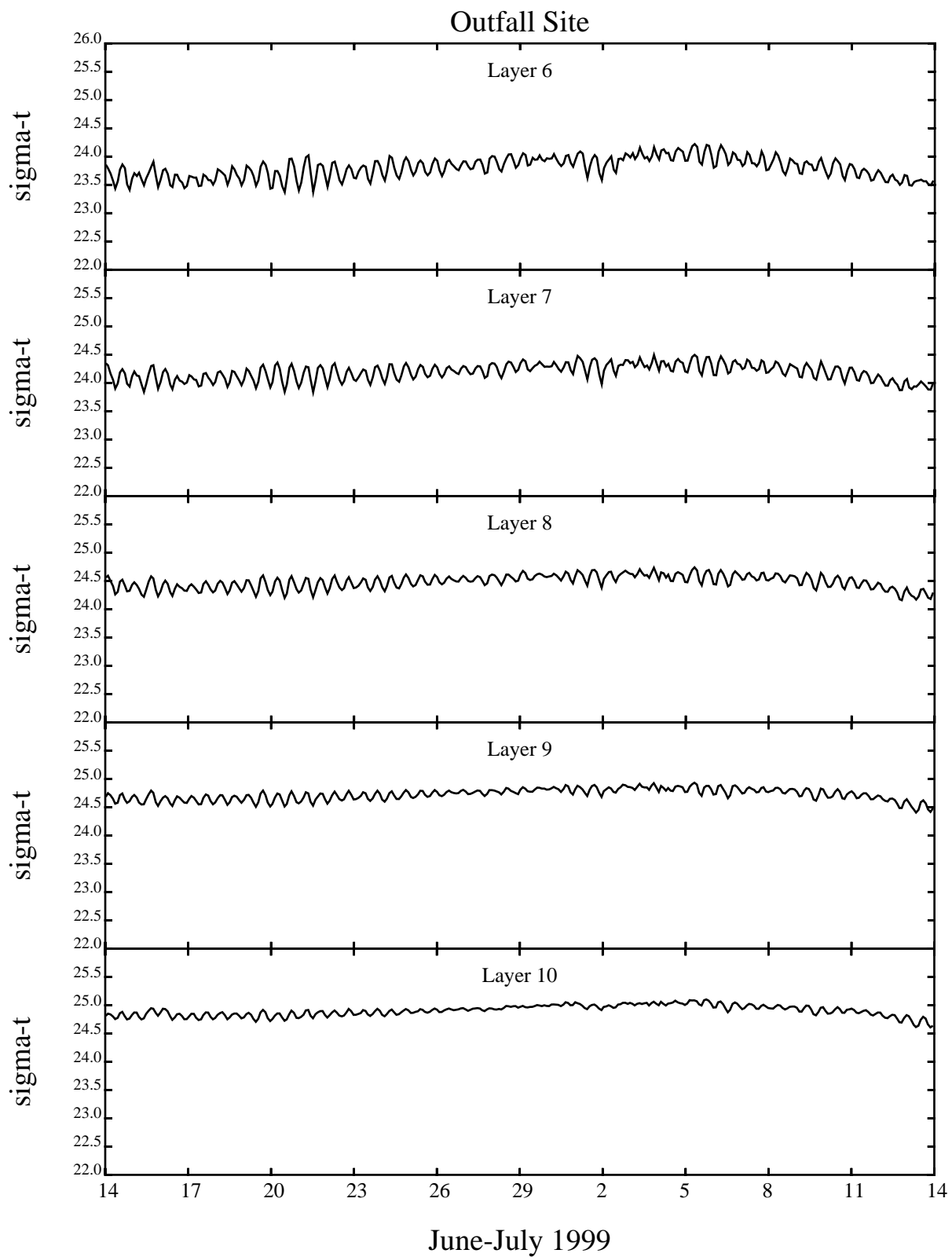Figure 2-24. Model computed vertical diffusivity at the top five model layer interfaces during May 1998 at Stellwagen Basin.

Stellwagen Basin

Layer 6-7

Layer 7-8

Layer 8-9

Layer 9-10

Layer 10-11

K_H (m^2/s)
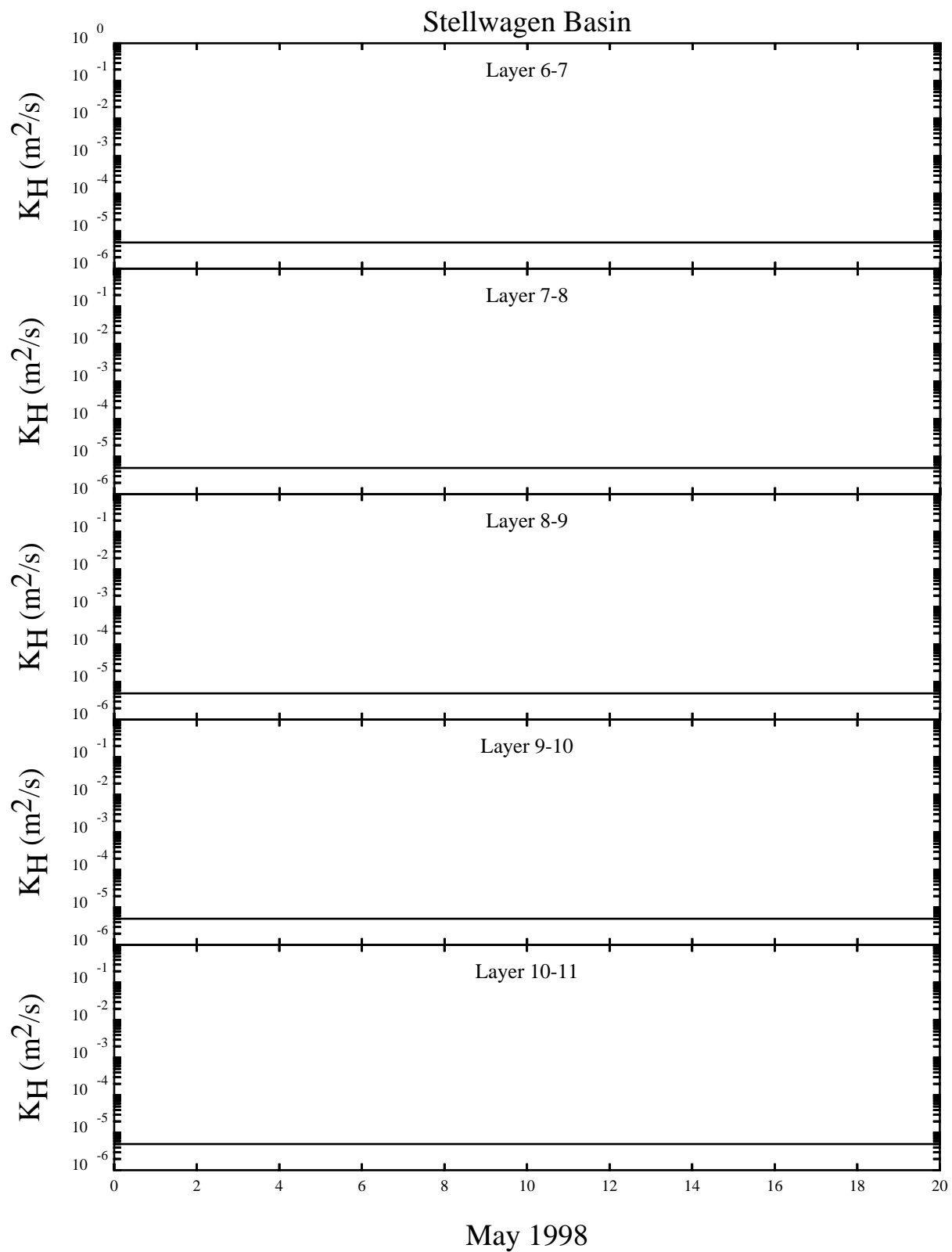
May 1998

Figure 2-25. Model computed vertical diffusivity at the interfaces of model layers 6-11 during May 1998 at Stellwagen Basin.
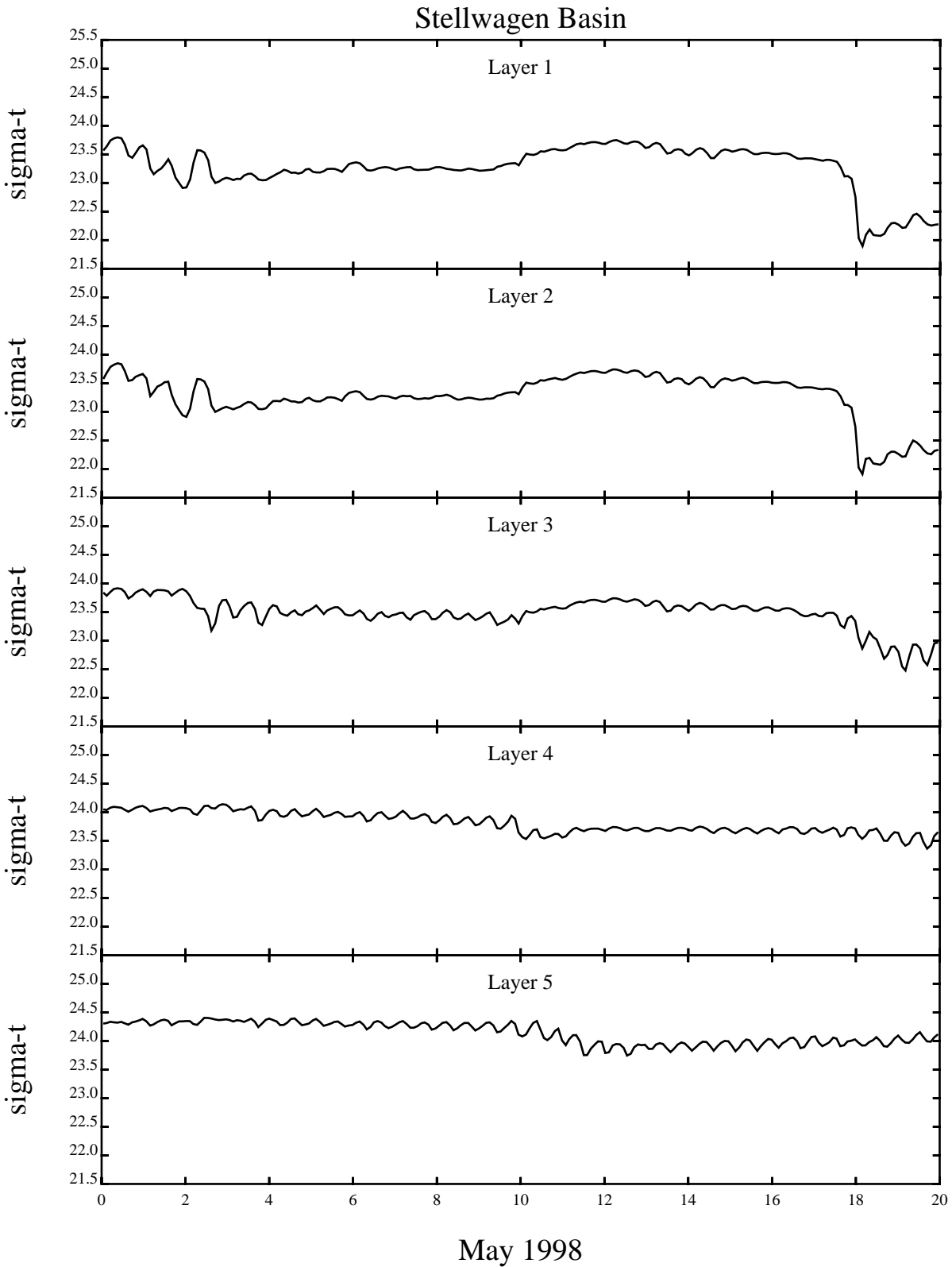
Stellwagen Basin

Figure 2-26. Model computed sigma-t in the top five model layers at Stellwagen Basin during May 1998.
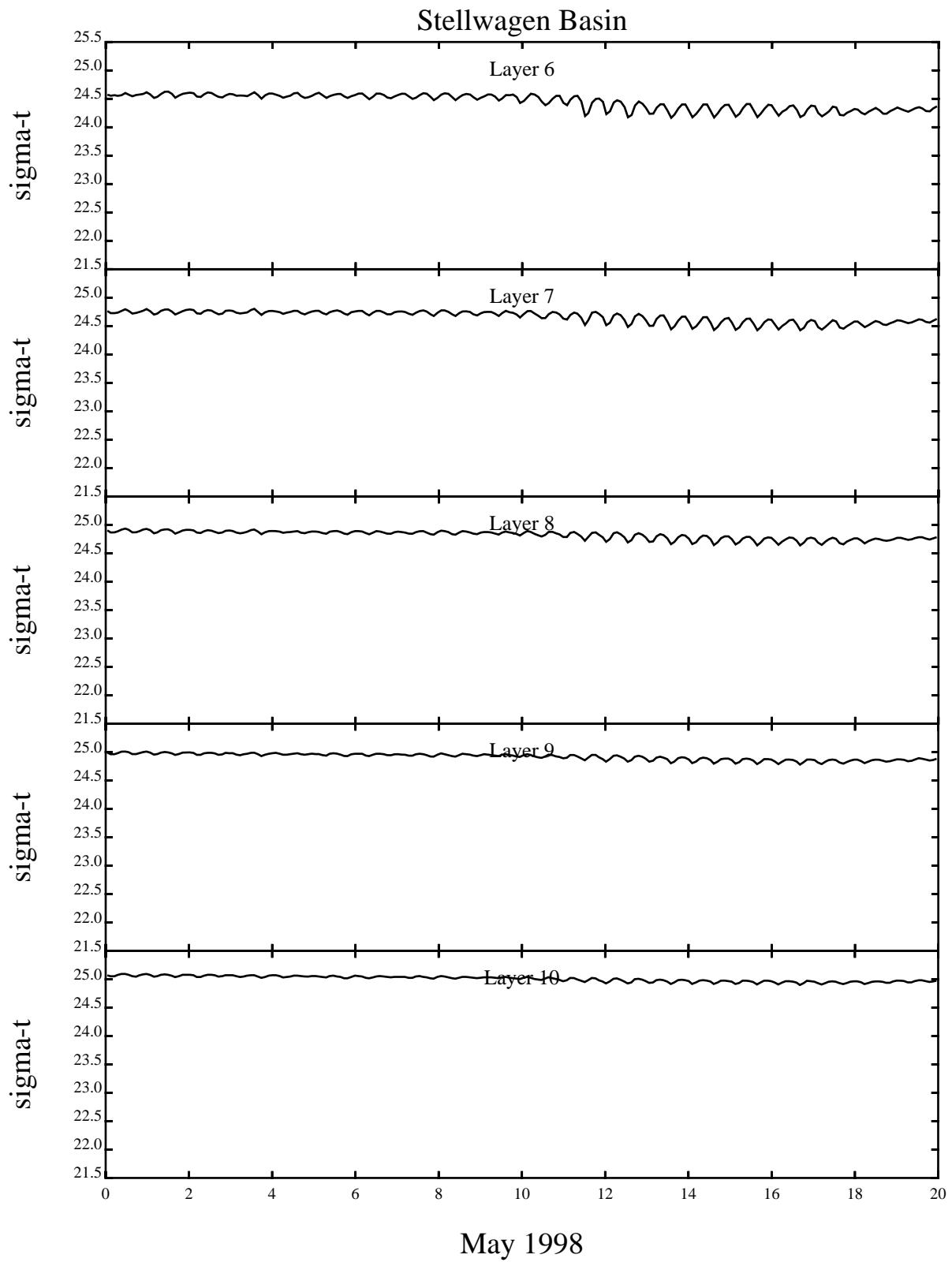
Figure 2-27. Model computed sigma-t model layers 6-10 at Stellwagen Basin during May 1998.

Figure 2-28. Vertical distribution of vertical diffusivity during a tidal cyle on
May 10, 1998 at Stellwagen Basin.
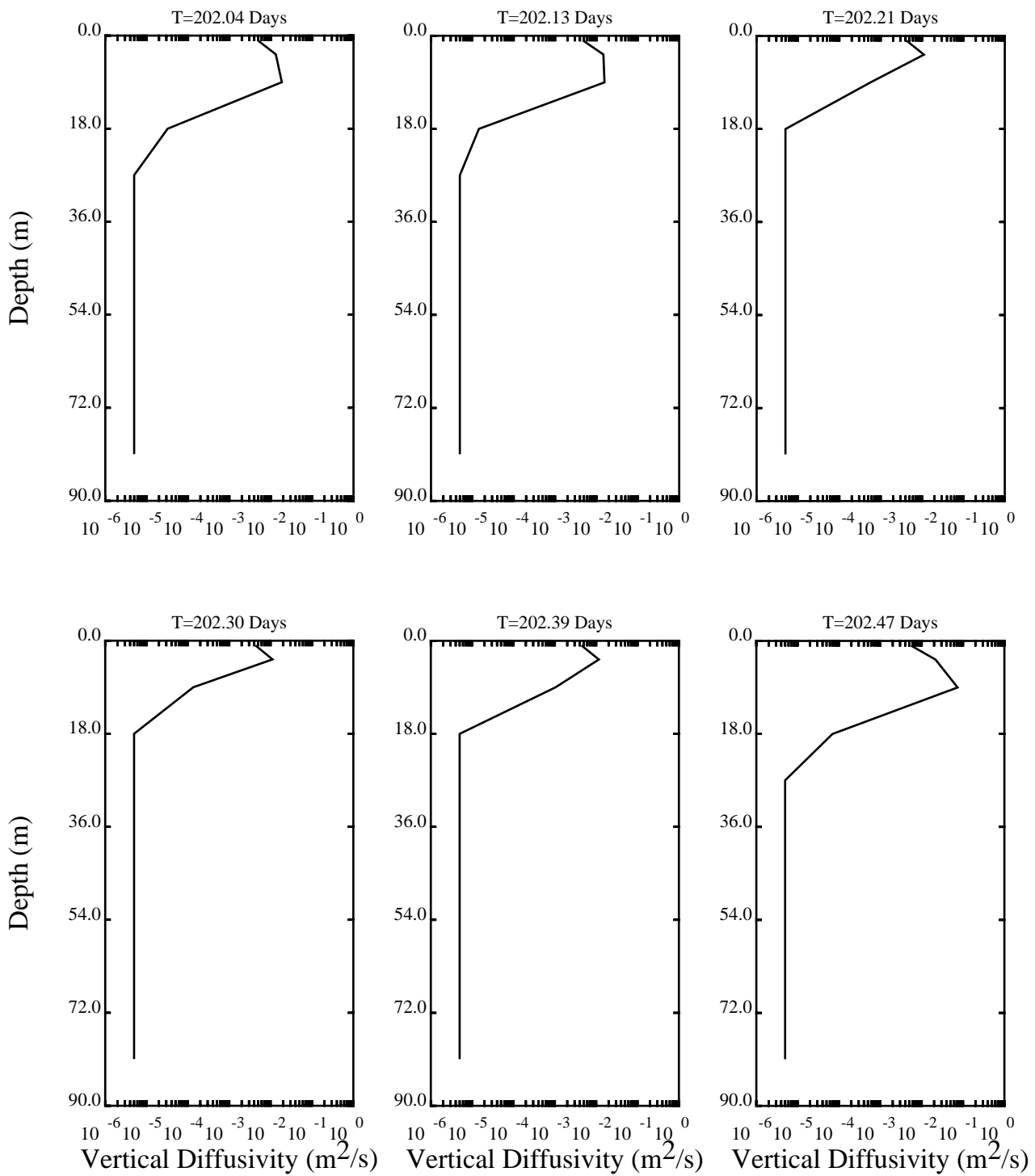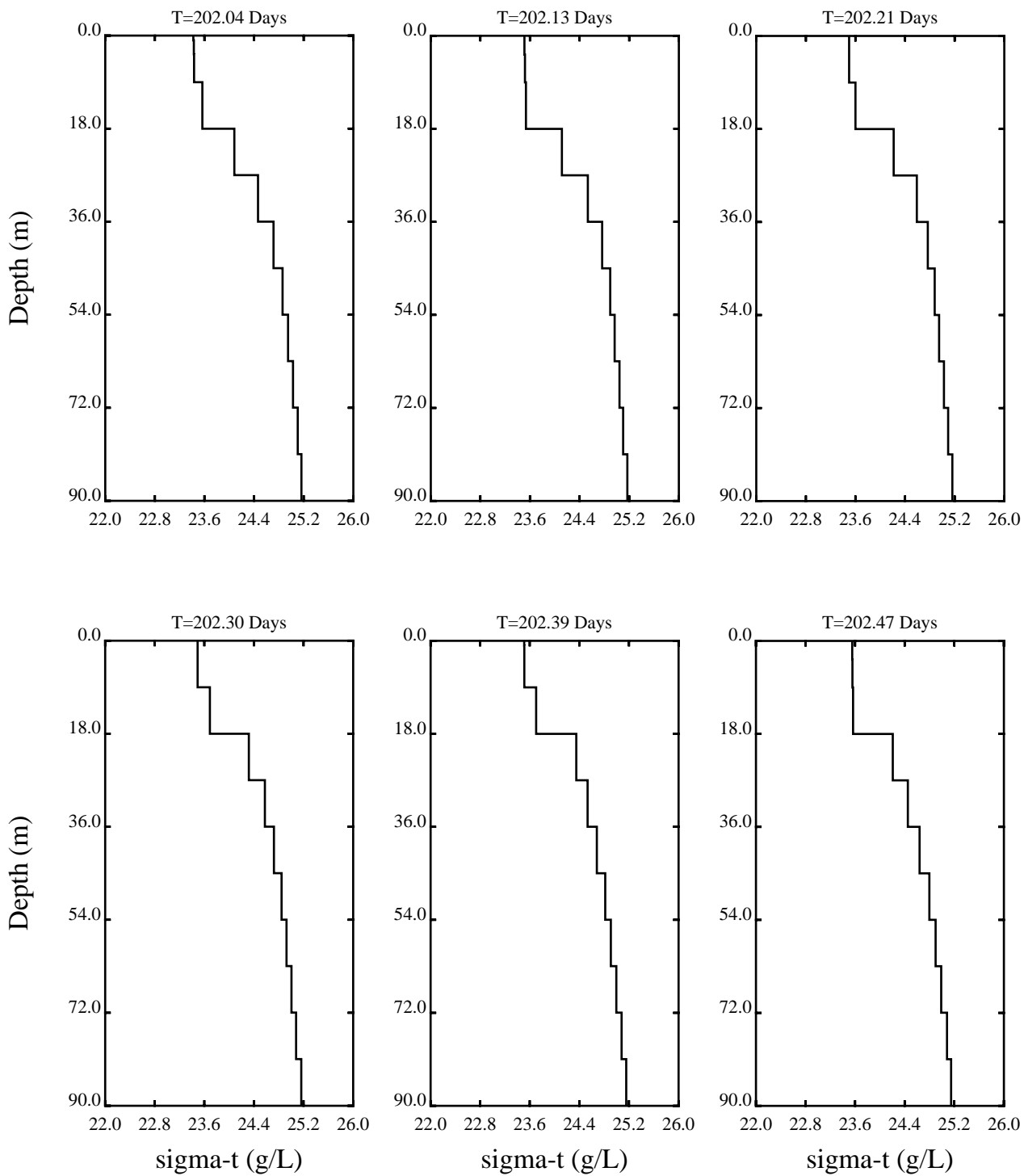
Stellwagen Basin - May 10, 1998

Figure 2-29. Vertical distribution of sigma-t during a tidal cycle on May 10, 1998
at Stellwagen Basin
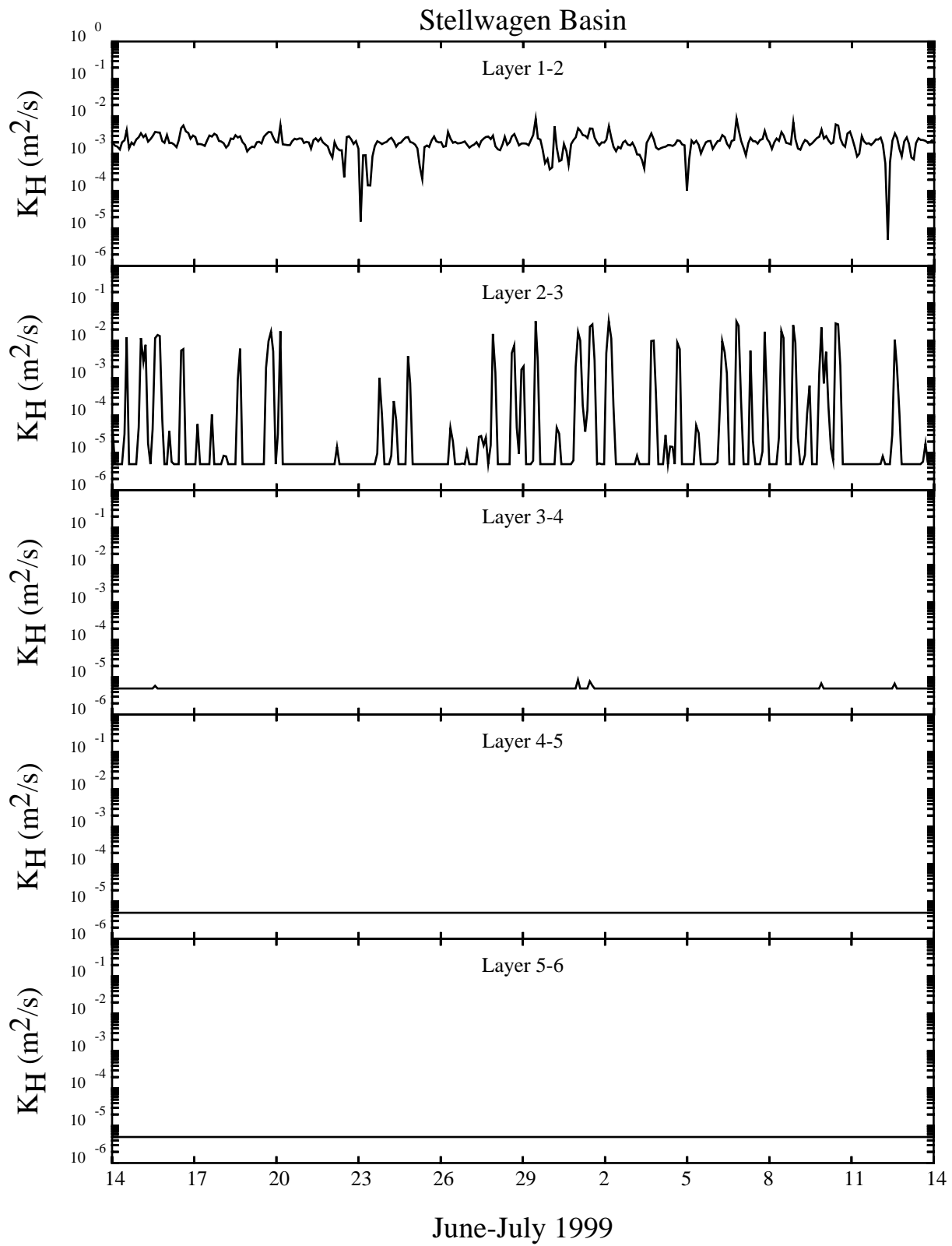
Figure 2-30. Model computed vertical diffusivity at the top five model layer interfaces during June-July 1999 at the Stellwagen Basin.
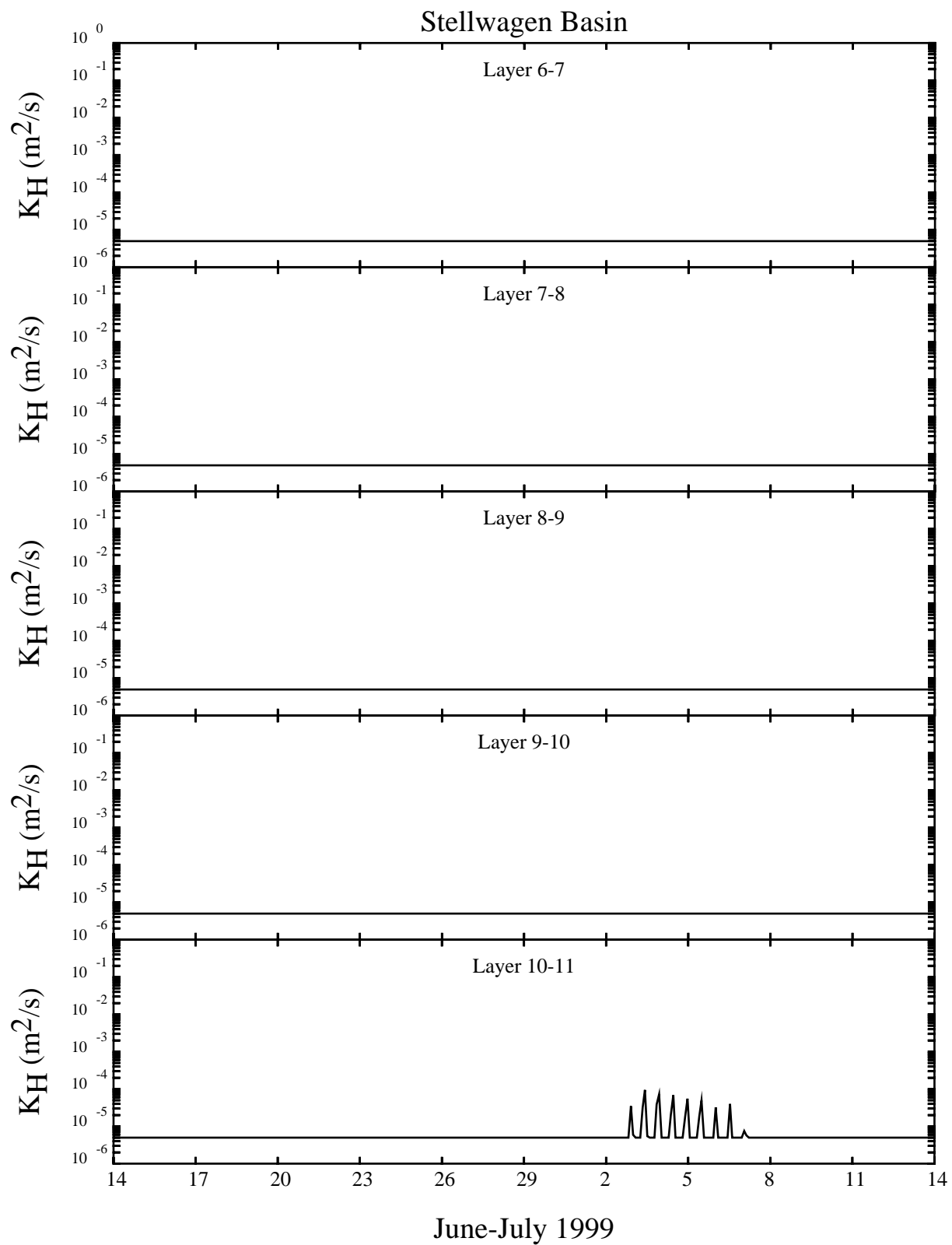
Figure 2-31. Model computed vertical diffusivity at the interfaces of model
layers 6-11 during June-July 1999 at Stellwagen Basin.
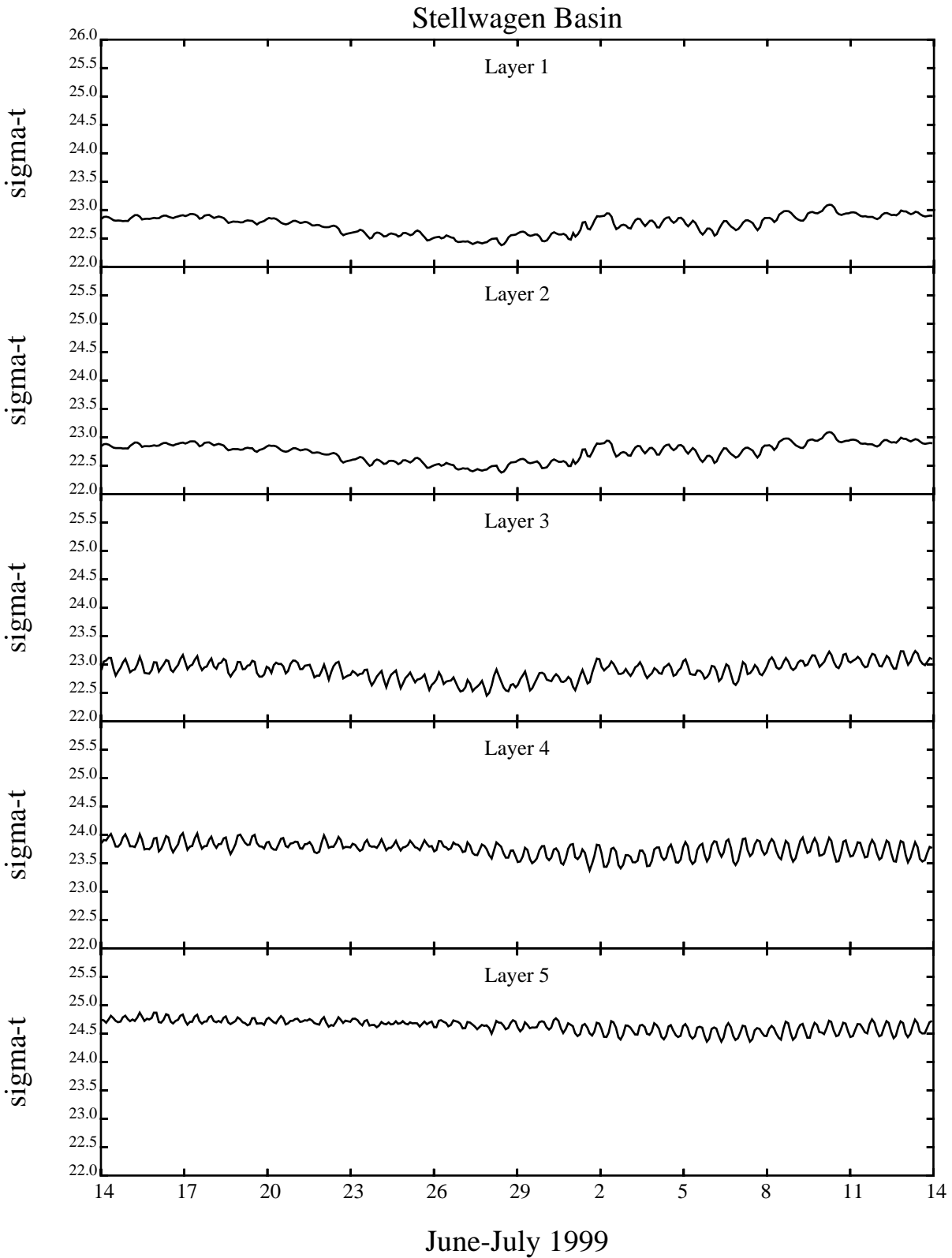
Stellwagen Basin

Figure 2-32. Model computed sigma-t in the top five layers at Stellwagen Basin during June-July 1999.
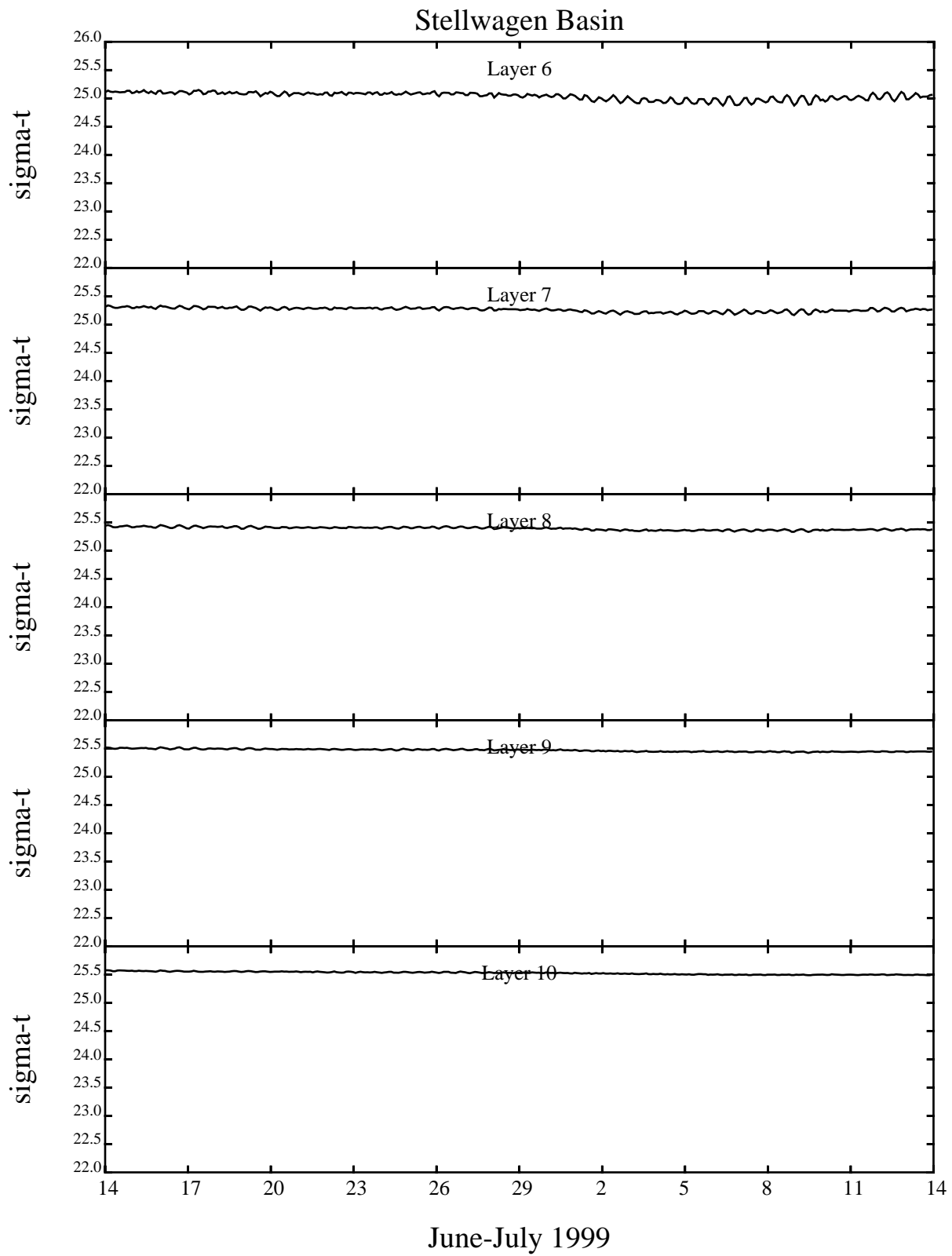
Figure 2-33. Model computed sigma-t in model layers 6-10 at Stellwagen
Basin during June-July 1999.
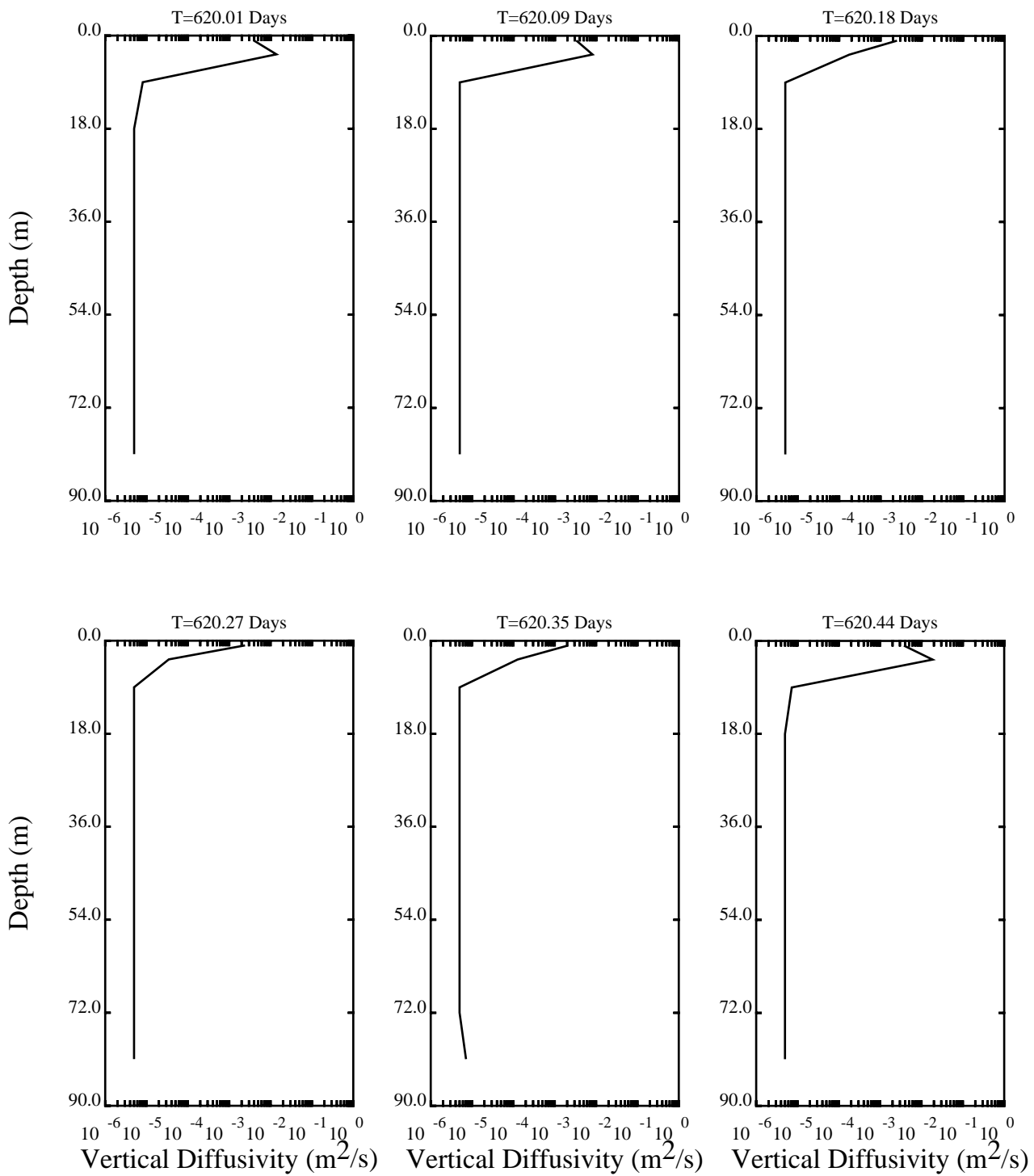
Stellwagen Basin - July 2, 1999

Figure 2-34. Vertical distribution of vertical diffusivity during a tidal cycle on
July 2, 1999 at Stellwagen Basin.

T=620.01 Days

T=620.09 Days

T=620.18 Days

T=620.27 Days

T=620.35 Days

T=620.44 Days

Depth (m)
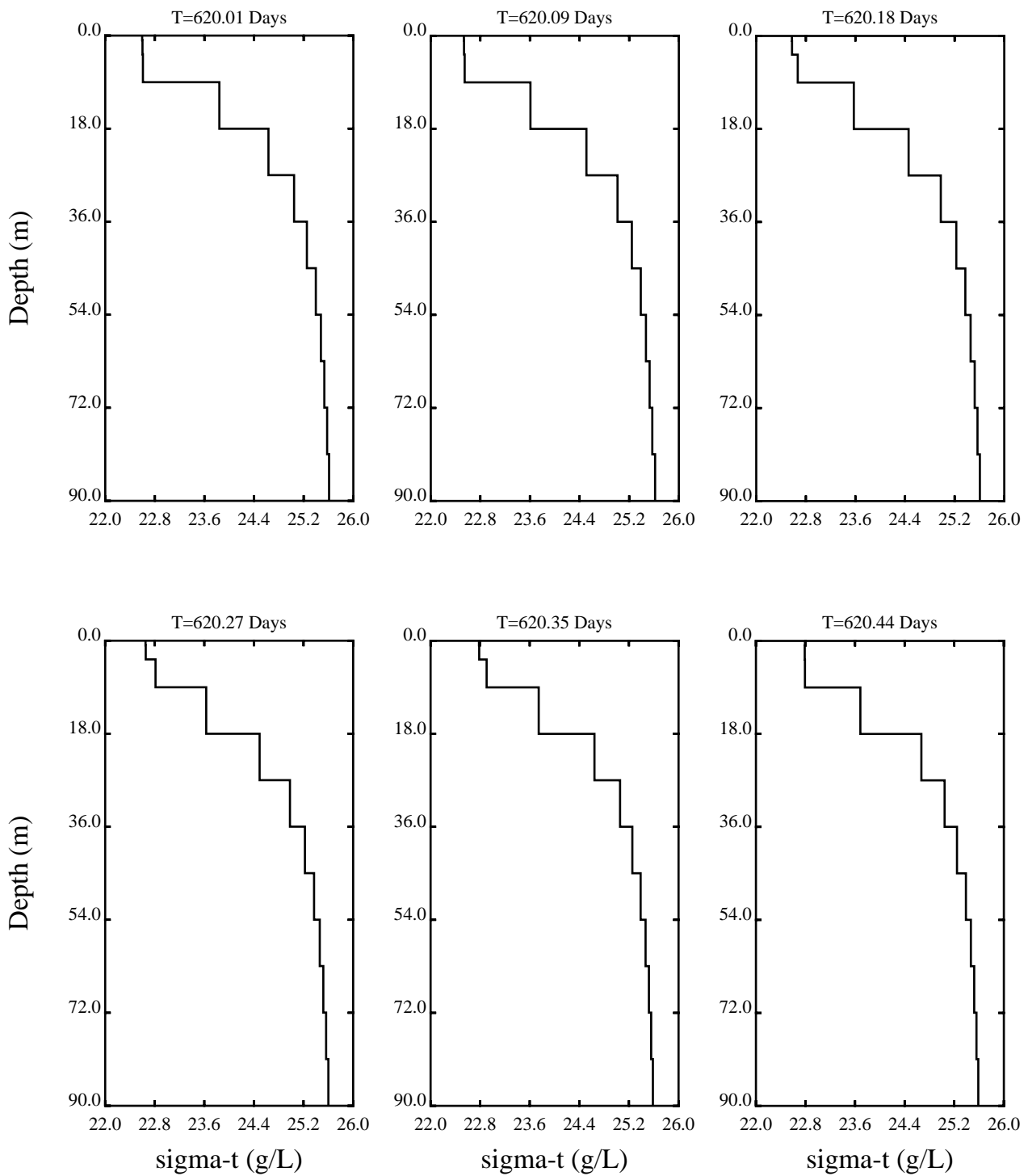
sigma-t (g/L)

Stellwagen Basin - July 2, 1999

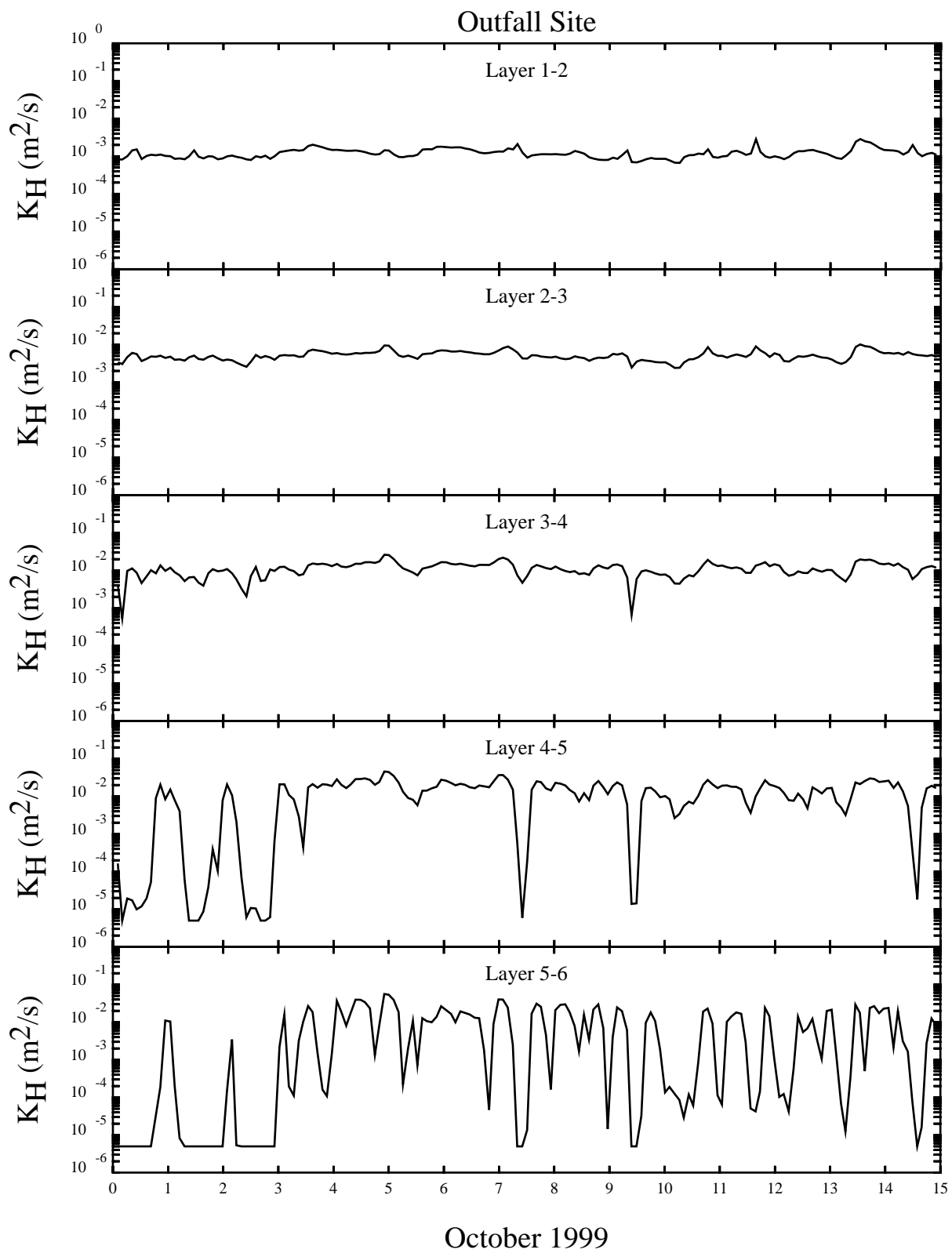Figure 2-35. Vertical distribution of sigma-t during a tidal cycle on July 2, 1999 at Stellwagen Basin.
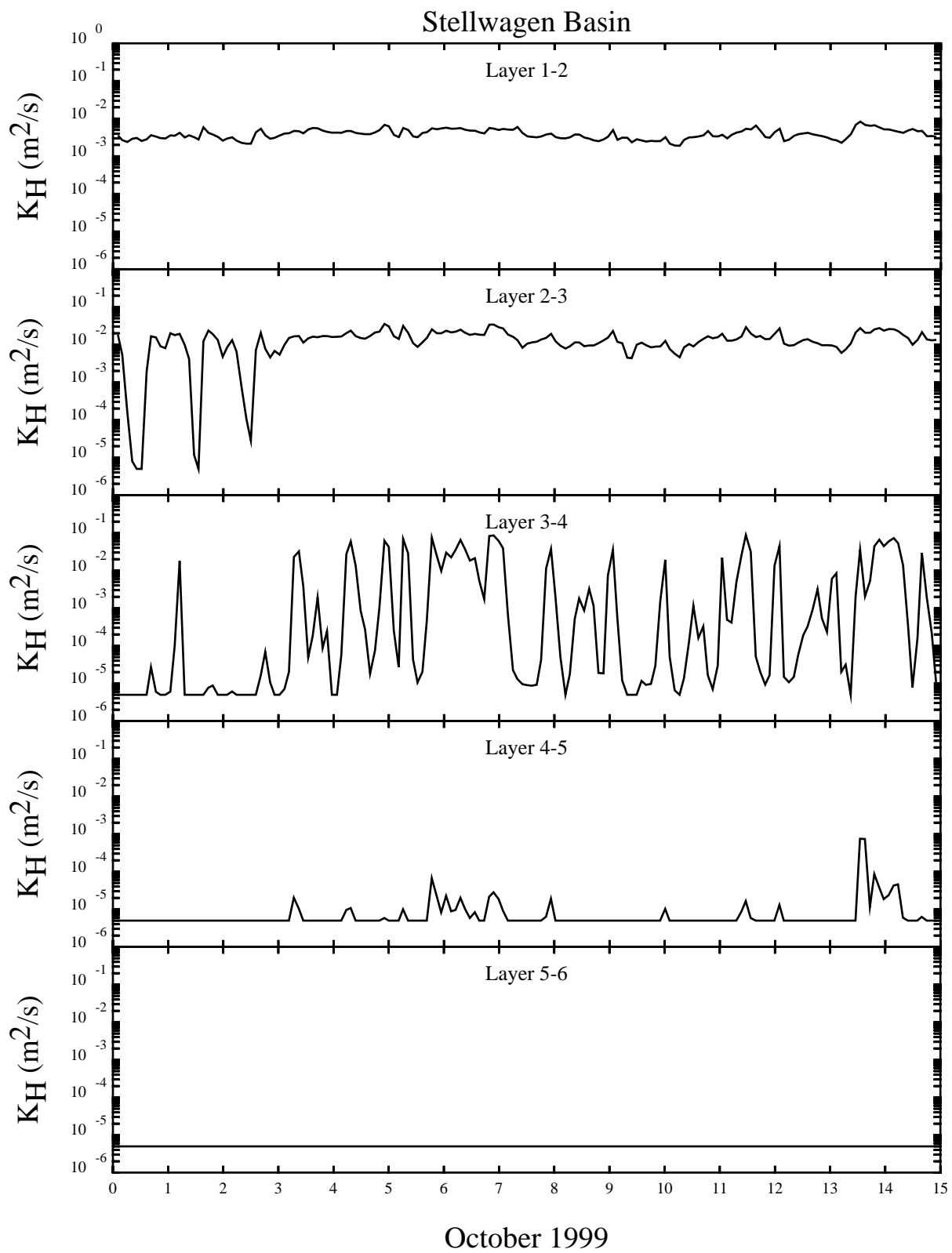
Figure 2-36. Model computed vertical diffusivity at the top five model
layer interfaces during October 1999 at Stellwagen Basin.

Stellwagen Basin

Layer 6-7

Layer 7-8

Layer 8-9

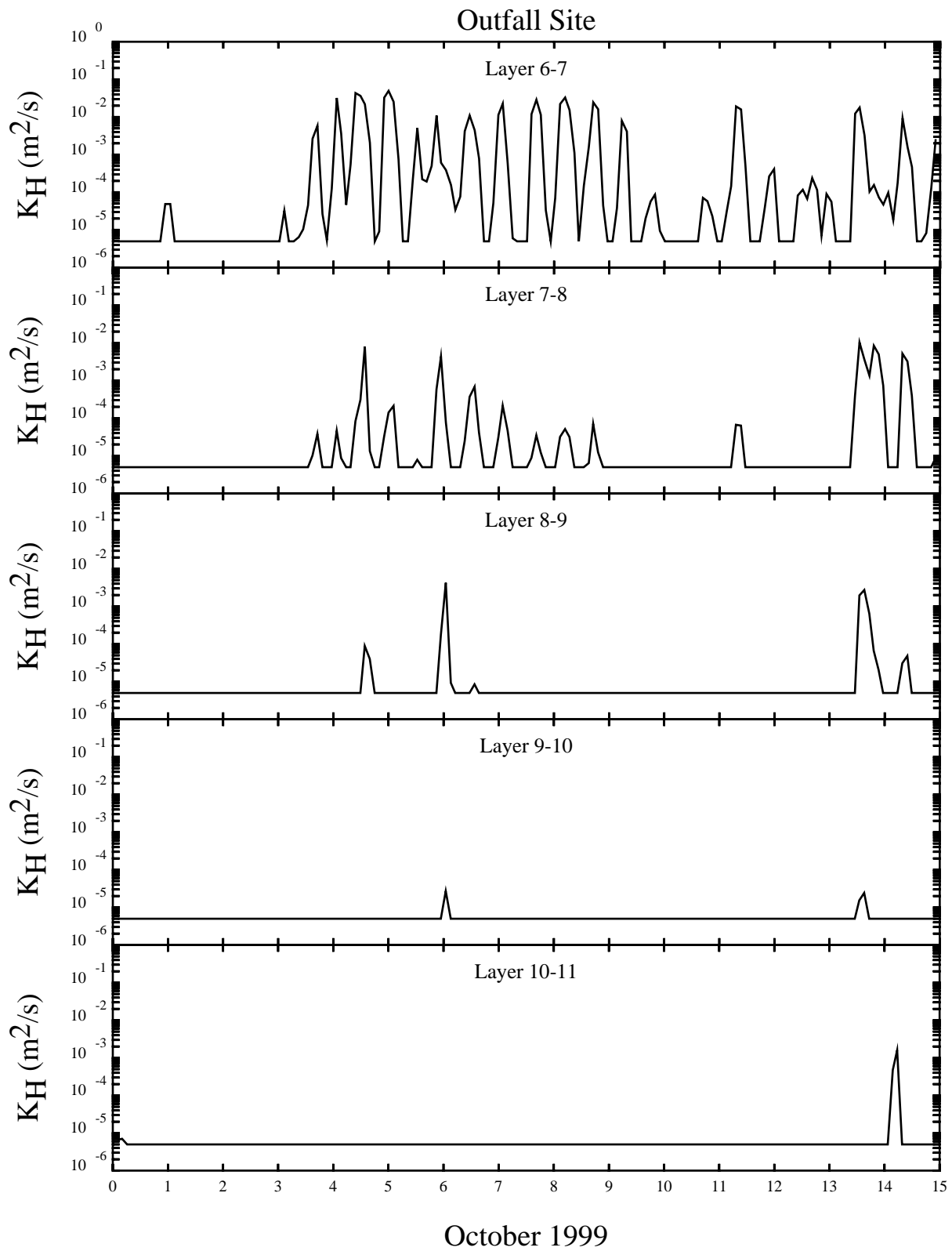Layer 9-10

Layer 10-11
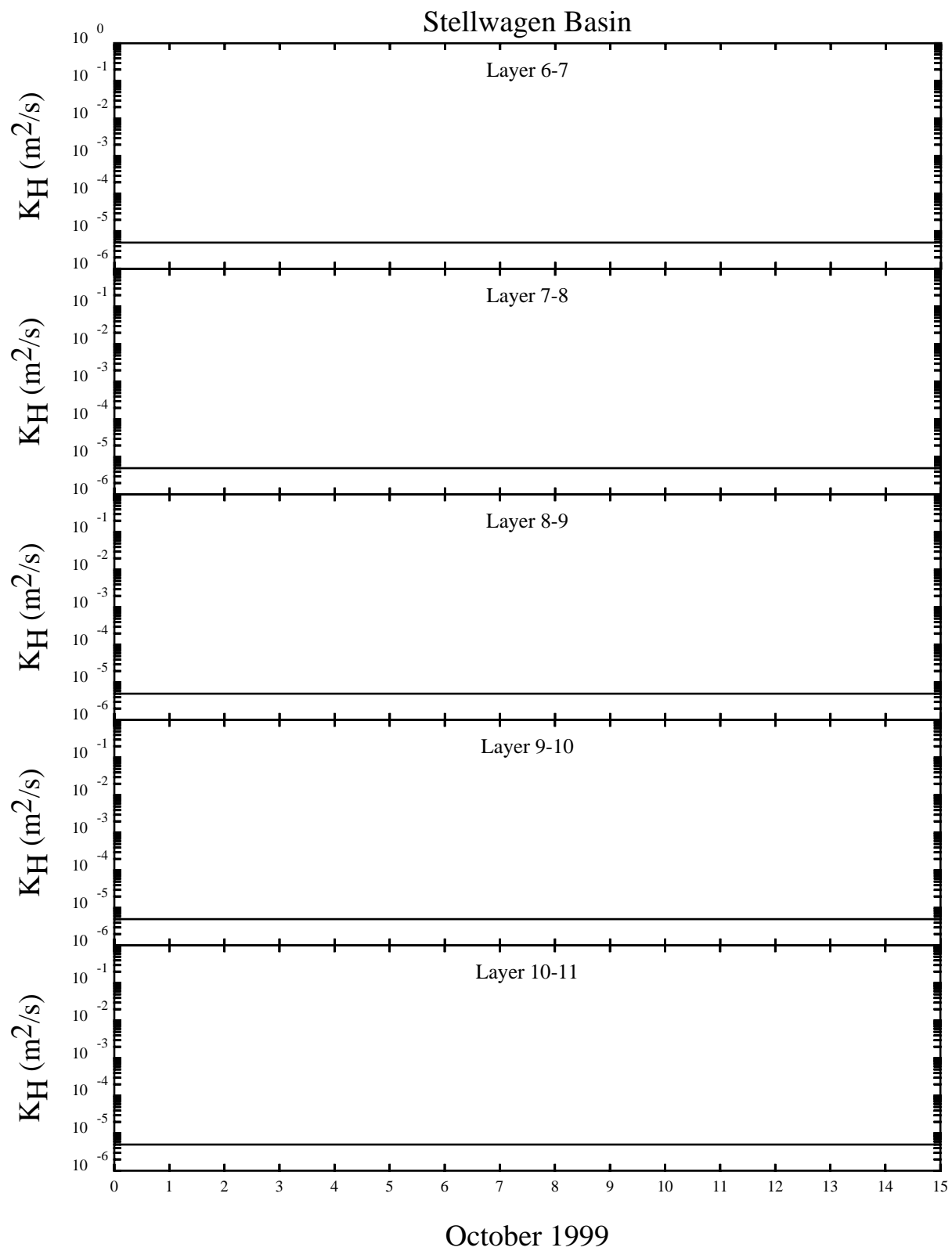
October 1999

Figure 2-37. Model computed vertical diffusivity at the interfaces of model
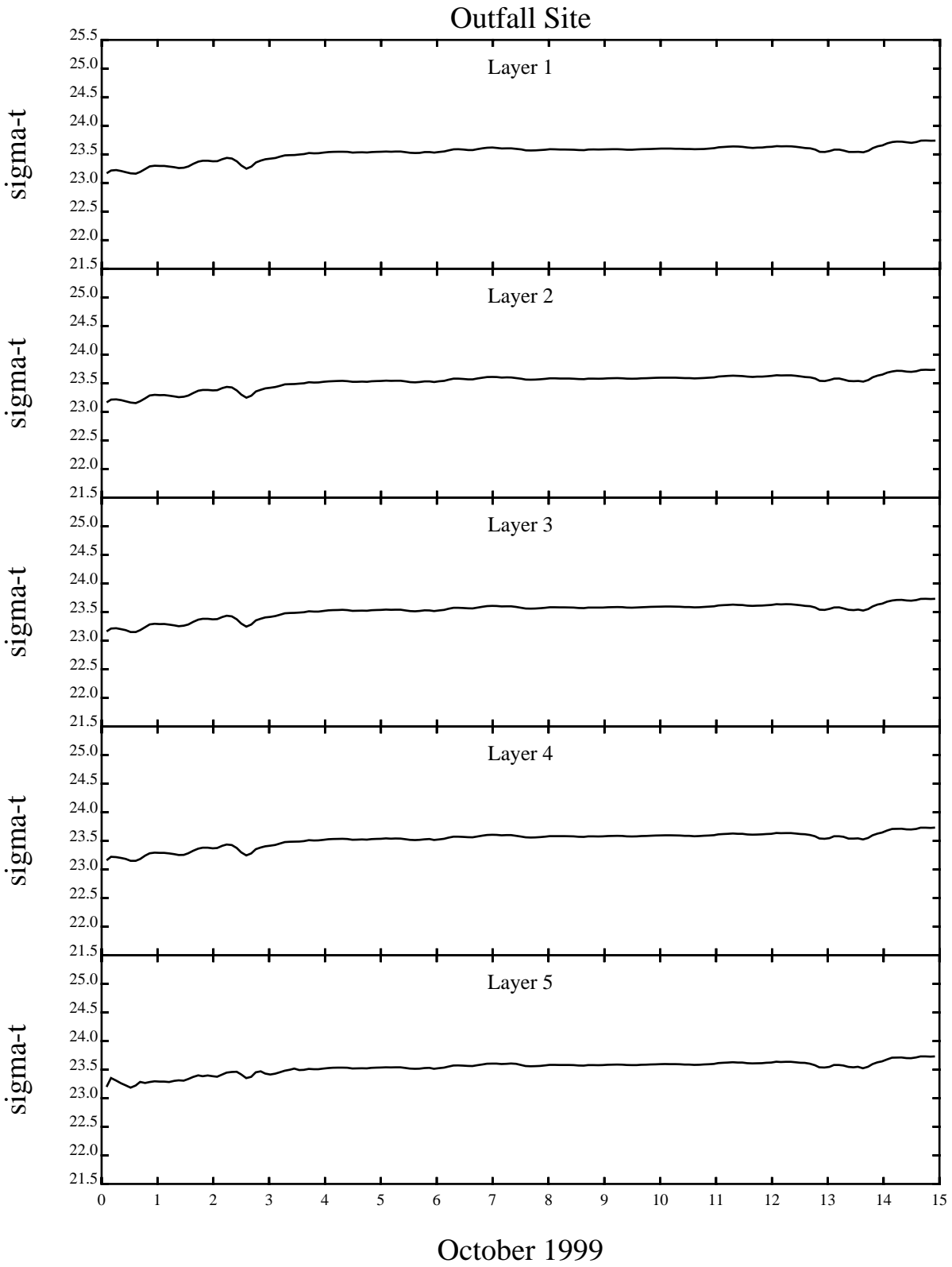layers 6-11 during October 1999 at Stellwagen Basin.
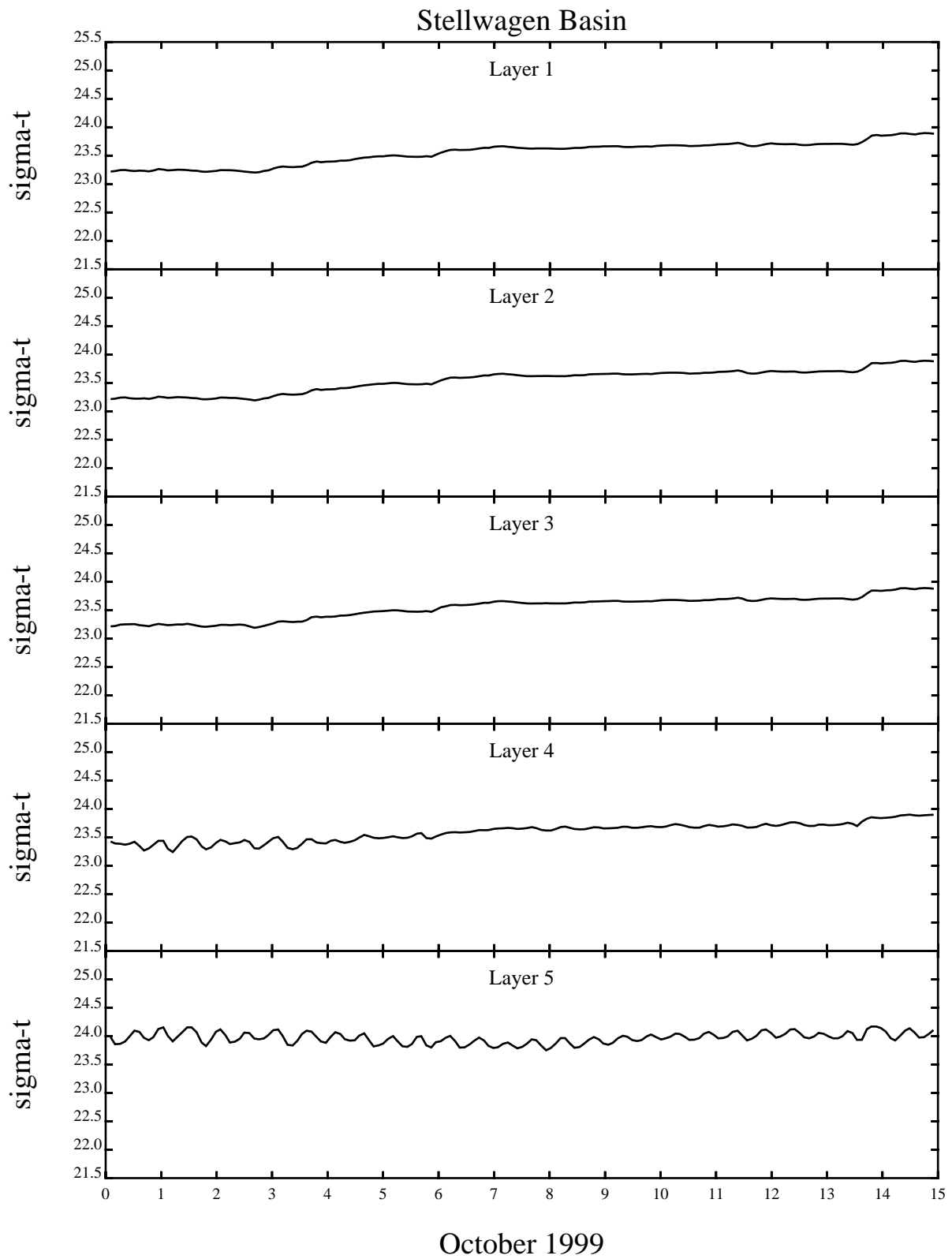
Figure 2-38. Model computed sigma-t in the top five model layers at Stellwagen Basin during October 1999.
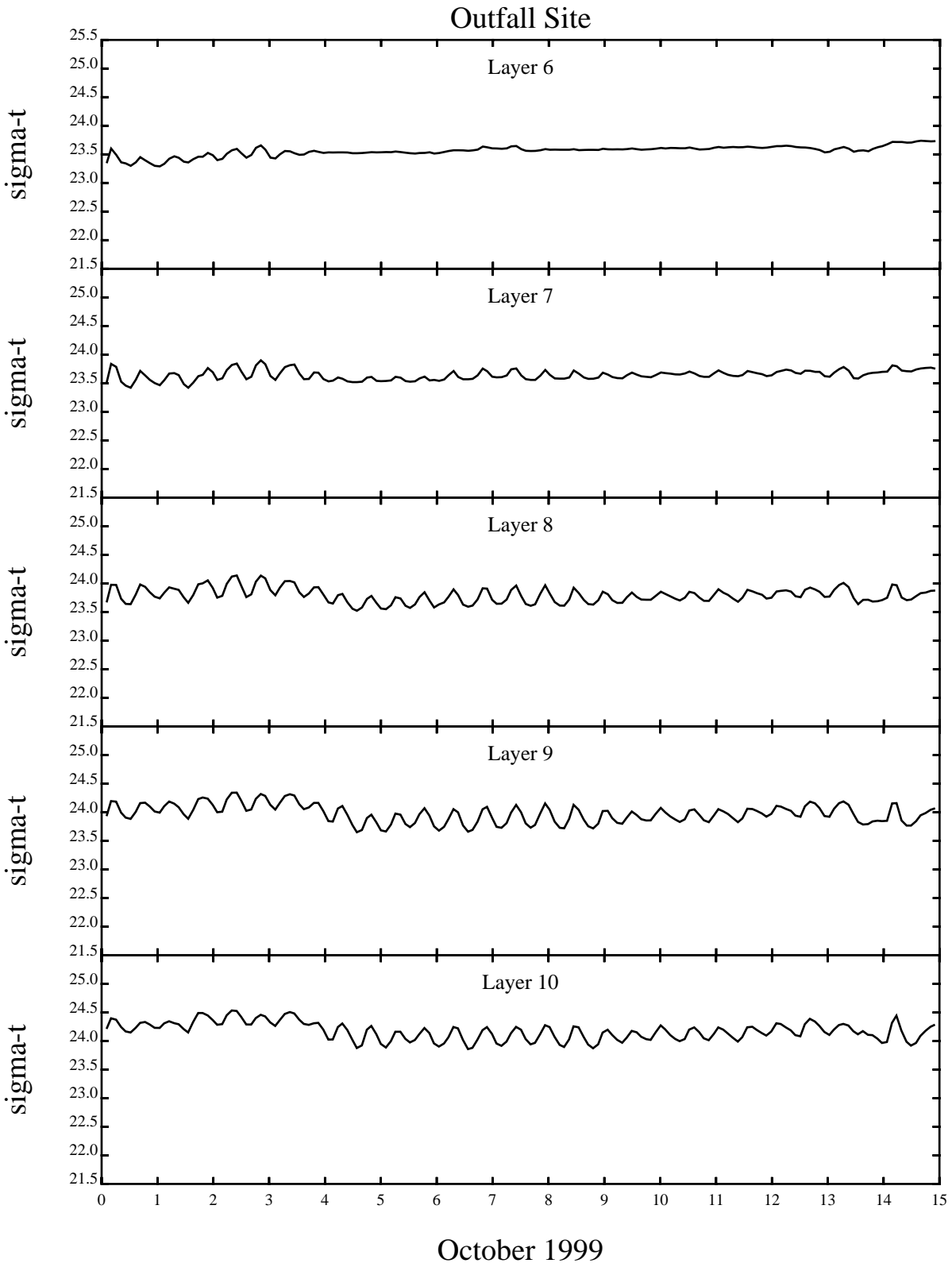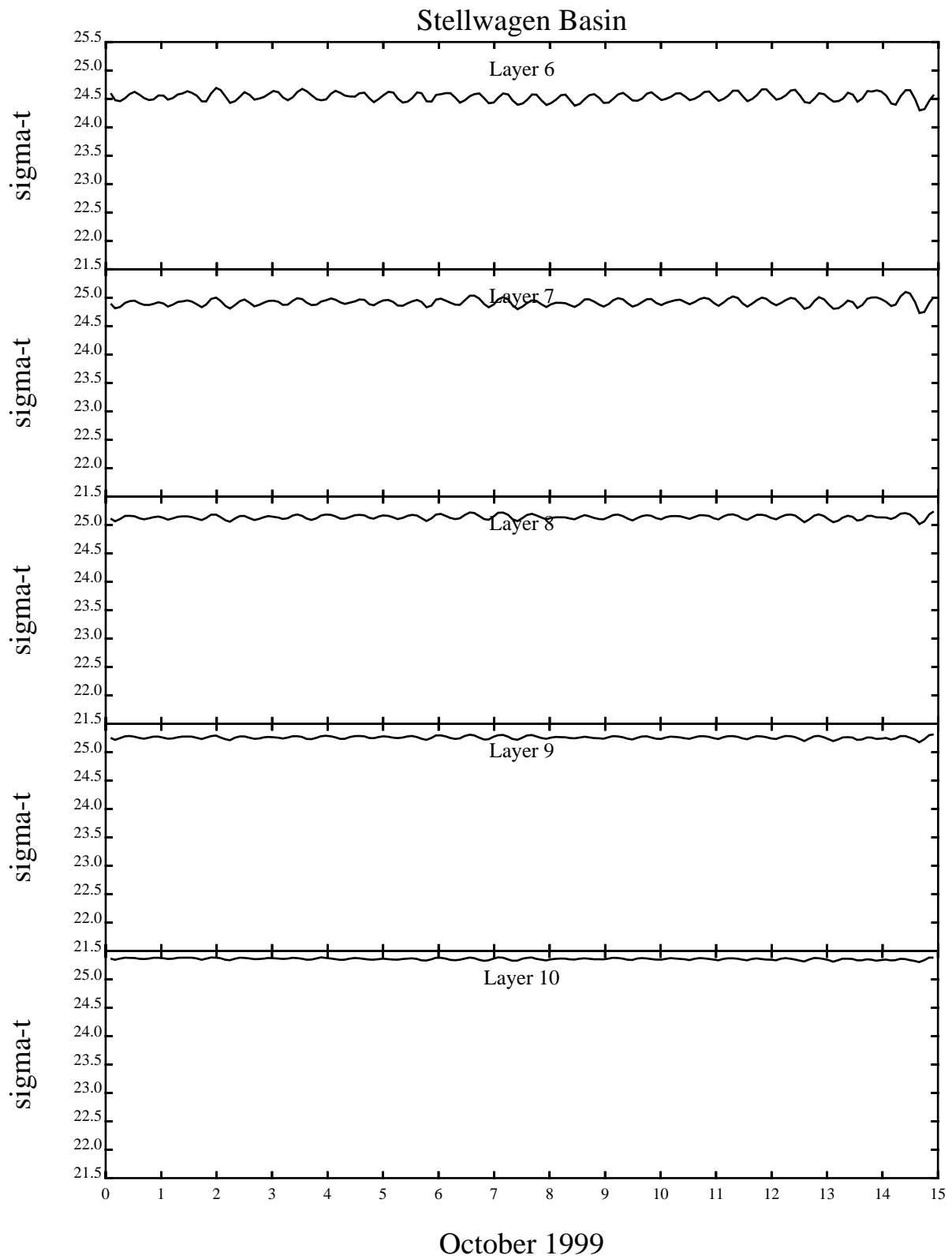
Figure 2-39. Model computed sigma-t in model layers 6-10 at Stellwagen Basin during October 1999.
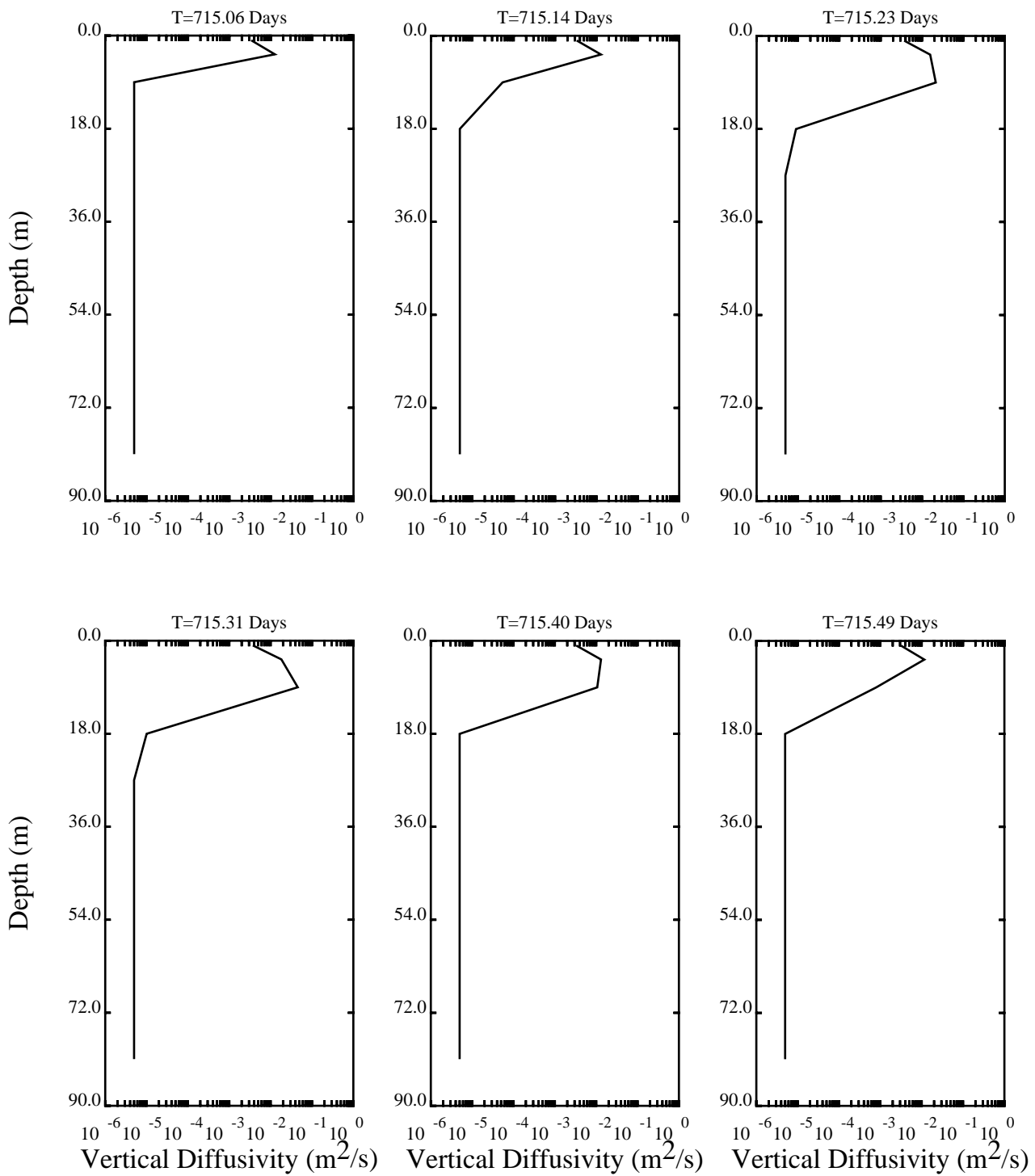
Stellwagen Basin - October 5, 1999

Figure 2-40. Vertical distribution of vertical diffusivity during a tidal cycle on October 5, 1999 at Stellwagen Basin.
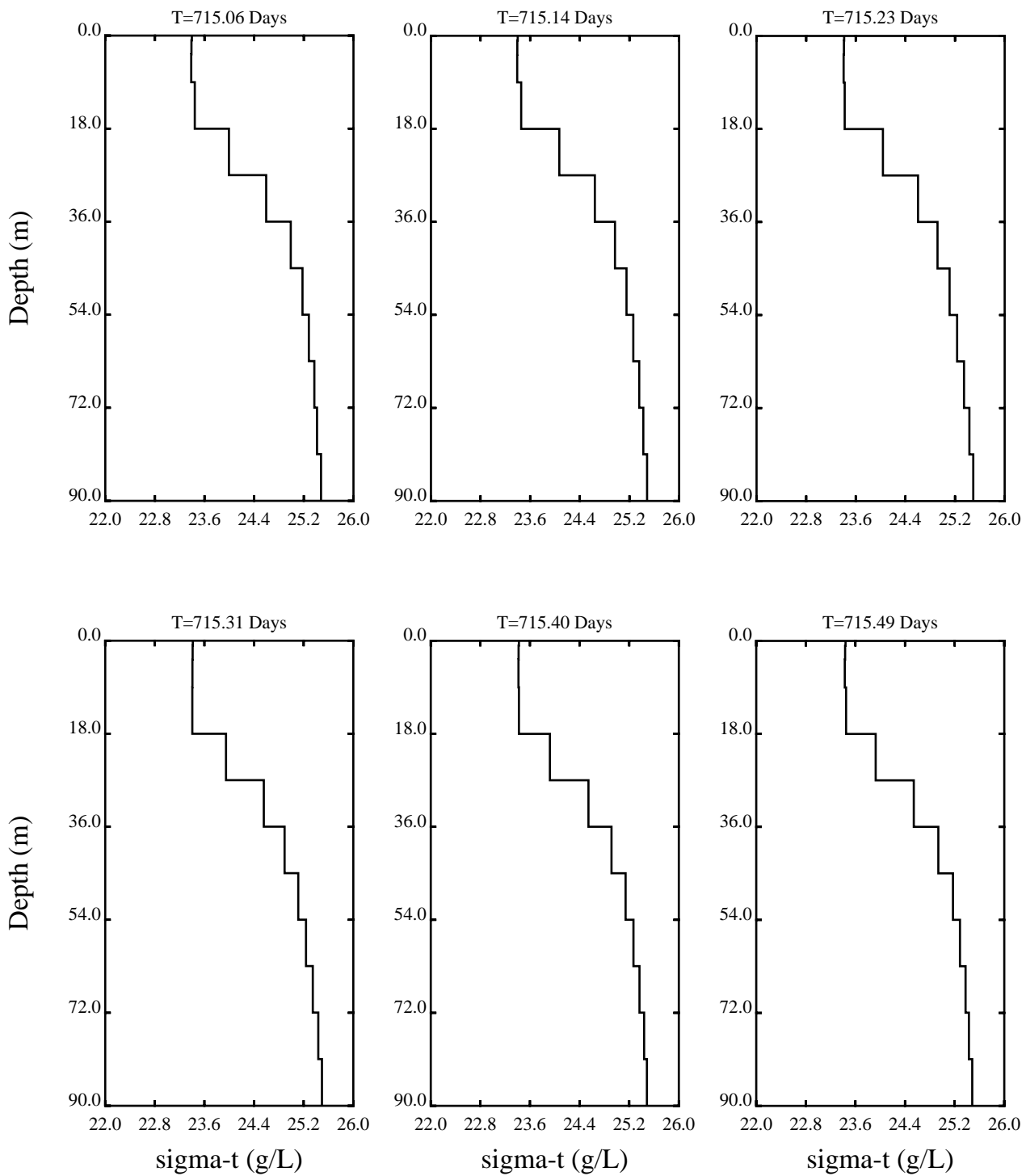
Stellwagen Basin - October 5, 1999

Figure 2-41. Vertical distribution of sigma-t during a tidal cycle on October 5, 1999 at Stellwagen Basin.

SECTION 3

HEAT FLUX MODEL

3.1   INTRODUCTION

The energy content in a surface water body is primarily governed by the surface heat energy exchanges. However, for shallow and transparent water bodies the heat exchanges through the water-sediment interface may also play an important role in the heat budget (Tsay et al., 1992). Measurements of heat fluxes such as atmospheric radiation, sensible heat and latent heat fluxes and solar radiation are very difficult and costly to make and are often parameterized to obtain the fluxes, using the most commonly available meteorological and atmospheric data. The processes that control the heat exchange between the water and atmosphere are well documented (Ahsan and Blumberg 1999; Cole and Buchak, 1995; Hondzo and Stefan, 1993; Rosati and Miyakoda, 1988; Schertzer, 1987; Fung et al., 1984; Large and Pond, 1982; Clark et al., 1974; Edinger et al., 1974). All of these works relied mostly on the bulk formulae to evaluate the components of the heat budget. It is important to note here that most of the bulk formulae, available in literature, for calculations of radiative fluxes are based on basically the same principles and generally agree with one another in general patterns of temporal and spatial variations of fluxes. However, significant differences in their magnitudes exist depending on the time period of the year and latitudinal position of the study area.

Estimation of net heat fluxes requires a great deal of judgement in choosing the bulk formulae which are dependent on many uncertain atmospheric parameters like cloud cover, humidity and temperature. Four major heat flux components including longwave atmospheric radiation, sensible heat and latent heat fluxes, and short wave solar radiation, have been used in the present study, largely based on the formulae reported in (Ahsan and Blumberg, 1999). Figure 3-1 shows the schematic diagram of these processes. Details of the formulation of all these pieces of heat fluxes are described below.

3.2   ATMOSPHERIC RADIATION

The net atmospheric radiation at the surface is the result of two processes, the downward radiation from the atmosphere and the upward radiation emitted by the water surface. This longwave radiation ranges in wavelength between 4 and 120 μm and has a peak intensity at about 10 μm. Atmospheric radiation depends primarily on the air temperature, humidity and cloud cover. The magnitude of the atmospheric radiation largely depends on the moisture content of the air and
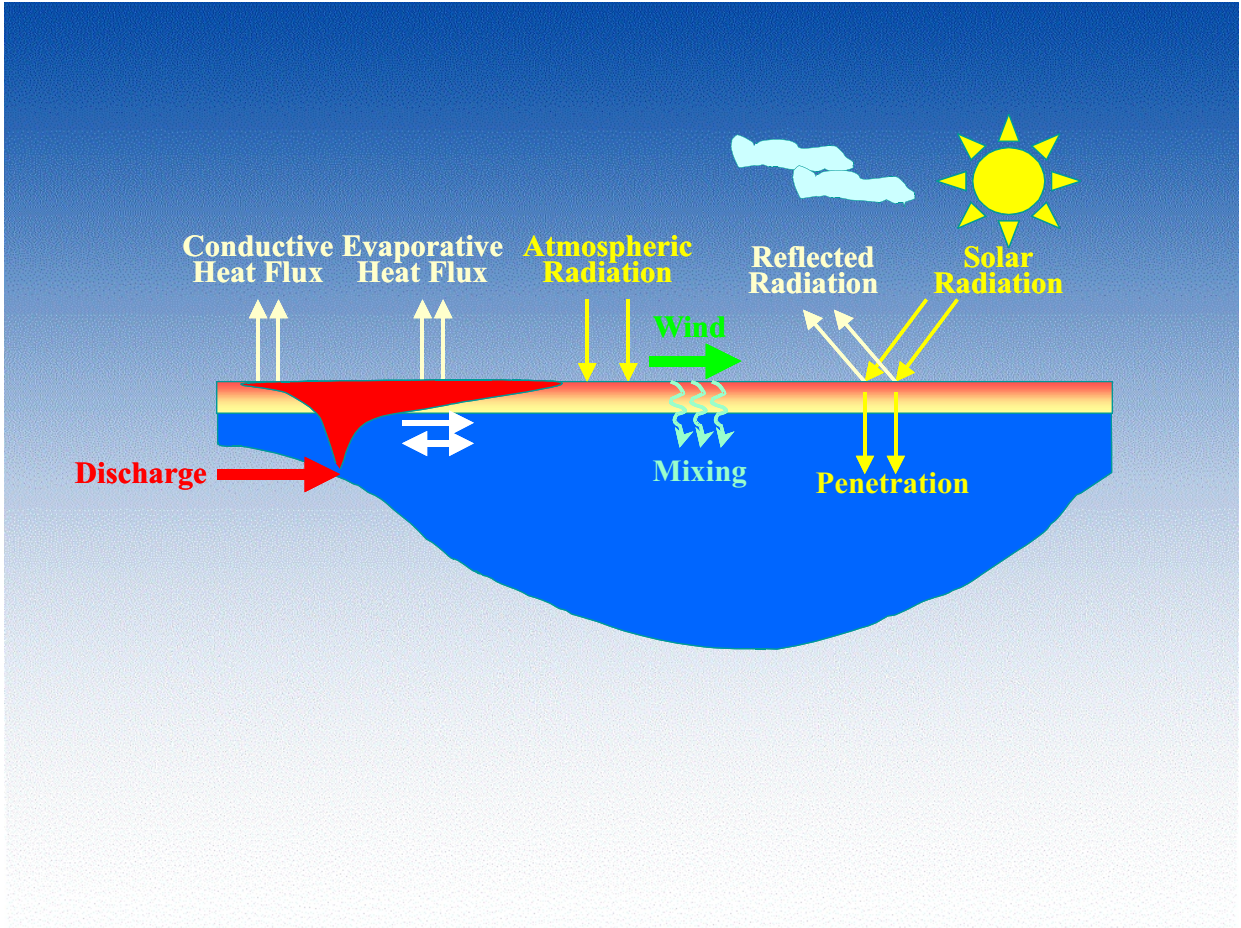
Figure 3-1. Heat budget components.

constitutes the major component of heat exchange processes during the night and during cloudy conditions (Edinger et al.,1974). The physics of the longwave radiation is simply a black body radiation, and the magnitude is directly proportional to the fourth-power of the absolute temperature. Nevertheless, the computation for the downflux is more complicated as it evaluates the effects of changes in atmospheric temperature, humidity, cloud cover, aerosol distribution, carbon dioxide, and other atmospheric constituents. Among several commonly referenced bulk formulae, Brunt (1932) suggested that the downflux depends on the square root of the near-surface vapor pressure (e_a). In the present study a Swinbank (1963) formulation has been used, which suggests that e_a is strongly correlated with the air temperature (T_a) and evaluates the downflux as a function of T_a alone. The net atmospheric flux is given as

$$H_a = \varepsilon\sigma\left((9.37 \times 10^{-6}T_a^6)(1 + 0.17C^2) - T_s^4\right) \tag{3-1}$$

where
H_a = net longwave atmospheric radiation (Wm^{-2})

ε = emissivity of the water body (0.97)

σ = Stefan-Boltzmann constant (5.67×10^{-8} $Wm^{-2}K^{-4}$)

T_a = atmospheric temperature in $^{\circ}K$

T_s = water temperature in $^{\circ}K$

C = cloud fraction (0-1)

Swinbank's formulation is sometimes found more attractive when surface humidity observations are not as readily available as air temperatures (Fung et al., 1984). This may also be attractive when a land based meteorological station is too far from the water body and may not provide site representative relative humidity data.

3.3 SENSIBLE HEAT FLUX, H_C

Heat exchange can occur between the atmosphere and a water body through conduction. The direction of the heat flux may be in either way depending on the sense of the temperature differences between the air and the water body. It has been shown (Edinger et al., 1974) that the daily rate of heat conduction is about an order of magnitude less than other dominant processes. The flux of conduction heat is commonly parameterized by the bulk transfer formula with dependencies on wind speed as suggested by Edinger et al., (1974).

$$H_c = C_c f(W)(T_s - T_a) \tag{3-2}$$

where, H_c = sensible (conduction) heat fluxes (Wm^{-2}), C_c = Bowen's coefficient (0.62 mb/K), f(W) = wind speed function, defined as $a_0 + a_1W + a_2W$ (Wm^{-2}mb^{-1}), T_s and T_a are water and air temperature respectively as defined earlier.

The coefficients a_0, a_1 and a_2 are chosen based on Brady et al., (1969) and suggested by Edinger et al.(1974). Significant discrepancies in formulating wind speed function have been reported in the latter studies, suggesting a wide variety of opinions among researchers. There is varying speculation as to whether conduction processes will remain at a negligible molecular scale in the absence of wind or whether other small scale processes such as conduction currents due to density instabilities may dominate. The latter concept gained significant favor due to the fact that density instabilities exist during conduction and evaporation from thermally loaded water surface, and during the night when air temperature may be less than the water temperature. Following Brady et al.(1969) and Edinger et al. (1974) a slightly conservative formulation has been adopted in this study:

$$f(W) = 6.9 + 0.345\,W^2 \quad (\text{Wm}^{-2}\ \text{mb}^{-1}) \tag{3-3}$$

Where W is wind speed in m/s measured at 7 m above the water surface. For both the sensible and evaporative heat flux computations the evaporative wind speed function f(W) is a somewhat uncertain parameter (Cole and Buchak, 1995). Various formulations of f(W) have been examined in Edinger et al.(1974). Cole and Buchak (1995) termed the wind speed in this function as "ventilation speed" rather than a vector velocity speed as used in the wind stress computations. This ventilation speed is somewhat lower than the actual wind speed measured in a distant land based meteorological station, which accounts for the sheltering and canopy effect by the surroundings of a water body. A wind shelter coefficient has been introduced by Cole and Buchak (1995) which has a range of 0 to 1 depending on the shape and size of the water body. No shelter coefficient was used in this study.

3.4 EVAPORATIVE HEAT FLUX, H_E

The evaporative heat fluxes are related to the conductive heat fluxes by the Bowen ratio and can be given as a function of wind speed and the difference between the saturated water vapor pressure at the water surface temperature and the water vapor pressure in the overlying air (Edinger et al., 1974).

$$H_e = f(W)(e_s - e_a) \tag{3-4}$$

where H_e = evaporative heat flux (Wm^{-2}), e_s = saturated vapor pressure at temperature T_s (mb), e_a = air-vapor pressure at temperature T_a (mb).

3.5 SOLAR RADIATION

The model uses observed solar radiation for this study and there are enough observed data to cover the entire calibration period. However, in cases when this solar radiation is not available then it computes the incident solar radiation on the ocean based on Smithsonian Meteorological Tables (List 1958). The radiation at the top of the atmosphere (extra-terrestrial) is:

$$I_e = \frac{J_0}{a^2} \cos z \ D_F \ (\phi, \lambda) \tag{3-5}$$

where the solar constant $J_0 = 1.35 \times 10^2 \ J \ m^{-2} \ s^{-1}$, a is the radius of the earth, and z is the zenith angle; cos z is given by

$$\cos z = \sin \phi \sin \delta + \cos \phi \cos \delta \cos h, \tag{3-6}$$

where ϕ is latitude, δ the sun declination angle, and h the sun's hour angle. The fraction of daylight D_F is a function of latitude and longitude when diurnal effects are included. The direct component of solar radiation reaching the ocean surface is then attenuated by an atmospheric transmission coefficient τ as

$$I_{DIR} = I_e \tau^{\sec z} \tag{3-7}$$

where $\tau = 0.7$. The diffuse sky radiation under cloudless conditions may be approximated by assuming that, when scattering of radiation occurs, half is scattered downward and half is scattered back. Thus

$$I_{DIFF} = \left[\left(1 - A_a \right) I_e - I_{DIR} \right] / 2 \tag{3-8}$$

The water vapor plus ozone absorption A_a is taken to be 0.09. The total radiation reaching the surface under clear skies is then approximated by the sum of (3-7) and (3-8), i.e.,

$$I_{tot} = I_{DIR} + I_{DIFF} \tag{3-9}$$

There are numerous empirical relations to predict the attenuation of solar radiation by clouds. Formula derived by Reed (1977) and suggested by Simpson and Paulson (1979) which is found to be in best agreement with observations:

$$I_0 = I_{TOT} \left(1 - 0.62C + 0.0019\beta\right)\left(1 - \alpha\right) \tag{3-10}$$

Here C is the fractional cloud cover, and B is the solar noon altitude in degrees and is computed by

$$\sin\beta = \sin\phi\sin\left[23.45\sin(t-82)\right] + \cos\phi\cos\left[23.45\sin(t-82)\right] \tag{3-11}$$

where t is the Julian day. The ocean surface albedo, α, is taken from Payne (1972), and these values agree very well with Simpson and Paulson's (1979) results. The variables, D_F, δ, h and β are all computed from present day astronomy.

Although more than half of this insolation that enters the ocean is absorbed within top half meter, the remaining fraction that penetrates can have significant effect on the development of thermal structure. Martin (1985) found that the penetration of solar radiation in the formation of the upper mixed layer is of particularly sensitive to various optical water types and turbidity. Parameterization of absorption of downward irradiance is given following Beers' law (Cole and Buchak, 1994):

$$I(z) = (1 - f_a)\, I_o e^{-kz} \tag{3-12}$$

where, I_0 = Incident solar radiation reaching the sea surface (W/m^2)

$I(z)$ = short wave radiation at depth z, (W/m^2)

f_a = fraction absorbed at the water surface

k = extinction coefficent

Many investigators use the two spectral component model to describe the vertical distribution of solar radiation. More than half of the radiation is of shorter wavelength and is absorbed in the surface and the remaining longer wavelength solar radiation penetrates deeper in the water column. The fraction of solar radiation absorbed in the surface, however, varies significantly from waterbody to waterbody. For example in the southern flank of Georges Bank the fraction is 0.8, Rosati and Miyakoda, (1988) used 0.58 in application of a general cumulative model for upper ocean simulation. Blumberg et. al. (1999) and Ahsan et. al. (2002) set this fraction equal to zero in the simulations of New York Harbor and Mississippi Sound, respectively.

3.6   MODEL SENSITIVITY

Figures 3-2 through 3-5 present the original vertical temperature calibration at eight far field stations and four near field stations for two time periods.   These are the same figures that were presented in the calibration report. The results were computed by setting the fraction of shortwave solar radiation absorbed in the surface layer equal to zero (the same value that was used in New York Harbor and Mississippi Sound).   The model results show a good reproduction of the surface temperatures during the warm periods of both 1998 and 1999, and a fair reproduction of the temperature throughout the water column. As a sensitivity, the model was rerun for two cases. The first case was specifying the fraction of shortwave radiation absorbed in the surface layer equal to 0.5. The second case was specifying this fraction equal to 1.0.

Figures 3-6 through 3-9 present the results of the 0.5 case. One can clearly see from Figure 3-6 that the surface temperatures are over predicted by the model. One might argue, however, that the calibration to temperature at depth may be slightly improved at stations F31 and F07. The model results compared to the data for the two cases are similar at stations F17, F26 and F27. The comparison to the data is a little less favorable at station F29 for the 0.5 case. Figure 3-7 shows similar results. In general, if the model under estimated the surface temperature in the calibration case, the 0.5 case improved the surface results. If the model over predicted the bottom temperatures in the calibration case, the 0.5 case improved the model to data comparison. However, where the model calibration was good, changing the short wave radiation absorbance had detrimental impacts on the comparison of the model to the data. Figures 3-8 and 3-9 tell the same story. The argument can be made that the results from the 0.5 case are as good as the calibration condition. The deciding factor was the very high temperatures calculated at the surface in the 0.5 case. Perhaps if the number of layers in the model had been reduced from 12 to 10 with each layer having an equal depth, the results could have been improved. The decision was made, however, to make as few changes as possible from Signell's original model while still producing reasonable model results.

Figures 3-10 through 3-13 present the vertical temperature model results to data comparison for the 1.0 case. As with the 0.5 case there are portions of the water column at certain stations where the model compares more favorably to the data than the calibration. Stations F31 and F07 during June 1998 are good examples of this. However, the very high surface temperatures make (Figures 3-10 through 3-13) this choice unreasonable.

Figure 3-2 Calibration of vertical temperature distribution at six far field stations during June 1998. Surface absorbance equal to 0.0.

Figure 3-3. Calibration of vertical temperature distribution at four near field and two far field stations during June 1998. Surface absorbance equal to 0.0.

Figure 3-4. Calibration of vertical temperature distribution at six far field stations during August 1999. Surface absorbance equal to 0.0.

Figure 3-5. Calibration of vertical temperature distribution at four near field stations and two far field stations during August 1999. Surface absorbance equal to 0.0.
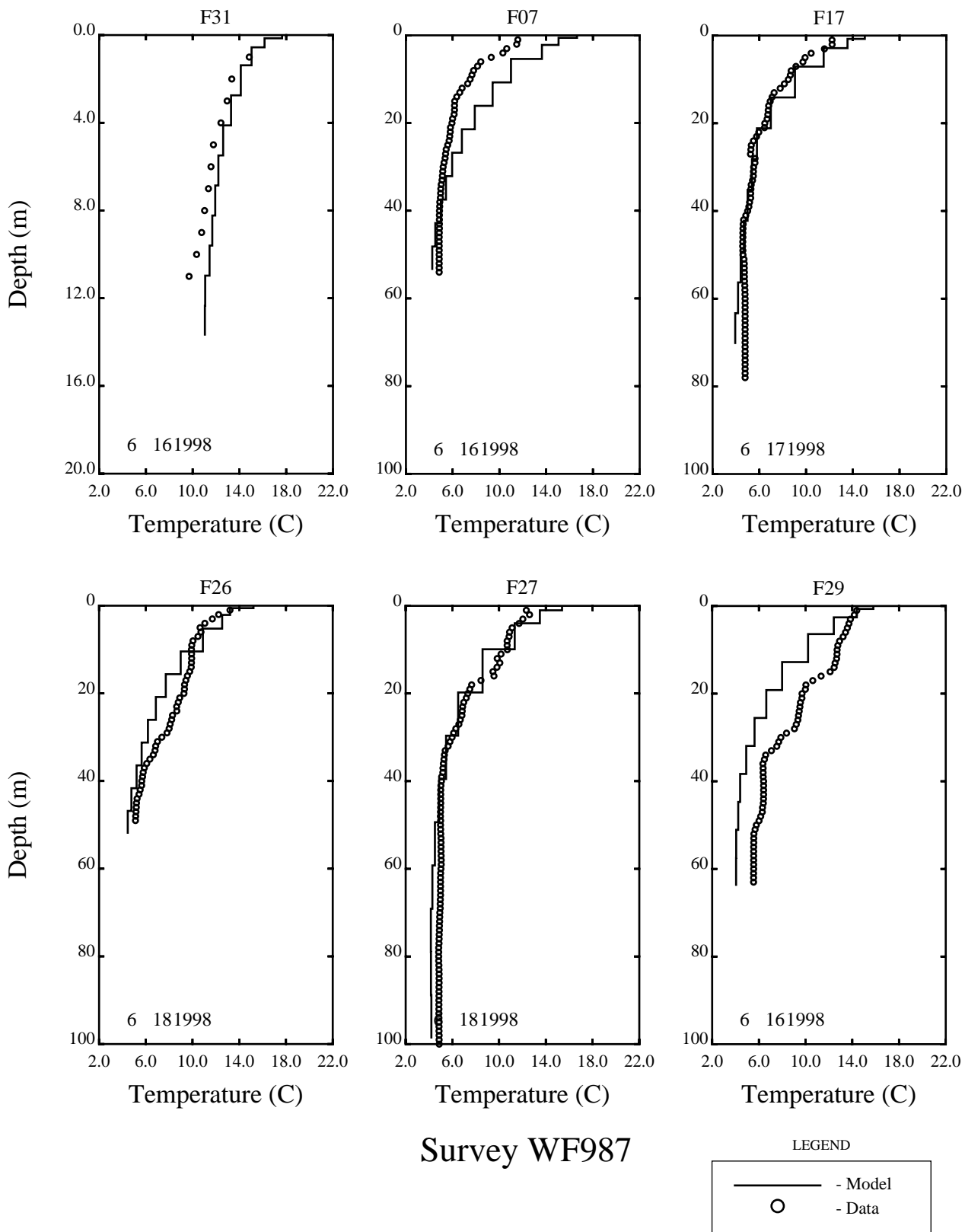
Figure 3-6. Model comparison to the vertical temperature distribution at six far field stations during June 1998. Surface absorbance equal to 0.5.
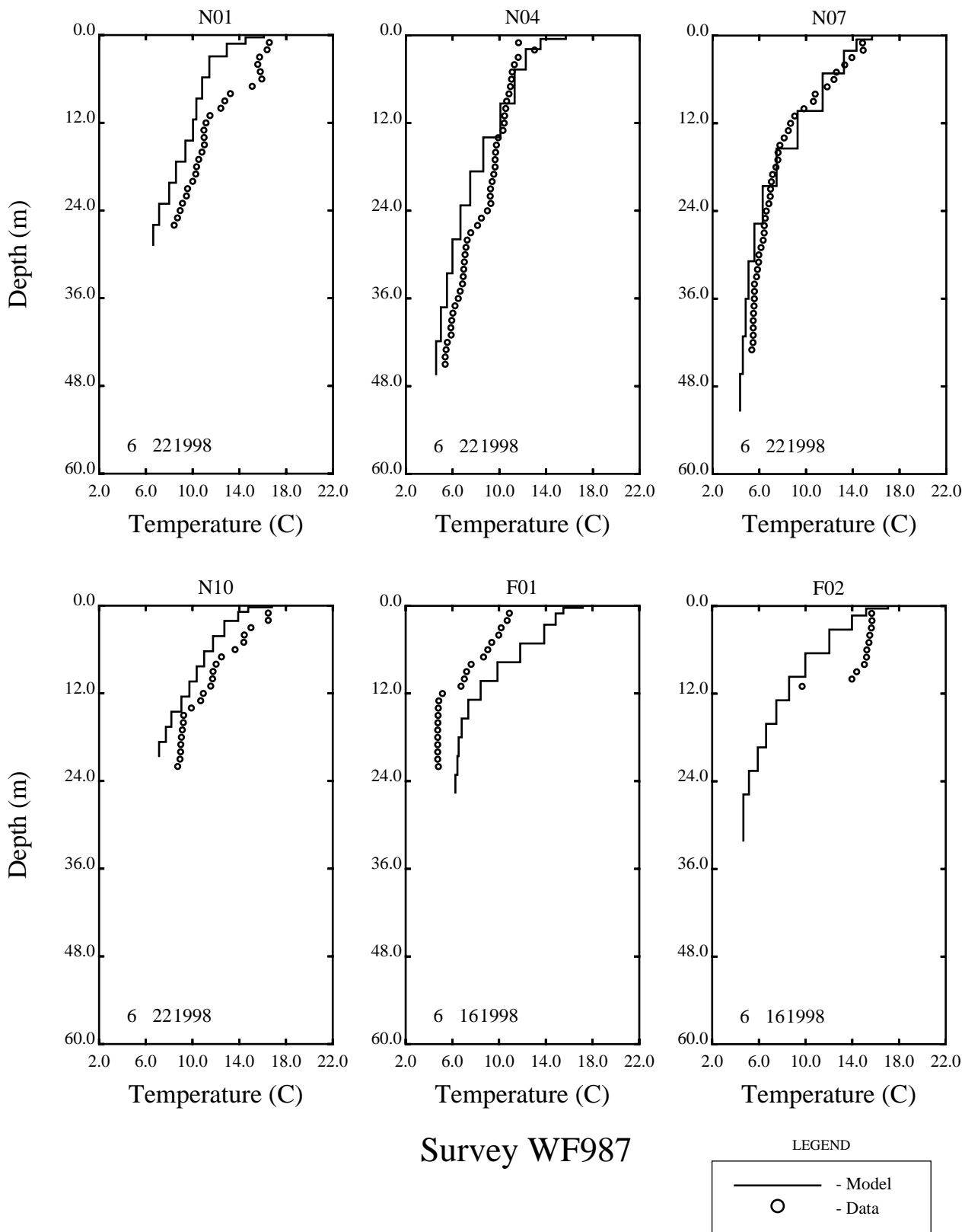
Figure 3-7. Model comparison to the vertical temperature distribution at four near field and two far field stations during June 1998. Surface absorbance equal to 0.5.
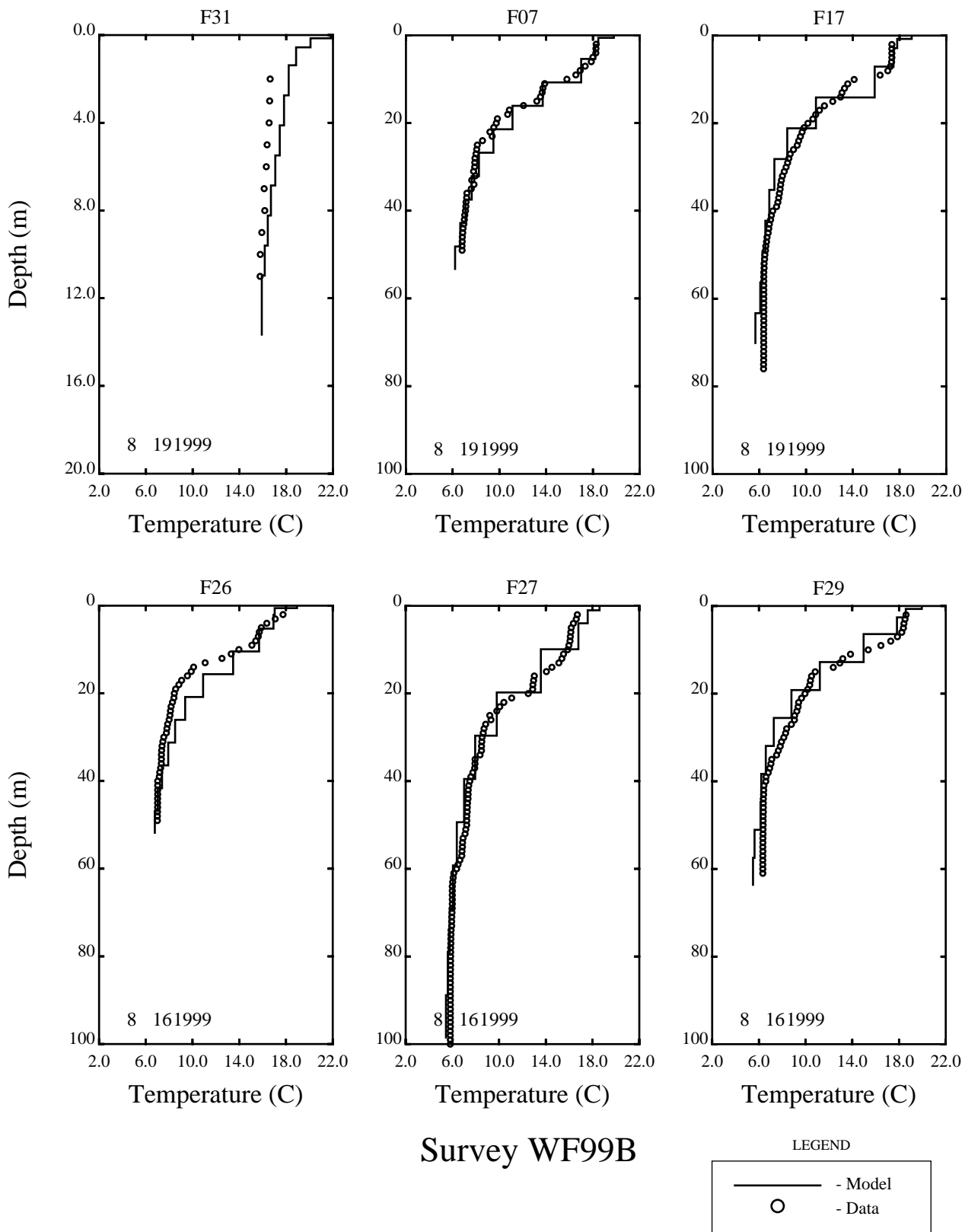
Figure 3-8. Model comparison to the vertical temperature distribution at six far
field stations during August 1999. Surface absorbance equal to 0.5.
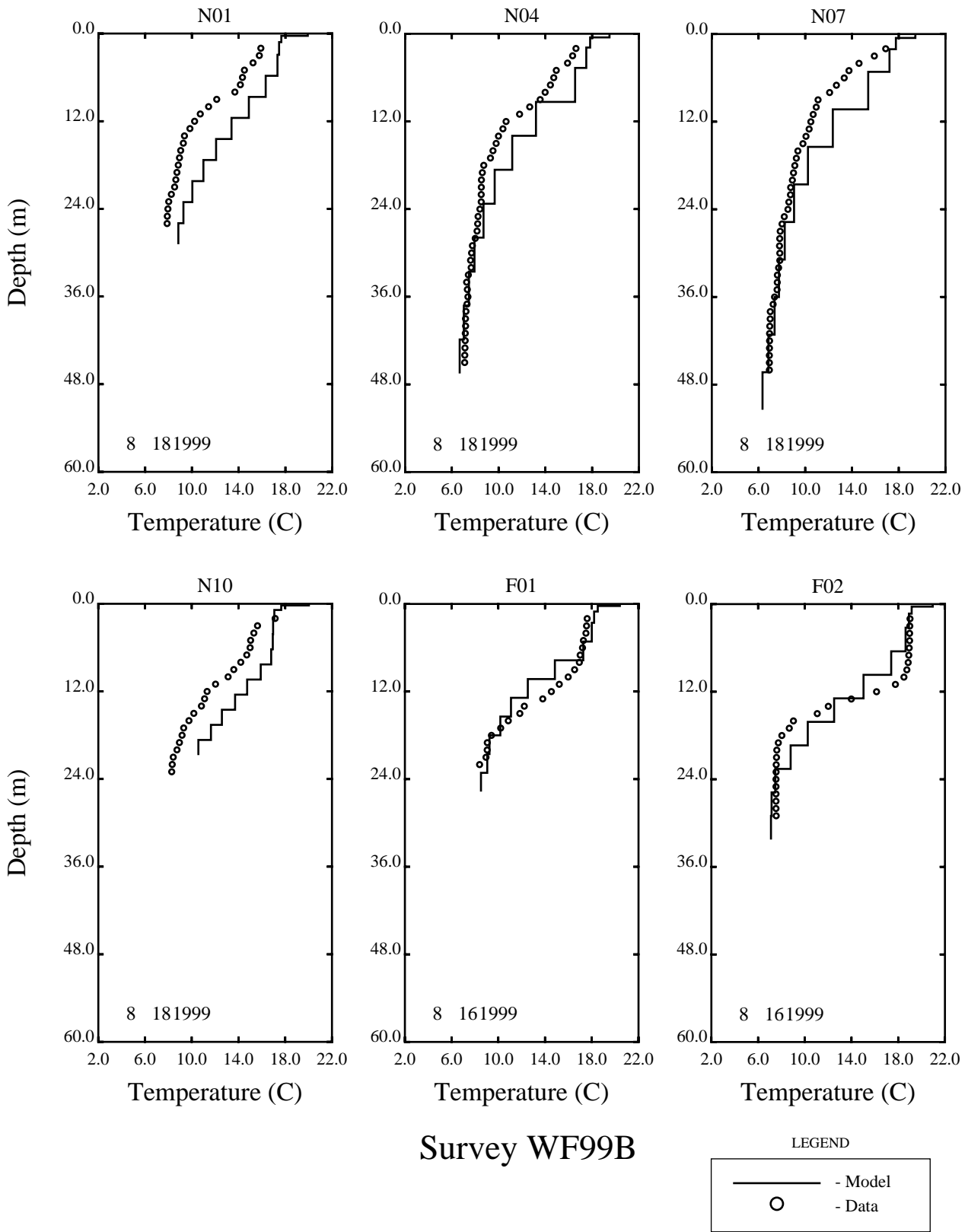
Figure 3-9. Model comparison to the vertical temperature distribution at four near field and two far field stations during August 1999. Surface absorbance equal to 0.5.
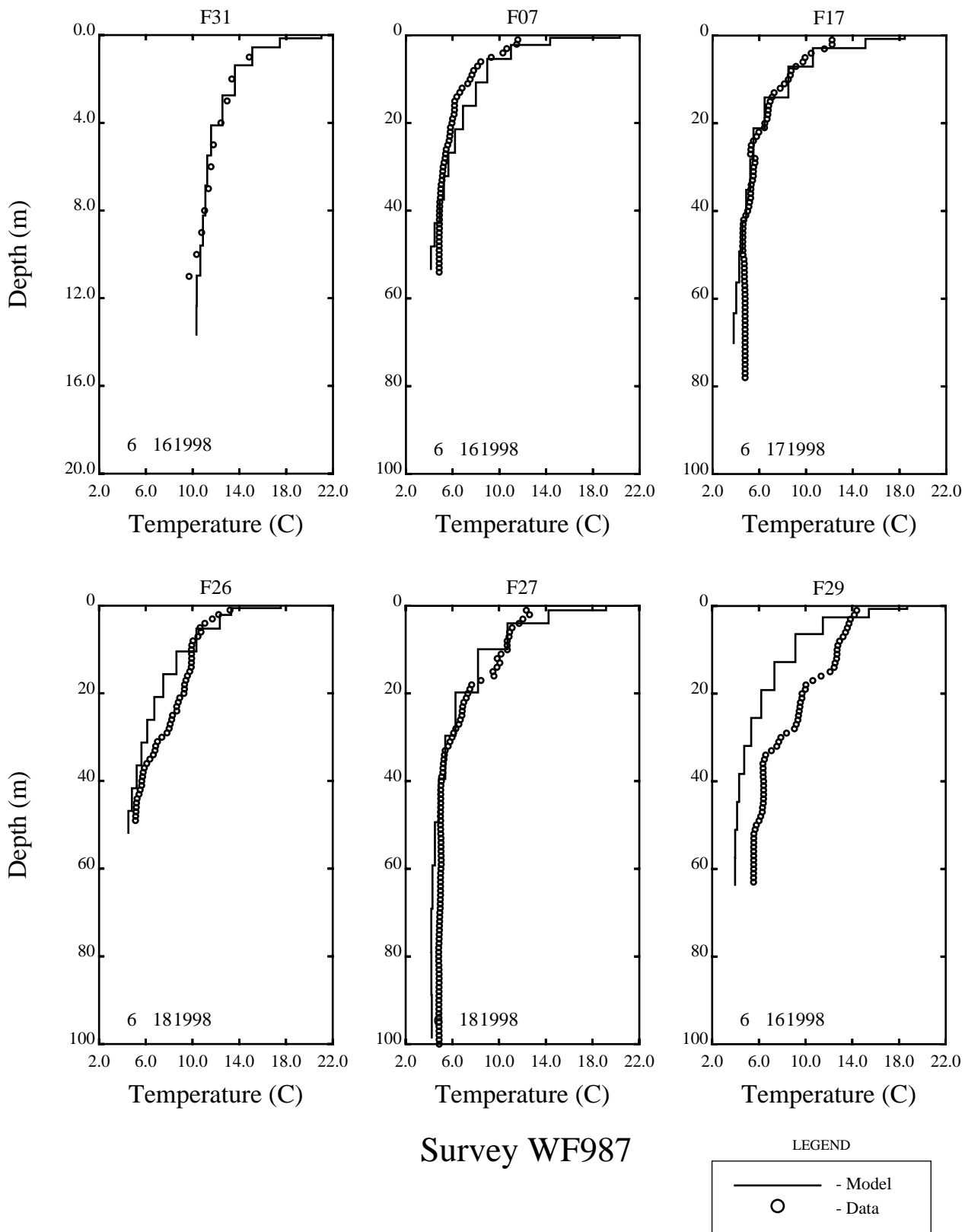
Figure 3-10. Model calibration to the vertical temperature distribution as six far field stations during June 1998. Surface absorbance equal to 1.0.
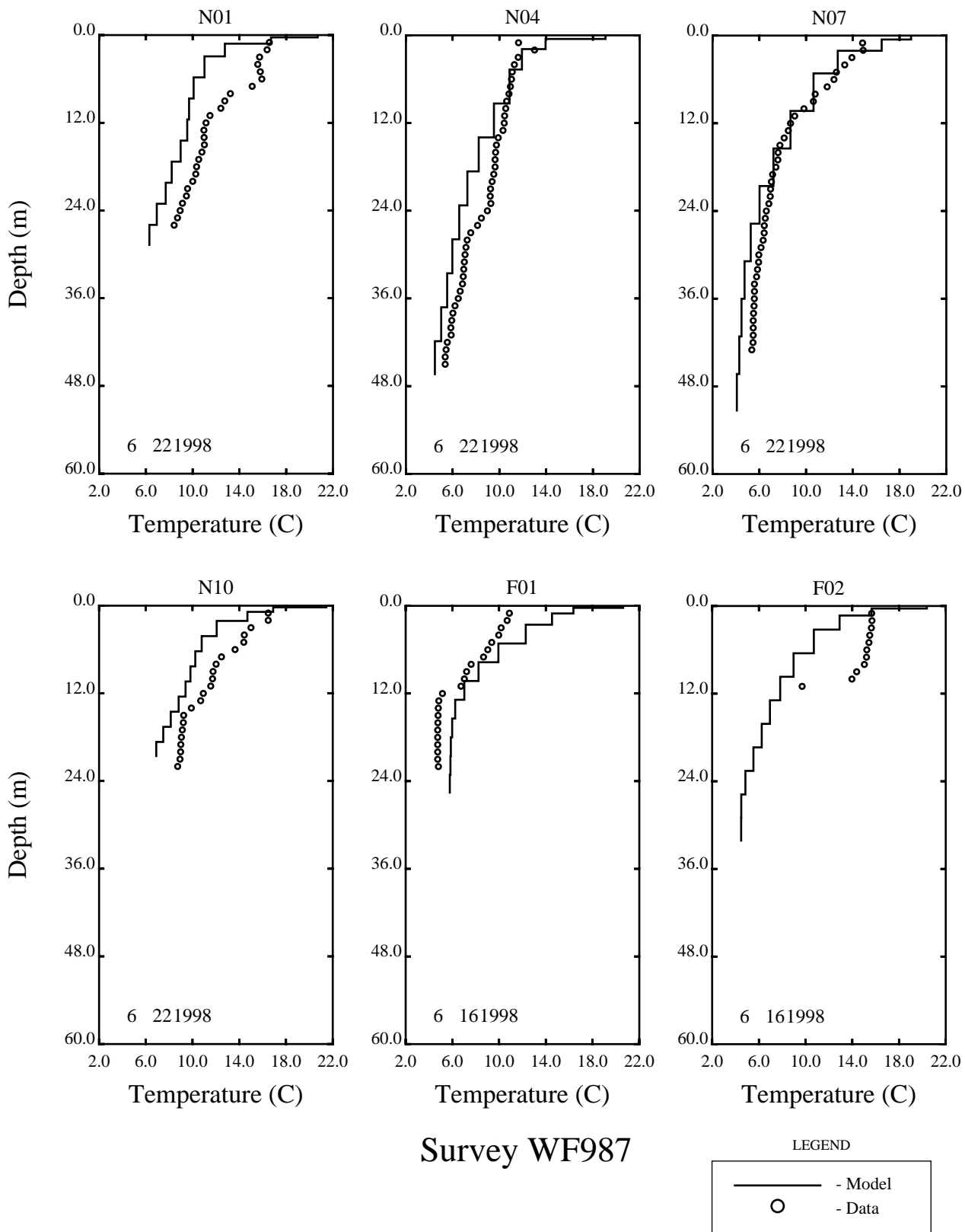
Figure 3-11. Model comparison to the vertical temperature at four near field and two far field stations during June 1998. Surface absorbance equal to 1.0.
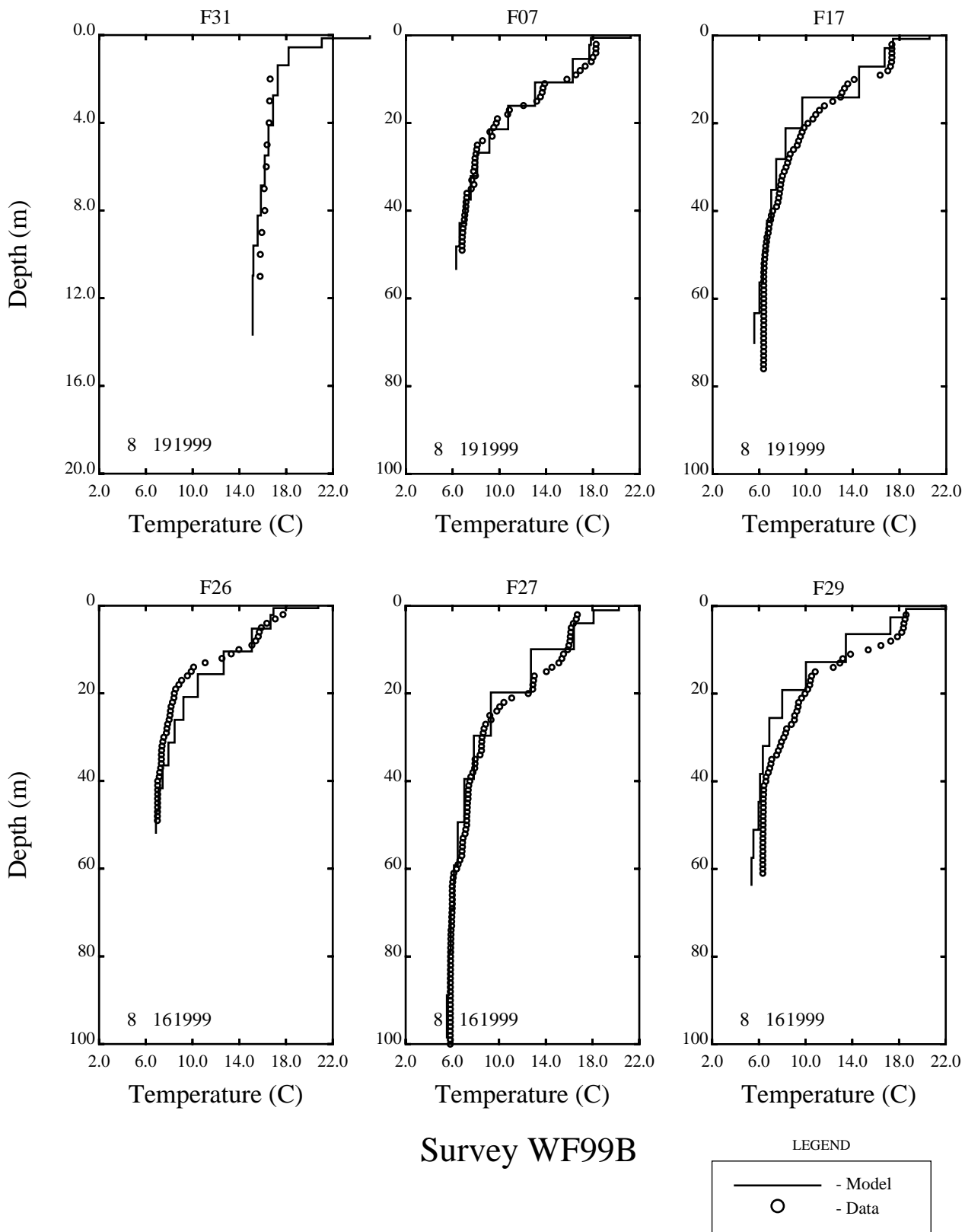
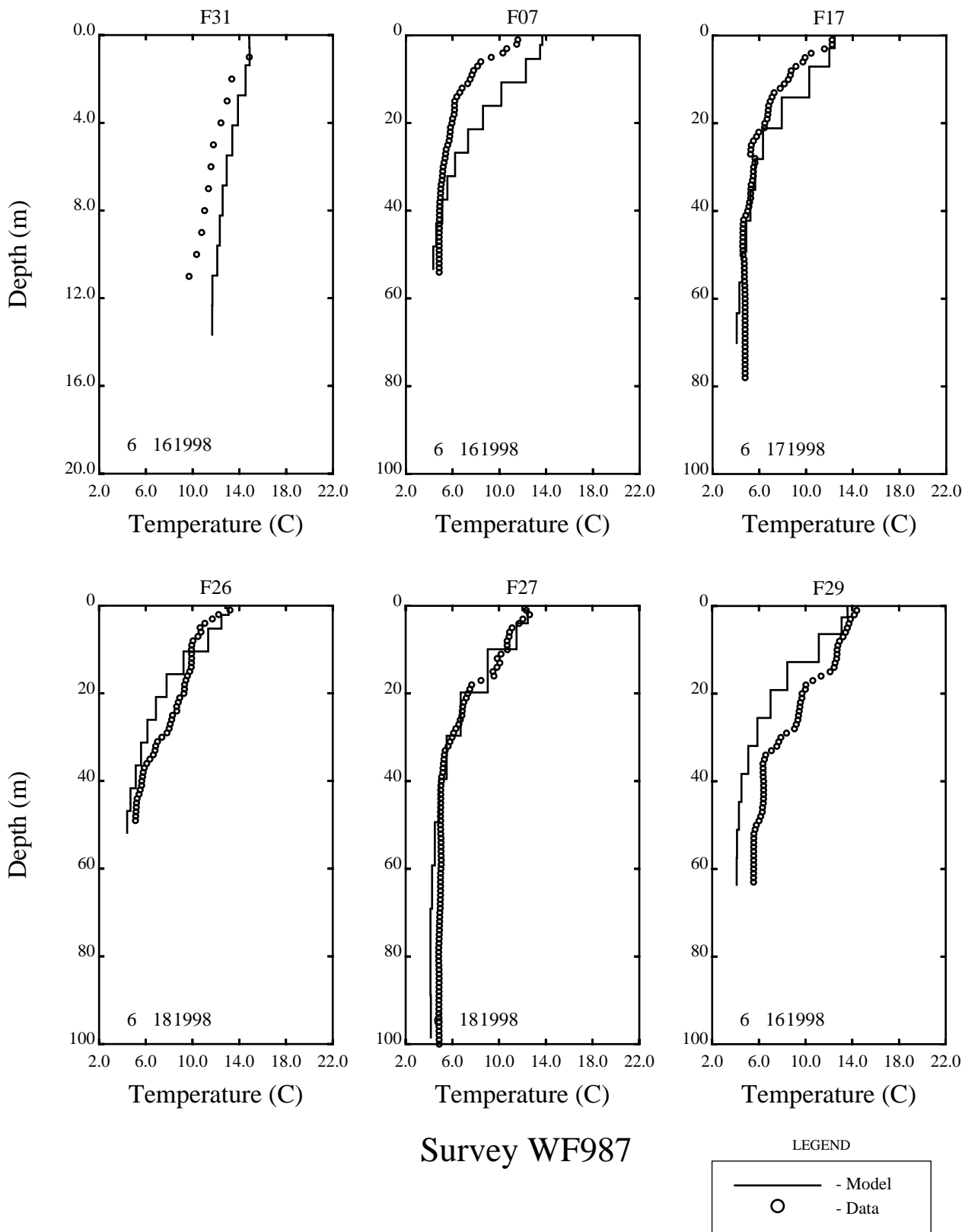Figure 3-12. Model comparison to the vertical temperature distribution at six far field stations during August 1999. Surface absorbance equal to 1.0.
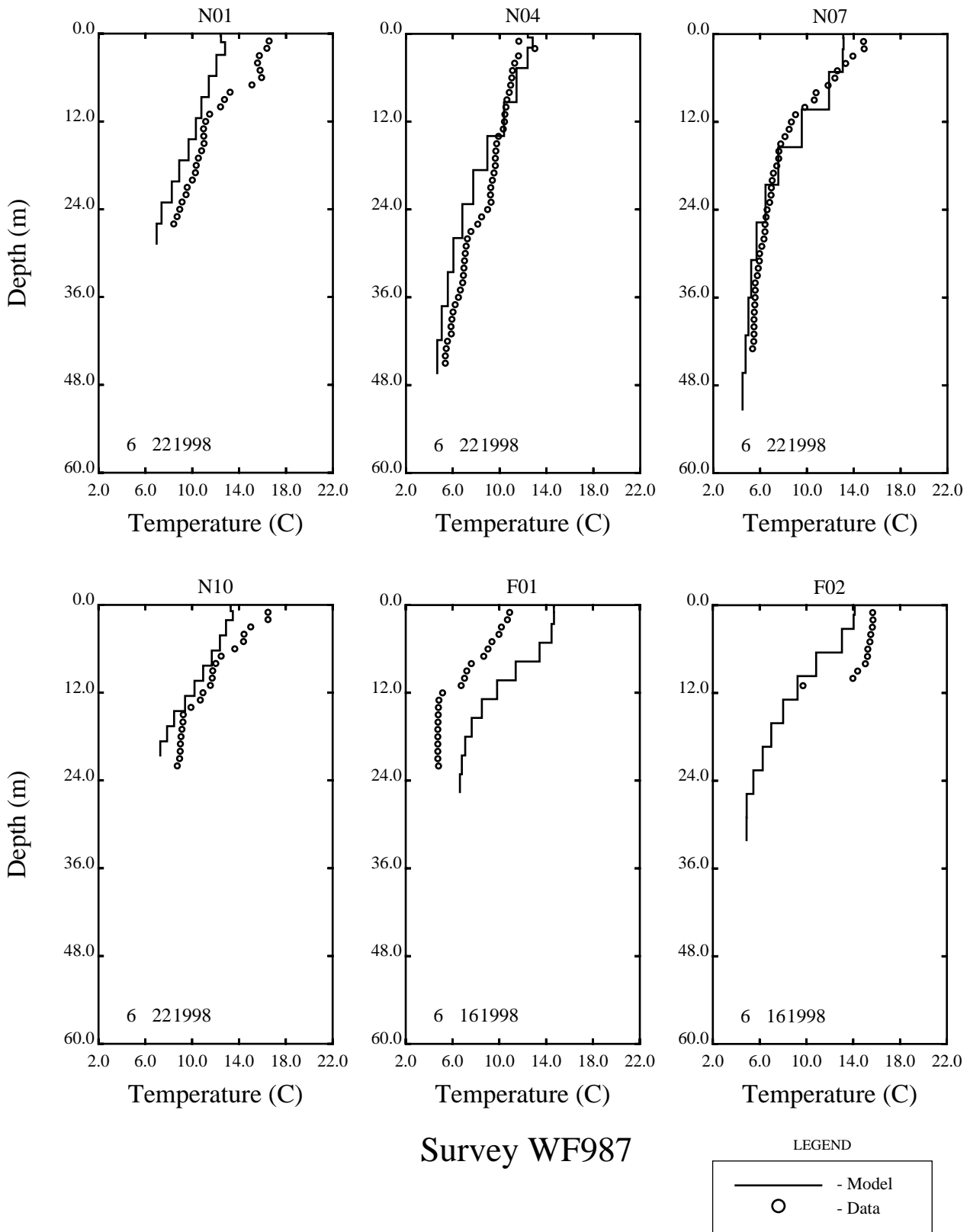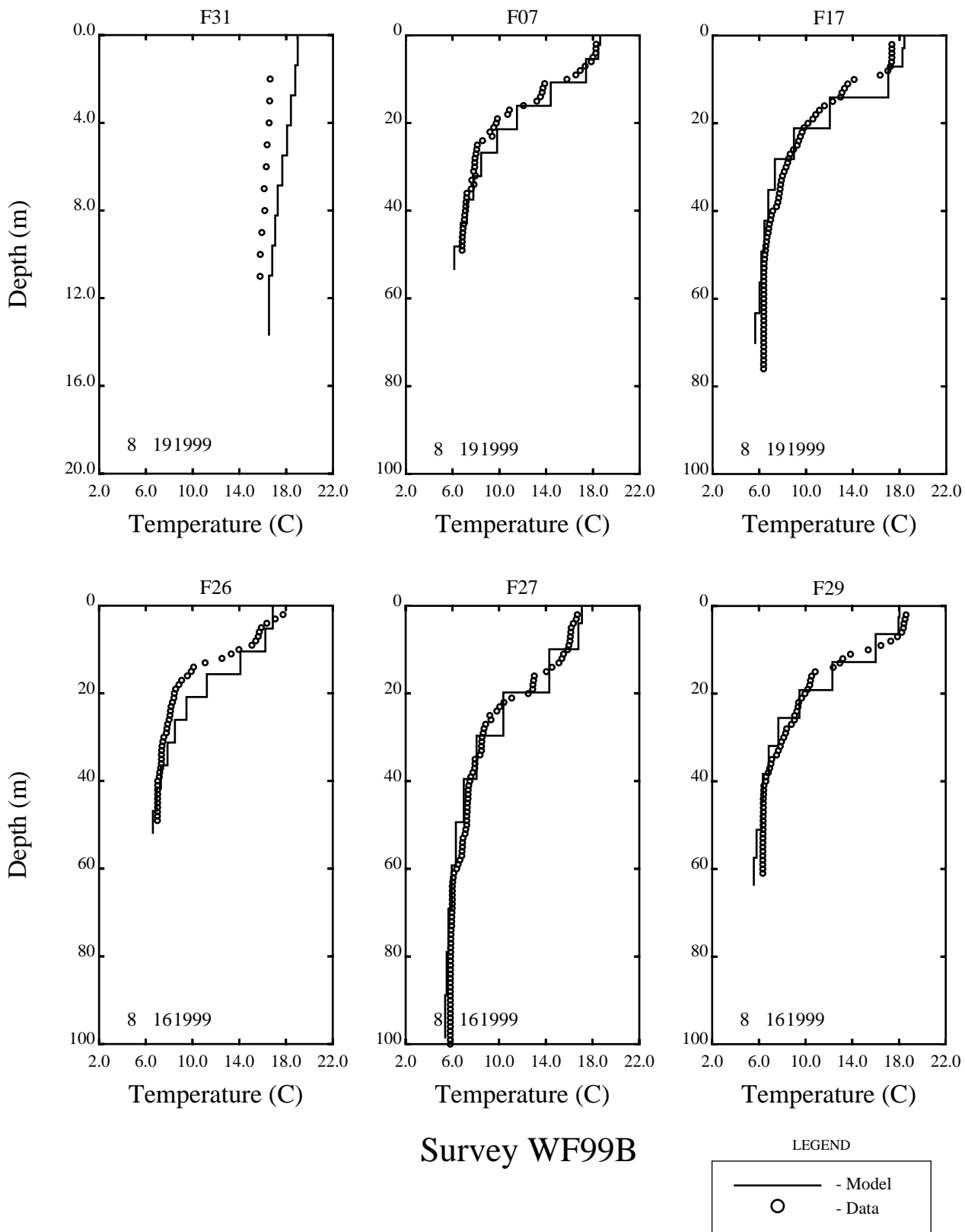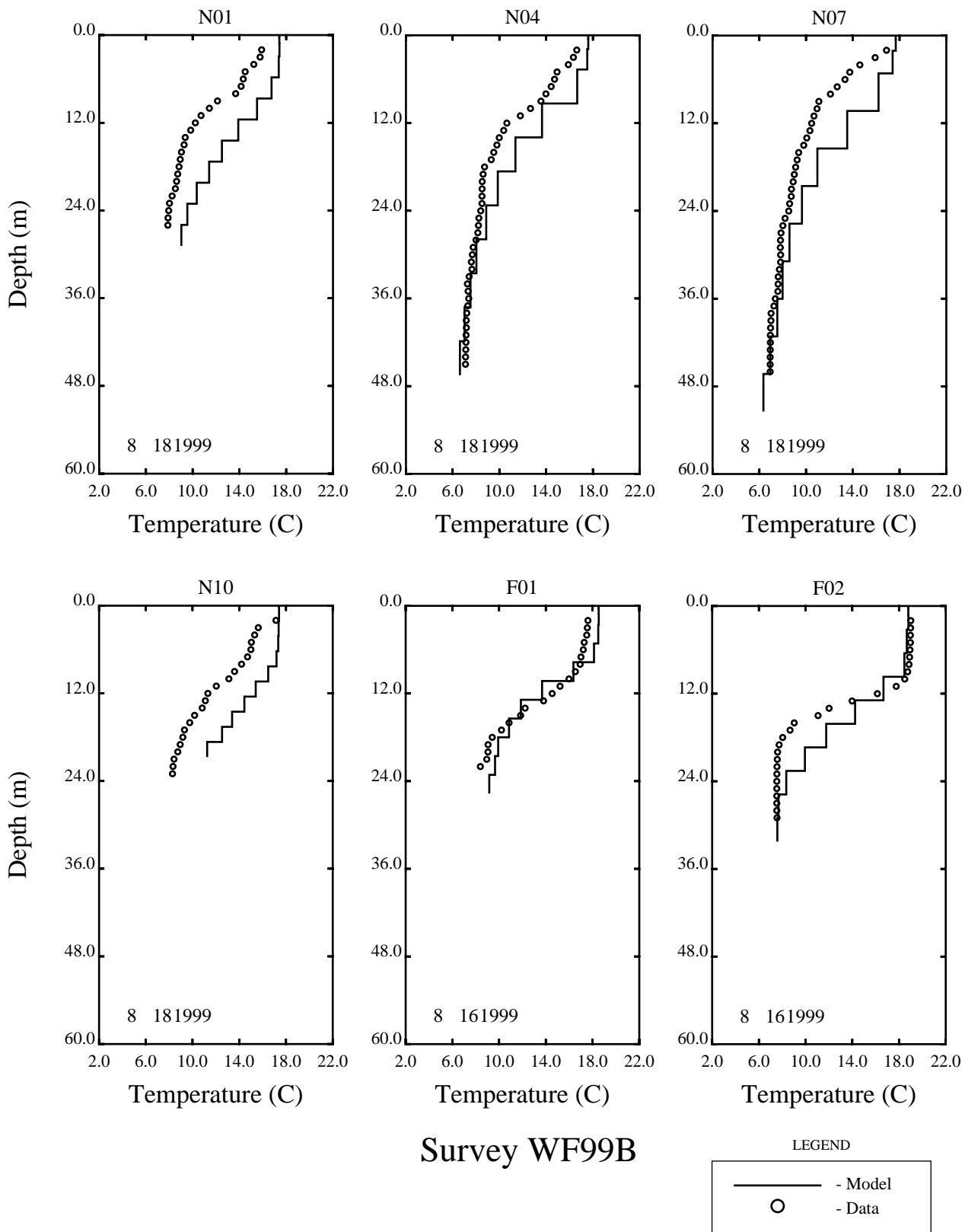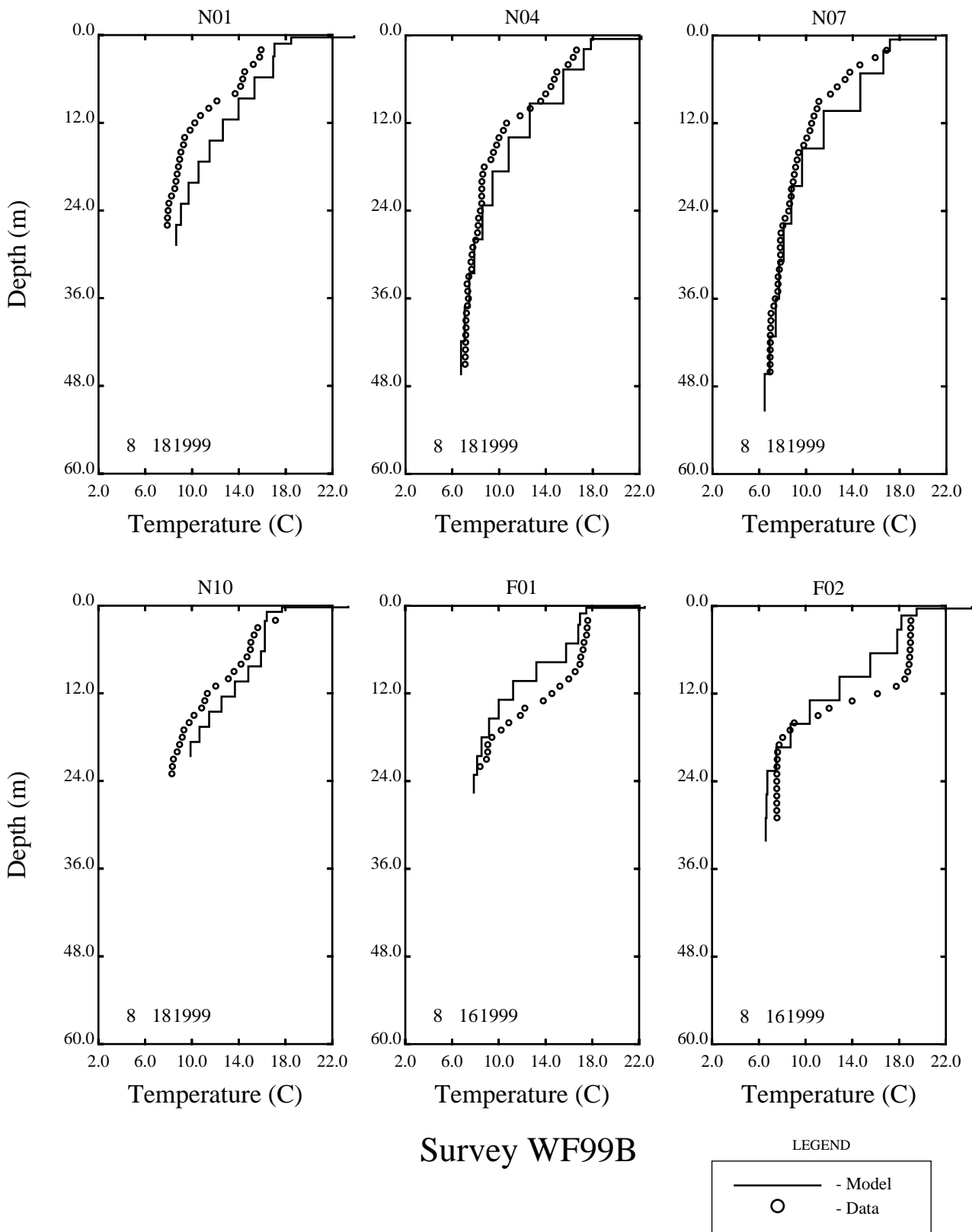
Figure 3-13. Model comparison to the vertical temperature distribution at four near field and two far field stations during August 1999. Surface absorbance equal to 1.0.

SECTION 4

EXTINCTION COEFFICIENTS

4.1   INTRODUCTION

The following section is an excerpt from HydroQual and Normandeau (1995) and describes the original development of the extinction coefficients used in the water quality model. These same extinction coefficients were used for the calibration of the hydrodynamic model in 1998 and 1999.

4.2   DEVELOPMENT OF EXTINCTION COEFFICIENTS

Water transparency and, therefore, the light extinction coefficient, plays an important role in primary productivity. Phytoplankton productivity is greater in areas of high light penetration than in light limited areas, given the same nutrient availability. The data indicate that higher light extinction coefficients are appropriate in the area around Boston Harbor. This is due to high suspended solids loadings associated with sediment resuspension and transport, riverine inputs and the discharge of sludge and effluent from the Nut and Deer Island wastewater treatment facilities. Extinction coefficients are also higher in regions of high algal biomass. This reflects the effect of algal self-shading. The extinction coefficients used as input to the model were determined from Battelle's measurements of vertical attenuation of surface light and chlorophyll-a. Estimates of the one percent light level were made from the vertical light profiles and total light extinction coefficients were made using the following equation:

$$k_{e_{obs}} = \frac{4.6}{H} \qquad \text{(Note: } e^{-4.6} \approx .01) \qquad\qquad (4\text{-}1)$$

where

$k_{e_{obs}}$ = the total water column extinction coefficient (m^{-1})

H   =   depth of the 1 percent surface light level (m),

These estimates were then corrected using the averaged vertical chlorophyll-a concentration, between the water surface and the one percent light level depth as per Equation 4-2

$$k_{e_{base}} = k_{e_{obs}} - k_c \cdot \text{chl-a}_{obs} \qquad\qquad (4\text{-}2)$$

where

$k_{e_{base}}$ =   the base or background extinction coefficient related to

non-algal turbidity (m^{-1}),

$k_{e_{obs}}$ = the total water column extinction coefficient (m^{-1}),

k_c = the extinction coefficient per unit of phytoplankton chl-a $(m^2/mg$ chl-a$)$,

chl-a_{obs} = the observed chl-a concentration (mg/m^3).

The resulting $k_{e_{base}}$ were plotted as a function of the depth of the model segment in which it was sampled, as shown in Figure 4-1. Two curves were fit through the data so as to be able to estimate for $k_{e_{base}}$ segments for which no light measurements were made. The following empirical equations resulted:

$$k_{e_{base}} = 0.6 \qquad (m^{-1}) \text{ Boston Harbor} \qquad (4\text{-}3a)$$

$$= 0.42e^{-0.065H} + 0.16 \quad (m^{-1}) \text{ North of Scituate Harbor} \qquad (4\text{-}3b)$$

$$= 0.06e^{-0.045H} + 0.16 \quad (m^{-1}) \text{ South of Scituate Harbor} \qquad (4\text{-}3c)$$

where H represents the depth of the segment. These equations represent the fact that Boston Harbor turbidity is influenced by sediment resuspension and transport, riverine inputs and by solids in the MWRA effluent and that shallow water near-shore areas are impacted by runoff and anthropogenic sources of solids while deeper mid-Bay segments are less impacted by these sources. The Bays system was divided into northern and southern regions, using Scituate as a dividing line, recognizing that there are greater anthropogenic inputs of suspended solids to northern Massachusetts Bay from Boston Harbor and other northern communities than enter the southern portion of the Bays system.

4.3   COMPARISON TO THE TWO-COMPONENT EXTINCTION RATE

Some MEG members indicated that a two-component shortwave radiation extinction rate, as described in equation 4-4 might be more appropriate than the single component exponential decay.

$$I(z) = I_o (a_1 e^{-k1z} + a_2 e^{-k2z}) \qquad (4\text{-}4)$$

where I_o is the total incident shortwave radiation corrected for reflection, a_1 and a_2 are the fraction of radiation carried by the shorter and longer wavelength components (with $a_1 + a_2 = 1$), and k1 and k2 are their extinction coefficients. (It should be noted that the original 1992-1994 model configuration forced all of the incoming shortwave radiation into the top one-percent of the water column (Signell et al, 1996 and HydroQual (2000).) Figure 4-2 presents a comparison of the two-component function with constants suggested by the MEG $(a_1 = 0.8, k1 = 1/1.4m, a_2 = 0.2,$ and $k2 = 1/6.3m)$
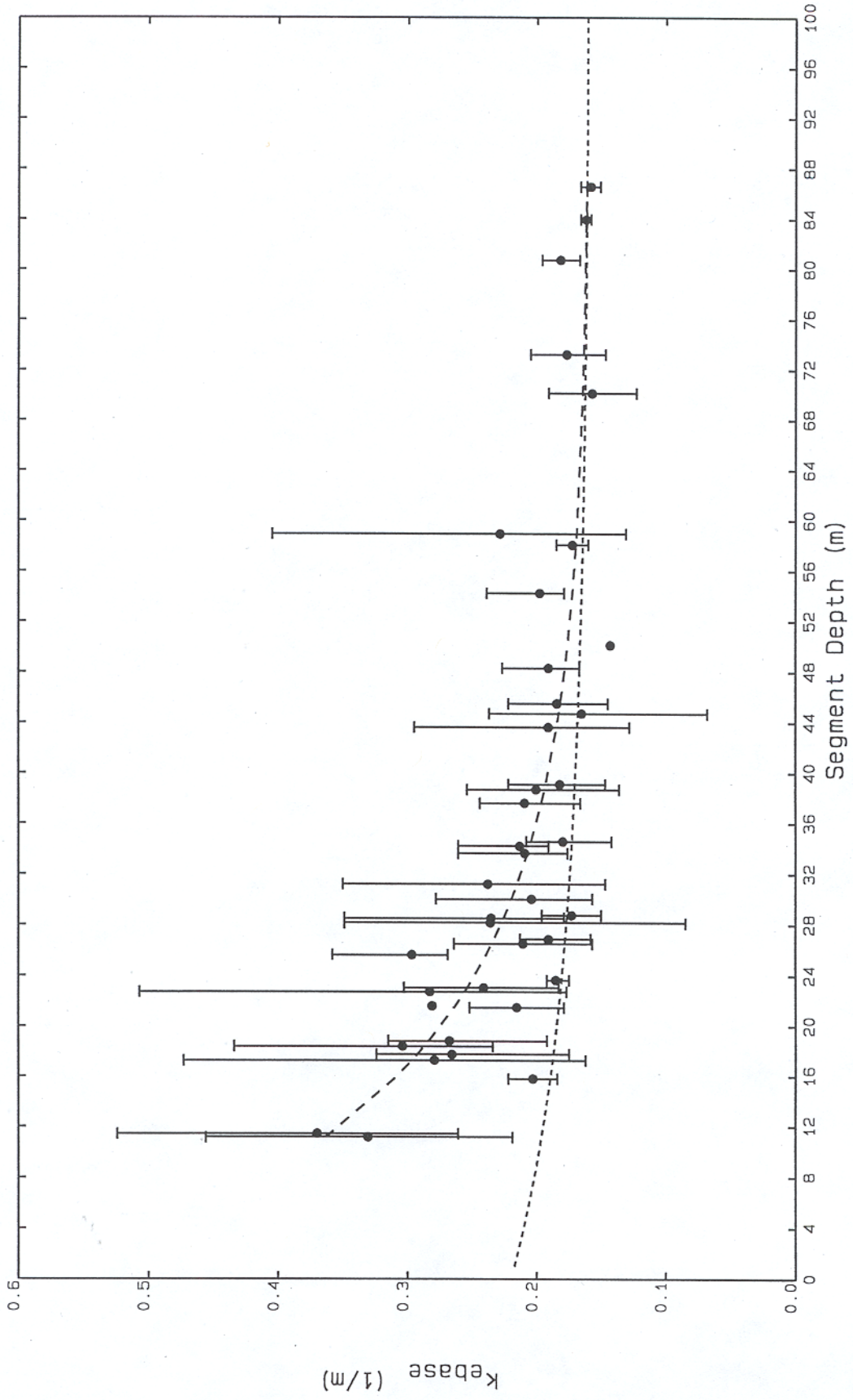
Figure 4-1. Estimates for k_{ebase}.

against the range of base extinction coefficients used in the 1998-99 calibration. The lines are plotted at one meter intervals. The range of base extinction coefficients bound the two-component function. Overall, however, the extinction coefficients used tended to be on the lower portion of the range, thereby allowing more shortwave radiation penetrate deeper into the water column. At the one meter depth, both the k_e of 0.6/m and the two component function have allowed approximately 55 percent of the incident shortwave radiation to penetrate. The k_e of 0.16/m allows approximately 86 percent of the incident shortwave radiation to penetrate. By five meters, the k_e equal to 0.6/m, the two-component function and the k_e equal to 0.16/m have allowed 5, 11, and 45 percent to penetrate, respectively. At k_e equal to 0.6/m the one percent light level is reached at 8 m. The two component function reaches the one percent light level at 19 m. At a k_e of 0.16/m the one percent level is reached at 29 m.
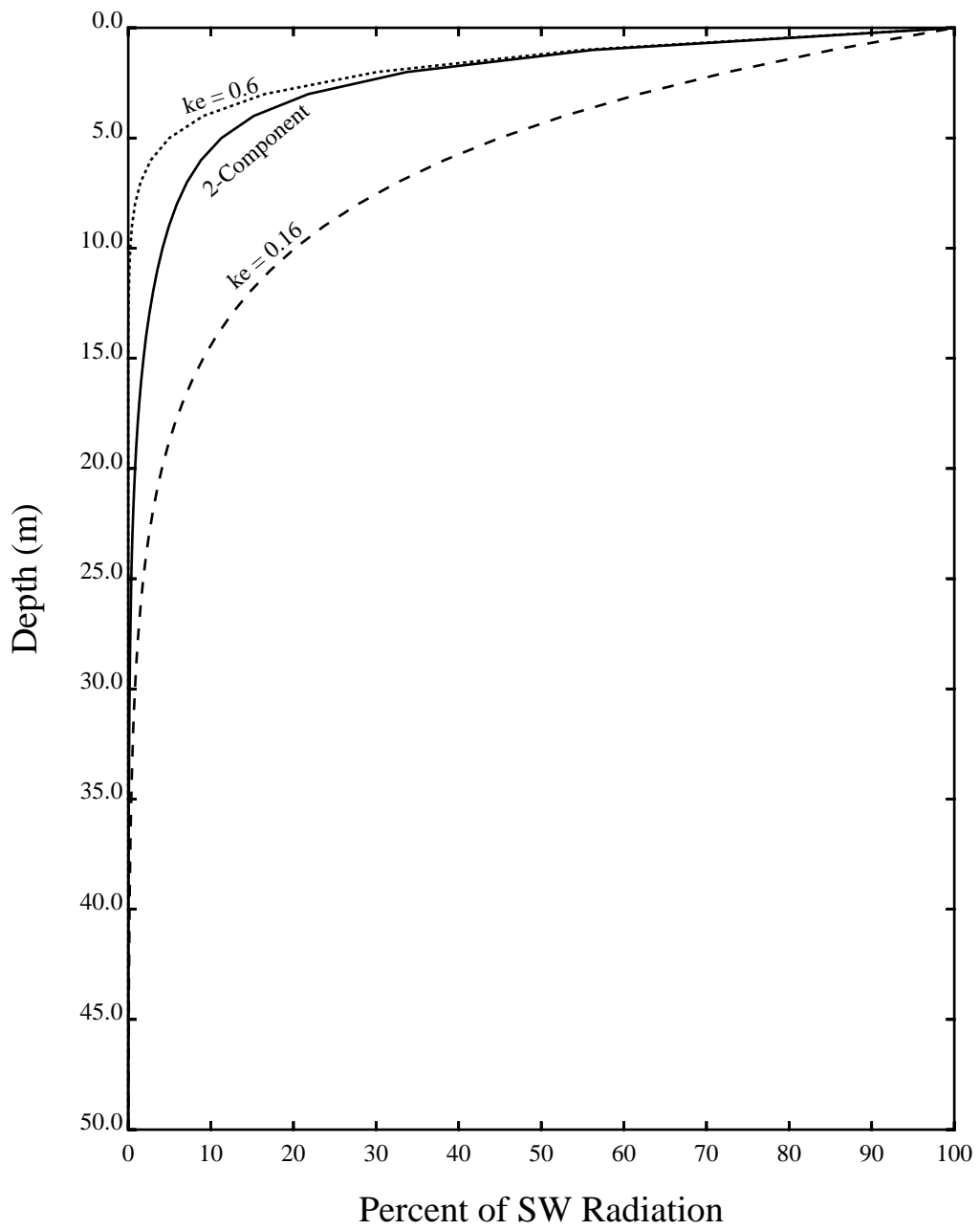
Figure 4-2. Comparison of light penetration depths with various light extinction equations.

SECTION 5

BOUNDARY CONDITION RELAXATION TIME

The boundary condition relaxation times, used in this modeling analysis, were developed by Signell, et al. (1996). On the northern portion of the eastern boundary of Massachusetts Bay, there is mostly an inflow of Gulf of Maine water. For this reason a short relaxation time was assigned to the northern boundary cells so that the northern bay would more closely follow the imposed temperature and salinity boundary conditions. On the southern side of the eastern boundary there is generally an outflow from the bay. In this portion of the bay near the boundary, the temperature and salinity values tend to diverge from the assigned boundary conditions because they are influenced more strongly by processes within the bay. In order to avoid "shocking" the system too much when the flow reverses direction for brief periods, a longer relaxation time was assigned.

Originally, fixed relaxation times were assigned along the boundary. Although several time scales were analyzed, none produced favorable results. The boundary condition relaxation times were then modified spatially across the boundary. Varying the relaxation times from 3 to 30 days produced reasonable results. Based on discussions with Signell (2002), the relaxation times were "empirically determined to produce reasonable results", but there could be "room for optimization based on some quantitative measure." The researchers at the University of Massachusetts may want to consider further analysis of the boundary relaxation times in the model.

SECTION 6

WESTERN GULF OF MAINE MODEL

An adjunct model of the western Gulf of Maine (GOMM) was developed to help provide boundary conditions for the Massachusetts and Cape Cod Bays Model during the calibration of the 1989-1992 period, (Signell, et al. 1996). Much of the description of this model that follows was pulled from Signell (1996). ECOMsi was used to develop the Gulf of Maine Model. The model grid is 90 x 45 cells and has a typical grid spacing of 2-4 km. The model grid and its relation to the Massachusetts Bay model grid is shown in Figure 6-1. The GOMM bathymetry was generated by the same method used for the Massachusetts Bay Model and both models were driven by the same wind and heat flux forcing. The GOMM elevation boundary conditions were specified as M2, S2, and N2 tides derived from Lynch and Naimie (1993). No subtidal fluctuations were specified, effectively clamping the low-frequency elevations at zero along the boundary. A mean sea surface slope is imposed at the northern boundary to drive a coastal current. The low frequency elevation varied linearly from 0.06 m to 0.00 m from the coast to the open boundary 45 km offshore. These values were chosen to drive a mean alongshore flow of 5-10 cm/s to coincide with measurements collected by Vermersch et al. (1979). The mean flow in GOMM is held constant throughout the year.

The temperature and salinity along the open boundary were specified by monthly climatology determined from the Bedford Institute of Oceanography AFAP database. Model output was specified at the cells that constitute the open boundary of the Massachusetts Bay model and averaged over a tidal cycle. These results were then converted into-low frequency elevation boundary conditions, and temperature and salinity boundary conditions at 12 standard levels (1, 2.5, 5, 7.5, 10, 15, 20, 30, 40, 50, 75 and 140m). The boundary conditions developed in this manner represent more variability than would have been possible with open boundary conditions based on climatology.

The use of the GOMM was abandoned by Signell during the calibration of the Massachusetts Bay model during the calibration of the 1993-1994 period due to a lack of data with which to drive the GOMM. The modeling analysis of 1998-1999 followed the method used by Signell for 1993-1994 as outlined in the report for which this addendum has been written.
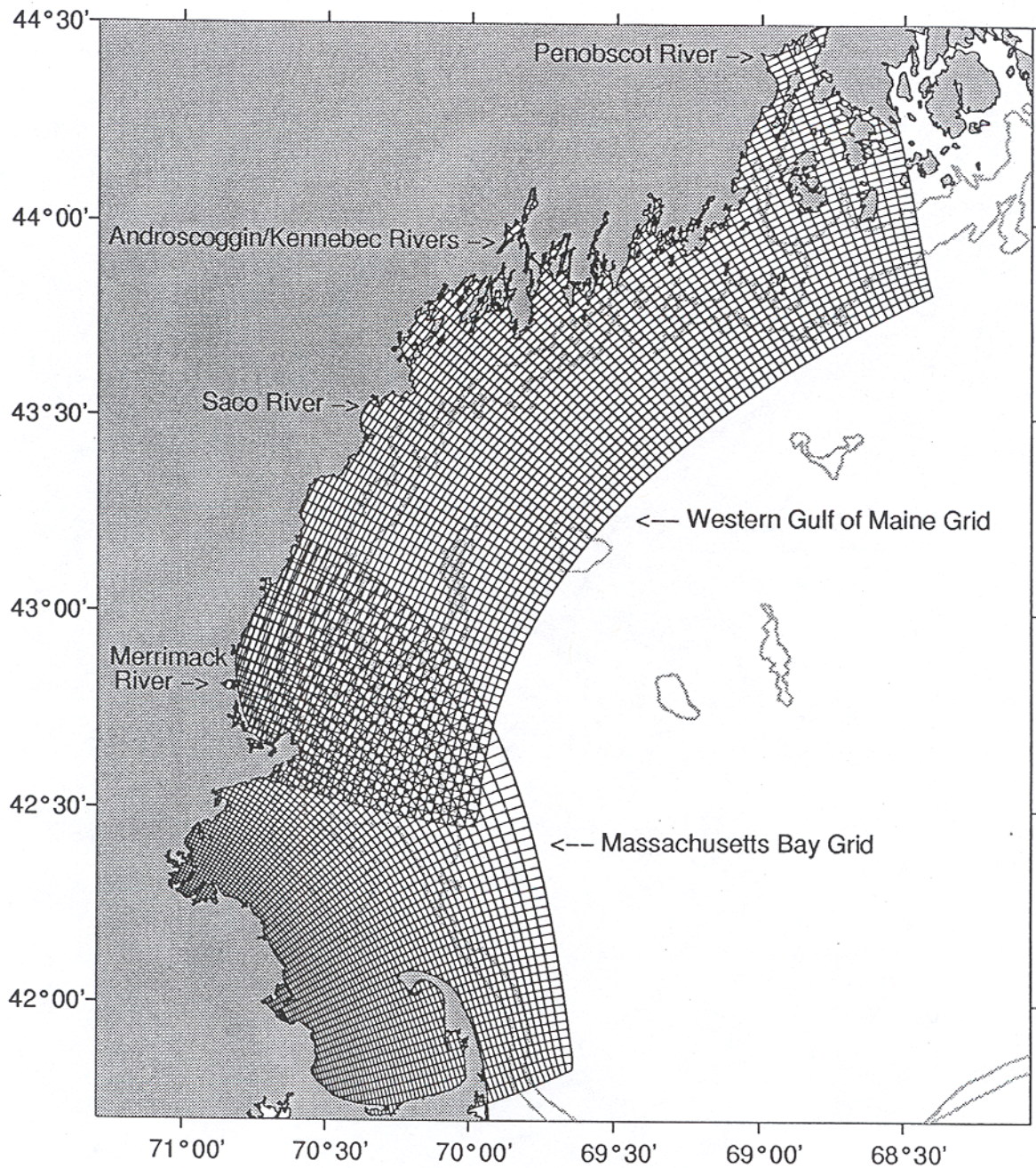
Figure 6-1. Western Gulf of Maine model grid and its relation to the Massachusetts Bay grid.

SECTION 7

REFERENCES

Ahsan, Q., A.F. Blumberg and H. Li, 2002. "Calibration/validation of a Coupled Mississippi Sound/Bight Forecast Model." Oceans 2002, October 29-31, 2002, Biloxi, Mississippi.

Ahsan, Q. and A.F. Blumberg, 1999. "A Three-Dimensional Hydrothermal Model of Onondaga Lake, New York." J. Hydr.. Engrg., Vol. 125, No. 9, September, 1999.

Blumberg, A.F., L.A. Khan and J. St. John, 1999. "Three-Dimensional Hydrodynamic Model of New York Harbor Region," J. Hydr. Engrg., Vol. 125, No. 8, August, 1999.

Brady, D.K., A. S. Brooks and N.L. Buske, 1969. "Future use of Chesapeake Bay for cooling thermal discharges." Water Sci. and Mgmt. Seminar Rep., Johns Hopkins University, Baltimore.

Brunt, D., 1932. "Notes on radiation in the atmosphere." Quarterly J. Royal Meteorol. Soc., Bracknell, U.K., 58, 389-420.

Clark, N.E., L. Eber, R.M. Laurs, J.A. Renner and J.F.T. Saur, 1974. "Heat exchange between ocean and atmosphere in the Eastern North Pacific for 1961-1971." NOAA Tech. Rep. NMFS-SSRF-682, U.S. Department of Commerce, Washington, D.C.

Cole, T.M. and E.M. Buchak, 1995. "CE-QUAL-W2: a two-dimensional, laterally averaged, hydrodynamic and water quality model, version 2.0 user manual." Instruction Rep. EL-95-1, U.S. Army Corps of Engineers, Washington, D.C.

Edinger, J.E., D.K. Brady and J.C. Greyer, 1974. "Heat exchange and transport in the environment." Rep. No. 14, Cooling Water Res. Project (RP-49), Electric Power Research Institute, Palo Alto, Calif.

Fung, I.Y., D.E. Harrison and A.A. Lacis, 1984. "On the variability of the net longwave radiation at the ocean surface." Rev. of Geophys. and Space Phys., 22(2), 177-193.

Hondzo, M. and H.G. Stefan, 1993. "Lake water temperature simulation model." J. Hydr. Engrg., ASCE, 119(11), 1251-1273.

HydroQual, Inc. and Nomandeau, 1995. "A water quality model for Massachusetts and Cape Cod Bay: Calibration of Bays Eutrophication Model." Boston: Massachusetts Water Resources Authority Report ENQUAD, 1995-08, 1-402.

HydroQual, Inc., 2000. "Bays Eutrophication Model (BEM): Modeling Analysis for the Period 1992-1994." Boston: Massachusetts Water Resources Authority Report ENQUAD, 2000-02.

HydroQual, Inc. and R.P. Signell, 2001. "Calibration of the Massachusetts and Cape Cod Bays Hydrodynamic Model: 1998-1999." Boston: Massachusetts Water Resources Authority Report ENQUAD, 2001-12, 1-170.

Large, W.G. and S. Pond, 1982. "Sensible and latent heat flux measurements over the ocean." J. Phys. Oceanogr., 12, 464-482.

Lynch, D. and C. Naime, 1993. "The M2 tide and its residual on the outer banks of the Gulf of Maine." J. Phys. Oceanogr., 11, 2222-2253.

Martin, P.J., 1985. "Simulation of the mixed layer at OWS November and Papa with several models." J Geophys. Res. 90(C0), 903-916.

Payne, R.E., 1972. "Albedo of the sea surface." J. Atmos. Sci., 29, 959-970.

Reed, R.K., 1977. "On estimating insolation over the ocean." J. Phys. Oceanogr., 7, 482-485

Rosati, A. and K. Miyakoda, 1988. "A general circulation model for upper ocean simulation." J. Phys. Oceanogr., 18, 1601-1626.

Schertzer, W.M., 1987. "Heat balance and heat storage estimates for Lake Erie, 1967 to 1982." J. Great Lakes Res., 13(4), 454-467.

Signell, R.P., H.L. Jenter, and A.F. Blumberg, 1996. "Circulation and effluent dilution modeling in Massachusetts Bay: Model implementation, verification and results." U.S. Geological Survey Open File Report 96-015.

Signell, R.P., 2002. Personal communication.

Simpson, J.J. and C.A. Paulson, 1979. "Mid-ocean observations of atmosphere radiation." Quart. J. Roy. Meteor. Soc., 105, 487-502

Swinbank, W.C., 1963. "Longwave radiation from clear skies." Quarterly J. Royal Meteorol. Soc., 89, 339-348.

Tsay, T.K., G.J. Ruggaber, S.W. Effler and C.T. Driscoll, 1992. "Thermal stratification modeling of lakes with sediment heat flux." J. Hydr. Engrg., ASCE, 118(3), 407-419.

Vermersch, J., R. Beardsley, and W. Brown, 1979. "Winter circulation in the Western Gulf of Maine: Part 2. current and pressure observations." J. Phys. Oceanogr., 9, 768-784.

Massachusetts Water Resources Authority
Charlestown Navy Yard
100 First Avenue
Boston, MA 02129
(617) 242-6000
http://www.mwra.state.ma.us